Manuscript Details

Manuscript number ENGEO_2017_1355_R1

Title Geomorphic impact and assessment of flexible barriers using multi-temporal LiDAR data: the Portainé mountain catchment (Pyrenees)

Article type Research Paper

Abstract

Multi-temporal digital elevation models (DEMs) obtained from airborne LiDAR surveys are widely used to detect geomorphic changes in time and quantify sediment budgets. However, they have been rarely applied to study the geomorphic impact of engineering structures in mountain settings. In this study, we assessed the influence and behavior of flexible sediment retention barriers in the Portainé catchment (Spanish Pyrenees), using three LiDAR data sets (2009, 2011 and 2016) that covered a 7-year period. Densely forested mountainous areas present some limitations for reliable DEM analysis due to spatial variabilities in data precision, accuracy and point density. A new methodological approach for robust uncertainty analysis along channels, based on changes in cross-sectional elevations, was used to discriminate noise from real geomorphic changes. The obtained results indicated that erosion occurs along most reaches covering a large area, whereas deposition is localized in specific areas such as those upstream of sediment retention barriers and in the debris cone. Despite the presence of 15 flexible sediment retention barriers, the channels presented net degradation during both 2009-2011 and 2011-2016, with 2,838 and 147 m3 of material exported from the basin, respectively. For the same periods, the barriers retained 33% and 25% of the total deposition (up to 1,300 m3 per barrier), respectively, but also induced lateral and downstream incision, the latter reaching 703 m3 for a single barrier. We detected a horizontal displacement of the net of up to 1.2 m in filled barriers, resulting from net flexion. The interference of the natural river evolution by defense measures has resulted in a complex erosion-deposition pattern. The presented methods show high potential for the hydrogeomorphic study of mountain catchments, especially for a high-resolution assessment of flexible barriers or other engineering structures in remote areas.

Keywords torrential flow; LiDAR; change detection; flexible barrier; sediment budget.

Taxonomy Earth Surface Sediment Transport, Geomorphic Hazard, Geomorphic Change, Barrier, Debris Flows, Lidar Remote Sensing

Corresponding Author Ane Victoriano

Order of Authors Ane Victoriano, James Brasington, Marta Guinau Selles, Glòria Furdada, Mariló Cabré, Myriam Moysset

Suggested reviewers Joe Wheaton, Christian Scheidl, Damià Vericat

Submission Files Included in this PDF

File Name [File Type]

Cover letter.pdf [Cover Letter]

Revision notes Victoriano_et_al.pdf [Response to Reviewers]

Manuscript changes marked Victoriano_et_al.docx [Revised Manuscript with Changes Marked]

Highlights.docx [Highlights]

Manuscript Victoriano_et_al.docx [Manuscript File]

Figure_1.tif [Figure]

Figure_2.tiff [Figure]

Figure_3.tiff [Figure]

Figure_4.tiff [Figure]

Figure_5.tiff [Figure]

Figure_6.tiff [Figure]

Table_1.docx [Table]

Table_2.docx [Table]

Table_3.docx [Table]

Table_4.docx [Table]

Table_5.docx [Table]

Table_6.docx [Table]

To view all the submission files, including those not included in the PDF, click on the manuscript title on your EVISE Homepage, then click 'Download zip file'.

UNIVERSITAT DE BARCELONA

Ane Victoriano Lamariano

Dpt. Dinàmica de la Terra i de l'Oceà
Facultat de Ciències de la Terra

Martí i Franquès s/n
08028 Barcelona

Tel. +34 93 4021376
Fax +34 93 402 13 40
www.ub.edu

Barcelona, January 23rd, 2018

Manuscript for *Engineering Geology*

Dear Editor Janusz Wasowski,

We would like to thank the two reviewers for their useful comments on our paper *"***Geomorphic impact and assessment of flexible barriers using multi-temporal LiDAR data: the Portainé mountain catchment (Pyrenees)"**. All the comments were taken into account and incorporated in the reviewed version.
Besides, you suggested us to check the English. We have followed your recommendation and the paper has been sent to an English correction professional service, where a person for whom English is the native language has made a thorough revision.

Enclosed you will find the following documents, which are the result of the revision:

- Revision notes: point by point response to each editor's and reviewers' comment indicating how and where the changes have been introduced in the manuscript (pdf document entitled "Revision notes Victoriano_et_al").

- Manuscript, changes marked: the tracked-changes version of the manuscript that includes all the changes as a result of the revision following reviewers' comments and the English correction (word document entitled "Manuscript changes marked Victoriano_et_al").

- Manuscript, unmarked: the new revised manuscript (word document entitled "Manuscript Victoriano_et_al").

This revision has considerably improved the quality of the manuscript, hoping it is now suitable for publication in ENGINEERING GEOLOGY.

Sincerely,

Ane Victoriano and co-authors

Correspondence to: ane.victoriano@ub.edu
Departament de Dinàmica de la Terra i de l'Oceà
University of Barcelona
RISKNAT Research Group

REVISION NOTES

We thank the reviewers for finding the paper interesting and for their useful revisions. We considered each comment and suggestion provided by the editor and the two referees, which improved the quality of the manuscript. The changes have been incorporated in the new revised version of the manuscript, and can be easily identified in the marked document. A point-by-point response to all the reviewer's comments is presented here, and the changes are referred by indicating the line numbers of the "Manuscript changes marked" document.

1. <u>EDITOR</u>

The authors thank the editor for his decision on the manuscript. Regarding the specific comments:

1) *English - generally fine. However, please check it again. For example, the English expression may need to be improved in the following sentences (in Conclusions): "Last but not least, the used data was not acquired for hydrogeomorphic nor engineering purposes, its usefulness and application has been proved though. The design of multi-temporal LiDAR campaigns choosing best flight parameters for data collection along channels would provide results that are even more accurate.*

Even if the English was generally fine, the editor mentioned that it should be checked again. The paper has been sent to an English correction professional service and a thorough revision has been done, correcting the entire paper, figures and tables. All the changes made by him have now been incorporated in the manuscript are. Regarding the mentioned expression in conclusions, it has been rewritten in a more concise way (line 753-758). However, all the manuscript has been corrected by a native speaker.

2) *Referencing - many references. Try to limit the number keeping in mind the typical audience of our Journal (more "engineering" than "geomorphologic"). Too many references in Spanish - select only the most important ones.*

Bibliography has been revised. Considering the "engineering" scope of the journal, we reduced the number of "geomorphologic" references due to the irrelevance of some of them (e.g. Cavalli et al 2008: "The effectiveness of airborne LiDAR data in the recognition of channel bed morphology"). Moreover, we removed many citations in Spanish (e.g. unpublished IGC reports), only keeping the most essential ones. In this revision process, a total of 20 references have been deleted.

2. <u>REVIEWER 1</u>

The reviewer considers that the paper fits within the scope of the journal. The commented points have been considered and incorporated, leading to a remarkable improvement of the manuscript.

1) *This paper present a procedure to estimate the error of the temporal Li-DAR data, however, it is kind of confusing and not easy to read. Since it is one of the major contributions of this paper, please consider to rewrite it in an independent section and in a more logic way with a flowchart.*

The new approach for error analysis corresponds to the estimation of the error for individual DEMs. This contribution is presented in a specific subsection, “Individual DEM error” indeed. As it is a step for the complete procedure of error analysis, we prefer to keep it as a subsection of section 3.3. As suggested by the referee, we have modified some parts of the text to avoid confusion and make it clearer and we have included a flowchart (Figure 2). This new figure synthetizes all the methodological approach of section 3.3 and makes it easier to understand it.

2) *About the LiDAR data and the data in the Tables (including Table 2 and 3), they are short of relevant references. Please include them in the References.*

LiDAR data was acquired by the Cartographic and Geological Institute of Catalonia (which are coauthors of the paper) and provided to us thanks to a special agreement between them and the University of Barcelona. We have added in Table 1 the information about where the data belongs to. Regarding tables 2 and 3, we have included missing citations (FGC, 2015, IGC, 2013 and Mr. Carles Fañanás, personal communication) both in the table footnote and in the list of references.

3) *About the resolution of the DEM from The Li-DAR, it is not clearly described. Please describe the method in more details, especially the 2009 data (there is one point in a 2m*2m in average, how do you obtain the 1m*1m DEM. More descriptions and/or discussions (with a Table perhaps) are necessary.*

The DEM was built in ArcGIS by triangulating LiDAR ground points and then interpolating the TIN using a linear interpolation algorithm and stablishing a 1 m grid resolution. Regarding 2009 data, it is true that the mean ground point density (Table 1) is lower than the DEM resolution, but it is essential to note that this is just an average value, so some areas show much higher density (and other lower). If we apply the formula proposed by Landridge et al. (2014), $S = \sqrt{A/n}$, the obtained resolution (s) for the data used in this paper is 1.86 m. Moreover, the optimal cell size differs between data sets, being up to 0.86 m for 2016 data. Considering that multi-temporal DEMs need to have the same resolution in order to be subtracted, the best choice is to use a mean value for DEM generation. 2x2 m DEMs would imply not taking advantage of a significant quantity of point (in the case of 2011 and 2016). Therefore, we consider that the most profitable option for DEM comparison is obtaining 1x1 m models for the three data sets. Finally, we are aware that, for 2009, in some areas the 1 m resolution DEM includes highly interpolated unreal surfaces. This supports the idea of quantifying the interpolation error and discarding areas where the error is too high, as done thorough the cross section based uncertainty analysis. The result is that sections with very low resolution show very high error and, at the end, they are not considered for morphological budgeting calculations. A better description and justification of 1m resolution DEM generation have been included in the methods section of the manuscript (line 271-272 and line 277-280). Also, we have added a new paragraph discussing the grid resolution, the problems associated to 2009 data and how these were solved (line 596-606).

4) *Since the results only possess a 68% confidence interval, it is essential to have more descriptions and discussions on the advantages and disadvantages (including comparison of the time and the cost) of the applied method(s). In addition, suggestions on improved this shortcoming are necessary.*

The main advantages and disadvantages of the method are presented in the discussion (section 5.1). The 68% confidence interval is not necessarily the real reliability of the results, it is just a threshold that we set due to our specific data characteristics (quite low point density; see reply to point 3). Comparing this approach to other DEM comparison procedures (classical DoD approach), it is noteworthy that the time and cost is higher. Indeed, DoD techniques are adequate enough in flat and/or poorly vegetated areas. However, the potential of the presented method lies on its usefulness for geomorphic change quantification along channels (where sediment retention barriers locate)in forested steep slopes, where a more accurate DoD thresholding is required. In such contexts, an unthresholded DoD analysis can be used as a preliminary inspection of geomorphic changes, whereas a detailed thresholded comparison is the best option to avoid errors and obtain the most reliable sediment budgets. This has been more clearly discussed in the new version of the manuscript, indicating the potential of the proposed method and how its shortcoming are overcome (line 607-636).

5) *The figures and tables might need to be modified according to the standards of ENGEO. Please recheck their quality.*

We have checked the standards of the journal. The design of the figures already fit with author guidelines. Regarding their quality, we have submitted all the figures separately as individual TIFF files with a 300 ppi quality. Tables, presented as editable text, have been modified according to the standards of ENGEO, avoiding shading and vertical rules.

3. REVIEWER 2

The authors appreciate the reviewer’s opinion that the paper is of great interest and that it is clear and well written. The referee also points out that the methodological approach is original and results are very well presented and discussed. The minor comments have been considered, as described below.

LINE 51 AND 58: *“hyperconcentrated”, here and throughout the text. I would prefer to refer to “floods with a high concentration of sediments” than using the term “hyperconcentrated” that is strictly defined in torrential classification schemes and, being a transitional phase between bed load transport and debris flow, it is quite difficult to be identified.*

As suggested by the reviewer, we have replaced the term “hyperconcentrated” by “floods with a high concentration of sediments” (line 55).

LINE 66: *an->and*

We corrected the error in this word.

LINE 110-113: *I totally agree. I would stress a little bit more the importance of point clouds alignment maybe also citing some literature (e.g. Lallias-Tacon et al., 2014).*

We have specified the importance and difficulty of the alignment of point clouds in complex terrains and referred to the work by Lallias-Tacon et al., 2013 (line 125-127).

LINE 119-120: *not only along channels but also on the hillslopes…*

We have indicated that difficulties for a reliable uncertainty assessment occur in mountain channels but also in the hillslopes (line 134-135).

LINE 172: *"one-year recurrence interval": you should state here that this is an estimate based on recent observations (you say it later in the text).*

This sentence has been modified (line 196) because the recurrence interval as not been calculated, it is just an estimation based on observations.

LINE 180-188: *is there a reason why flexible barriers where preferred to the more conventional check dams? The latter type could be better fixed to the banks and limit damages due to the lateral incision. Maybe a comment on hydraulic control measure typologies could be added to discussion chapter.*

The reasons for preferring flexible ring-net barriers to check dams were mainly three. On the one hand, the most important factor was the lower environmental impact of the measures. Flexible barriers were the most environmentaly-friendly option because they are quite rapidly installed using a helicopter, without affecting and degradating the hillslopes. For the construction of other conventional structural measures, acess paths need to be created to reach the specific channel stretches where they would be implemented. Indeed, not only one but much more dams would need to be constructed considering the extent of the problem, so the impact on the mountain would be remarkable. On the other hand, the economic cost of flexible barriers is much lower. Due to the limitations on the budget, these were the best option because a greater quantity of retention barriers than check dams could be installed. Finally, flexible barriers have been proved an effective hydrological correction measure in torrential channels, as they let small flow to pass through and they only act when flows are extremely voluminous, retaining big boulders and letting water flow downstream due to their ring-porous nature. A comment on the suitability of flexible barriers in the studied area has been added in the discussion (line 700-704).

LINE 243-248: *It would be nice to see the mask in a figure.*

The mask is indeed shown in a figure (Figure 3 in the new manuscript) and is marked with a black line named "analysis area".

TABLE 5 AND LINE 431-435: *Why did you present the volumetric results without an error indicating the associated uncertainty?*

The error associated to the total eroded and deposited volumes has not been indicated because it is not homogeneous in the whole extent but highly variable from section to section. The propagated error ($\delta\mu$) after the probabilistic thresholding process varies between 0.12-5.4 and 0.10-5 m in 2011-2009 and 2016-2011 comparison respectively, but the median is quite low, indeed 0.9 m for 2011-2009 and 0.66 m for 2016-2011. As the variability of the error is large, the mean error would not be representative, so we prefer not to indicate it in the volumetric budget calculations of table 5. Nevertheless, we have added the uncertainty ranges in the text (line 474-477) in order to give an idea of the error associated to volumetric calculations.

4. OTHER CHANGES

- References have been updated. Some papers were under review when the initial manuscript was submitted to Engineering Geology, but they are now accepted and we provide the complete citation.
- The figure numbers have been modified according to the new manuscript, considering that it now contains a newly added one.

Geomorphic impact and assessment of flexible barriers using multi-temporal LiDAR data: the Portainé mountain catchment (Pyrenees)

Ane Victoriano[a,*], James Brasington[b], Marta Guinau[a], Glòria Furdada[a], Mariló Cabré[c], Myriam Moysset[c]

[a] RISKNAT Group, Geomodels ~~Research~~ Institute, Departament de Dinàmica de la Terra i de l'Oceà, Universitat de Barcelona (UB), Barcelona, Spain.

[b] School of Geography, Queen Mary University of London (QMUL), London, UK.

[c] Geoprocessing Area, Institut Cartogràfic i Geològic de Catalunya (ICGC), Barcelona, Spain.

* Corresponding author at: Departament de Dinàmica de la Terra i de l'Oceà, Facultat de Ciències de la Terra, Universitat de Barcelona (UB), Martí i Franquès s/n, 08028 Barcelona, Spain

E-mail address: ane.victoriano@ub.edu (A. Victoriano).

Abstract

Multi-temporal ~~D~~digital ~~E~~elevation ~~M~~models (DEMs) obtained from airborne LiDAR surveys are widely used to detect geomorphic changes in time and quantify sediment budgets.~~;~~ ~~but~~However, they have been rarely applied to study the geomorphic impact of engineering structures in mountain settings ~~contexts~~. In this study, we assessed the influence and behavior of flexible sediment retention barriers in the Portainé catchment (Spanish Pyrenees), using three LiDAR data sets (2009, 2011 and 2016) that covered a 7-year ~~time~~ period. Densely forested mountainous areas present some limitations for ~~a~~ reliable DEM analysis due to spatial variabilities ~~of~~ in data precision, accuracy and point density. A new methodological approach for robust uncertainty analysis along channels, based on changes in cross~~-~~sectional elevations, ~~changes is presented~~was used to discriminate noise from real geomorphic changes ~~for robust uncertainty analysis along channels, in order to discriminate noise from real geomorphic changes~~. The ~~O~~obtained results indicated that erosion occurs along most reaches covering a large area, whereas deposition is localized in specific areas such as those upstream ~~from~~ of sediment retention barriers and ~~at~~ in the ~~most downstream~~ debris cone. Despite the ~~existence~~ presence of ~~fifteen~~ 15 flexible sediment retention barriers, the channels ~~were~~ presented net degradation~~al~~ during both ~~for the~~ 2009-2011 and 2011-2016 ~~periods~~, with 2,838 and 147 m^3 of material exported from the basin, respectively~~, corresponding to a net erosion of 2,985 m³.~~ For the same periods, the barriers retained 33% and 25% of the total deposition (up to 1,300 m^3 per barrier), respectively, but also induced lateral and downstream incision, the latter~~st~~ ~~one~~ reaching 703 m^3 for a single barrier. We detected a~~n~~ horizontal displacement of the net of up to 1.2 m ~~horizontal displacement of the net~~ in filled barriers, resulting from ~~the~~ net flexion. The interference of ~~defense measures with~~ the natural river evolution by defense measures has resulted in a complex erosion-deposition pattern. The presented ~~tools and~~ methods show high potential for the hydrogeomorphic study of mountain catchments, ~~and~~ especially~~,~~ for a high~~-~~resolution assessment of flexible barriers or other engineering ~~measures~~ structures in remote areas.

Keywords: torrential flow, LiDAR, change detection, flexible barrier, sediment budget.

1. Introduction

Hydrometeorological events represent the most frequent natural disasters occurring on a global scale (Munich Re, 2016), producing significant economic and human losses. In 2015 alone, floods caused damages~~an~~ estimated ~~economic to cost of~~to be worth US$ 21.3 billion (c. ~~EUR~~ €20,108 million) and claimed 3,449 lives (Guha-Sapir et al., 2016). In mountainous ~~environments~~areas, high~~-~~-intensity~~,~~ sediment-laden torrential floods are the most destructive geomorphological hazards. Several areas in the Pyrenees have been affected by these phenomena in recent years and their management continues to pose an ongoing challenge (Batalla et al., 1999; Chevalier et al., 2013~~; Lorente et al., 2003; Palau et al., 2017; Portilla et al., 2010~~).

Such phenomena are highly unpredictable, often resulting from short and intense localized~~, short duration, high intensity~~ precipitation events. The rapid accumulation of drainage through ~~the~~ steep mountain basins can ~~then give rise~~lead to high-~~-~~velocity flows that entrain large volumes of sediment from the bed and banks. ~~and may~~These can quickly evolve into ~~hyperconcentrated~~ floods with a high concentration of sediments that continue to bulk-up downstream, with potentially catastrophic consequences. Such ~~floods~~ flows ~~have considerable destructive power, posing~~pose a severe risk to infrastructure, ~~and~~ riparian assets and ~~a major threat to~~ life, particularly where the floods discharge onto the valley floor through populated fans and floodplains. ~~Central to this is an understanding of how l~~Lithology, gradient and the pattern of drainage accumulation~~, gradient and lithology~~ combine to affect the distribution of stream power and sediment transport in mountain catchments. This interaction ~~affects~~determines whether the ~~potential for switching~~ flow ~~between~~becomes a clearwater, hyperconcentrated ~~fluid one and~~ or a debris ~~flow~~ one ~~behaviour as water flows can evolve into hyperconcentrated or debris flows~~ in a single event, depending on the sediment load ~~involved~~ (Pierson and Costa, 1987). This in turn~~,~~ influences the distribution of runout across the receiving ~~piedmont~~ fan piedmont or floodplain (~~Chiang et al., 2012;~~ Scheidl and Rickenmann, 2011).~~ Throughout the paper, w~~We will use the term "torrential" throughout this paper to include all the mentioned flow types and events.

~~The control of h~~Hydrogeomophic hazards ~~is~~ can be ~~faced~~ dealt with using various kinds of defense measures, depending on the characteristics of the site. Engineering structures are considered a fast and effective way of mitigating risk~~ mitigation,~~ and ~~among them,~~include the recently-developed flexible debris flow barriers that are increasingly being ~~used~~ emplaced in torrential channels (Luis-Fonseca et al., 2011; Wendeler et al., 2008). While much attention has been paid to the safe design of such retention barriers (Ferrero et al., 2015; Volkwein et al., 2015), ~~the study of~~ their geomorphic effects still require~~s~~ further research, as ~~it has~~these directly impact~~lications~~ on the effectiveness and stability of the structure itself. Thus, the question ~~being~~ that needs to be addressed ~~would be~~is how barriers actually behave and influence ~~landscape~~ geomorphological evolution.

Geomorphological risk assessments have been facilitated by the emergence of high-resolution topographic data that have~~s~~ provided new opportunities to quantify the transfer of mass and energy across landscapes (Passalacqua et al., 2015). The acquisition of detailed 3D topographic data, ~~in~~ particularly through airborne laser scanning (~~ALS, also called~~ airborne LiDAR), has ~~fast~~ rapidly become ~~established as~~ routine practice for many national mapping agencies ~~and it is used~~ to support ~~flood and~~ geological risk assessment. Moreover, such data are now increasingly available to the wider public through open-access data portals, presenting unrivalled opportunities for broad-scale research. Airborne LiDAR data have~~s~~ been used ~~to support a~~for a wide range of research into natural hazards, ~~including~~ such as the geomorphic research on past and/or recent active surficial processes (Abellan et al., 2016; ~~Jaboyedoff et al., 2012;~~ Roering et al., 2013). In ~~the specific context of~~ fluvial and torrential environments, these data have been used to provide enhanced characterization of drainage systems and ~~to provide~~ the boundary conditions for kinematic and physical models of fluid and sediment transport (Bailly et al., 2012; Biron et al., 2013; ~~Cavalli et al., 2008; Cavalli and Tarolli, 2011; Jones et al., 2007;~~ Notebaert et al., 2009~~; Thoma et al., 2005~~).

The ~~I~~increasingly ~~the~~ routine ~~approach to~~use of LiDAR data acquisition has led to the development of multi-temporal data sets that sample the same region as a series of timeslices. The derived ~~D~~digital ~~E~~elevation ~~M~~models (DEMs) can then be differenced sequentially to obtain DEMs of ~~D~~difference (DoDs), which reveal not only the horizontal, but also the vertical pattern of topographic change. Such assessments of geomorphic changes ~~assessment~~ based on DoDs ~~gives insights into~~provide information on landscape morphology and evolution ~~(Anders et al., 2013)~~, as it ~~allows~~ enables a detailed study of the spatial and temporal patterns ~~of~~ in erosion and deposition~~, and also~~as well as the net changes from morphological sediment budgeting~~. Sequential DEM differencing has been applied to a wide range of fluvial systems, including braided~~,~~ gravel-bed rivers with high sediment loads (Brasington et al., 2000; Lane et al., 2003), ~~and~~ steep mountain channels (Cavalli et al., 2017), ~~but also for the analysis of~~and specific flood or debris flow events (~~Breien et al., 2008; Bremer and Sass, 2012;~~ Bull et al., 2010; Croke et al., 2013; ~~Imaizumi et al., 2016; Rathburn et al., 2017;~~ Scheidl et al., 2008).

It is essential to consider data uncertainty ~~in order~~ to avoid the misinterpretation of ~~the~~ real geomorphic changes~~,~~ by distinguishing them from background noise generated by different ~~error~~ sources of error. Over the last few decades, much attention has been paid to the assessment of DoD uncertainties ~~that come from DEM quality~~ (Brasington et al., 2003; Cavalli et al., 2017; Lane et al., 2003~~, 1994~~; Wheaton et al., 2010). ~~The need for the estimation of a~~It has been reported that ~~the~~a minimum level of detection ($_{min}$LoD) should be estimated ~~to~~ for the detection of small elevation changes that are probably associated ~~to~~ with errors ~~has been reported~~ (Brasington et al., 2000; Fuller et al., 2003).

Regarding mountain environments, ~~many difficulties for a~~the reliable application of airborne LiDAR data ~~are~~ is still ~~unsolved~~hampered by many difficulties. Comparability between data sets is ~~a key point~~ ~~that becomes~~ a hard task in morphologically complex terrains. ~~On the one hand~~However, ~~there is a bias resulting from differences in the~~ point cloud georeferencing and the adjustment/alignment process becomes~~ an~~ arduous ~~task~~in mountain regions (Lallias-Tacon et al., 2014). ~~On the other hand~~Moreover, elevation accuracy and point density decrease in steep densely forested ~~steep~~ areas (Cavalli et al., 2008), leading to data sets with temporally variable characteristics among them and spatially variable uncertainties within each~~ one~~. With~~hen~~ these limitations~~ exist~~, DoD-based analyses cannot be ~~applied~~ performed properly due to many areas lacking ~~of~~ source data, ~~that produce~~resulting in merely interpolated surfaces~~,~~ that are different in each DEM. ~~At this point~~Thus, there is a need for a methodology for LiDAR uncertainty ~~assessment~~ analysis based on spatial variabilities along mountain channels and hillslopes~~ arises~~.

In this paper, we present a new ~~methodological~~ approach for ~~the~~ quantifying~~ication of~~ geomorphic changes in active and densely forested mountain catchments using multi-temporal airborne LiDAR data. The ~~major~~ main objective ~~is to~~of this study was to assess the behavior, effectiveness and geomorphic influence of flexible retention barriers. This~~e interest and contribution of this~~ research ~~lie on the~~provides a high-resolution assessment of the existing engineering ~~features~~structures in ~~difficult-access~~ remote channels that are difficult to access, ~~as well as on the detection of~~identifying the priority areas for the maintenance and future management ~~actions~~of the barriers.

2. Study area and torrential activity

This study ~~i~~was carried out in the Portainé (5.7 km long;~~,~~ average gradient, 24.7%) and ~~the~~ Reguerals (3 km long;~~,~~ average gradient, 31.3%) mountain torrents of the Pyrenees, the latter being a tributary of the former and ~~named~~ referred to as Caners downstream ~~from~~ of the confluence (Fig. 1a). The two torrents constitute the Portainé catchment (5.72 km^2), which is located in the Pallars Sobirà County (Catalonia, Spain), and they flow into the Romadriu River, which is part of the Ebro River draining into the Mediterranean Sea. Elevation ranges ~~between~~ from 2,439 m a.s.l. (the Torreta de l'Orri peak) ~~and~~ to 950 m a.s.l. (the Vallespir hydropower dam), and the torrents merge at 1,285 m a.s.l.~~ In the headwaters, a~~A ski resort is located at the headwaters, ~~and an~~with its access road ~~goes~~ along the hillslopes crossing the channels ~~repeatedly~~several times. The basin can be divided into two sectors that differ in morphology and hydrogeomorphic processes. The southern one corresponds to the ~~less vegetated~~ headwaters~~,~~ ~~coinciding with~~containing less vegetation and the ski ~~domain~~resort. This area is characterized by ~~G~~gentler slopes (10-25º) and a less entrenched drainage network~~ characterize this area~~, where torrential processes are not especially relevant. The northern sector is densely forested and shows ~~an~~ intense torrential activity along the steep (>25º) and strongly entrenched and confined torrents. These ~~are human-altered~~ channels have been affected by human activity ~~with~~ via the implementation of a multi-barrier system that ~~highly~~ strongly influences sediment transfer processes. In the~~i~~se reaches, severe flows have occurred in the last decade and a debris cone has ~~been~~ formed in the most downstream part.

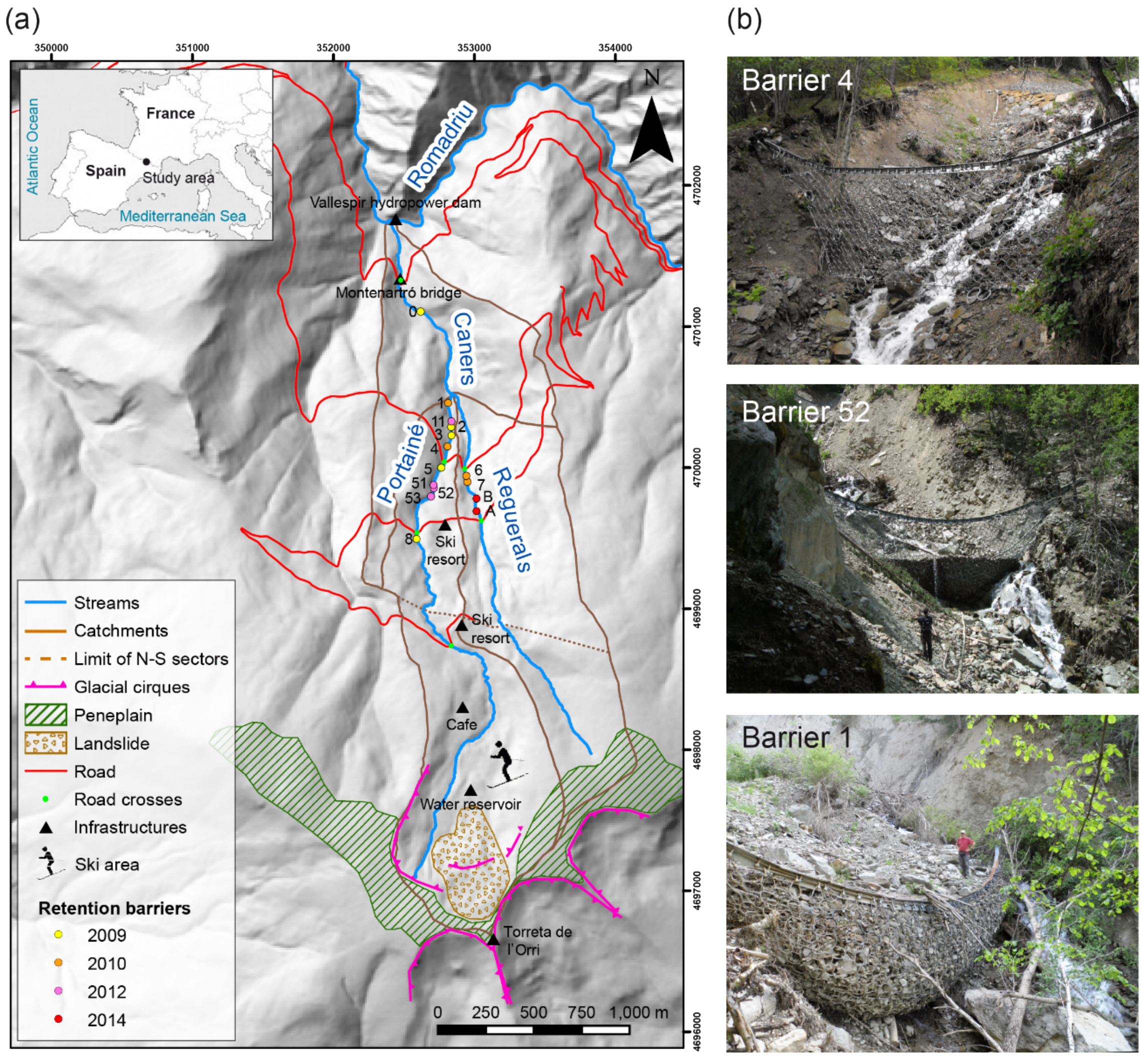

Figure 1. (a) Setting of the study area showing the main geomorphological and anthropic features. The Portainé and ~~the~~ Reguerals torrents, ~~and~~ as well as the code of each sediment retention barrier, ~~is~~ are also indicated. (b) Photographs of some of the barriers showing examples of an empty (barrier 4 in June 2010), partly filled (barrier 52 in June 2013) and completely filled (barrier 1 in June 2013) ~~status~~barrier.

2.1. *Geological setting and climate~~ic setting~~*

The region is dominated by highly folded, fractured and weakened Cambro-Ordovician metapelites. Glacial and periglacial processes during the Pleistocene glacial periods gave rise to intense weathering, ~~and~~ with the subsequent fluvial erosion ~~has~~ resulting~~ed~~ in steep slopes and entrenched torrents. Apart from the bedrock, two types of surficial deposits ~~are present~~crop out in the Portainé catchment. ~~First,~~ One is the colluvium, up to 10 m thick, which covers the bedrock ~~is covered~~ along most of its extension~~by an up to 10 m thick colluvium along most of its extension~~. ~~Second,~~ The other are the torrential deposits ~~are~~ found in the valley bottoms~~, which~~ that have been formed by the deposition of different sediment-laden flows. Both are unconsolidated materials that can be easily eroded and transported, as well as the bedrock (Ortuño et al., 2017).

The climate of the study area is Alpine Mediterranean, with a mean annual rainfall of 800 mm and ~~5-7 °C~~ a mean annual temperature of 5-7°C (Meteocat, 2008). Maximum precipitation in terms of intensity and frequency ~~is recorded~~occurs in the spring and summer, mainly as convective storms. It ~~is noteworthy~~should be noted that ~~the~~ orography controls the generation of convective cells at the top of the drainage basins (Trapero et al., 2013), ~~influencing~~ affecting the local meteorological conditions.

2.2. Hydrogeomorphic hazards and flexible barriers

Fluvio-torrential processes are very intense in the Portainé and ~~the~~ Reguerals torrents~~, andthe torrential flows posinge a significant hazard to this catchment~~. ~~These events~~Torrential flows, which include some well-known debris flows, produce considerable economic damages to infrastructures and facilities in the catchment, especially due to the obstruction of the access road ~~that connects with~~to the ski resort. Since 2009, €5~~.~~,800~~.~~,000 ~~€~~ have been invested in road works and €510,~~.~~000 ~~€~~ in mitigation measures ~~since 2009~~ (Pinyol et al., 2017). Dendrogeomorphological studies have proved the occurrence of at least ten ~~previous~~ events from 1969/1970 to 2009/2010 (recurrence interval of 4.5 years), based on the dating of damage indicators on riverbank trees in different geomorphic positions (Génova et al., ~~under review~~accepted; Victoriano et al., ~~in press~~2018). T~~he t~~orrential activity has intensified since 2006, ~~showing a one-year recurrence interval~~with extraordinary flows occurring almost yearly. This~~e~~ increase ~~o~~in the occurrence of torrential events has been ~~related~~ linked to ~~the~~ anthropic ~~changes~~ activities in the ski resort area,~~;~~ mainly to the loss of vegetation cover~~,~~ decreasing ~~the~~ infiltration capacity, and to the construction of artificial drainage channels ~~to~~ for gathering the runoff, all of these together producing higher peak discharges (~~de las Heras, 2016;~~ Furdada et al., 2017). The largest recorded debris flow occurred in September 2008 (prior to the available LiDAR data) and its volume was estimated ~~in the field~~ to be 26,000 m^3 (Portilla et al., 2010), with an average~~d~~ erosion rate of 2.12 m^3/m (Abancó and Hürlimann, 2014).

~~In order t~~To reduce the impacts of the torrential events, mid-term hydrological corrective~~on~~ measures have been ~~carried out~~implemented (Luis-Fonseca et al., 2011), consisting of~~n~~ placing VX-160 flexible ring-net barriers along the channels (Fig. 1b). These aim ~~is~~ to retain part of the transported material and ~~to~~ induce a stepped river profile to reduce ~~the~~ flow energy and, therefore, ~~avoid~~ prevent erosion. Since 2009, ~~fifteen~~ 15 barriers have been placed in the Portainé catchment, ~~eleven of them~~11 in Portainé and ~~seven~~ 4 in Reguerals (Fig. 1a). Due to the large sediment loads ~~involved during~~that are associated with extraordinary events, the barriers were quickly filled, even after a single event. Currently, torrential events still occur, leading to progressively more entrenched ravines and posing a risk to the effectiveness and stability of the barriers.

3. Methods

3.1. Documentary data

We searched for documentary data on recent torrential events and compiled all the available data on their effects ~~and impacts~~ on infrastructures. The main data sources were the technical reports of the *Institut Geològic de Catalunya* (IGC) and *Ferrocarrils de la Generalitat de Catalunya* (FGC) ~~(FGC and ICGC, 2016, 2015, IGC, 2013a, 2013b, 2011, 2010a, 2010b, 2008)~~ (e.g., FGC and ICGC, 2015~~;~~ IGC, 2013), as well as other scientific works (Palau et al., 2017; Victoriano et al., ~~in press~~2018). The relative magnitude of the events was established according to their repercussion on infrastructures (number of obstructed road crosses and filled barriers) and geomorphological processes (incision, sediment transport and accumulation). Regarding anthropic activities~~ons~~, the emplacement dates and ~~place~~ locations of the sediment retention barriers (Fig. 1a) were~~as~~ established thanks to the information provided by Mr. Carles Fañanás (Department of Environment, Government of Catalonia) ~~and recorded phenomena were compiled from different IGC reports~~. ~~With all the information, a~~A complete database was prepared with all this information.

3.2. LiDAR data acquisition and processing

Sequential data sets were collected in August 2009, August-September 2011 and August-September 2016, using a Cessna Caravan 208B aircraft equipped with a Leica ALS50-II topographic LiDAR sensor, owned by the *Institut Cartogràfic i Geològic de Catalunya* (ICGC). The LiDAR flight parameters and data specifications are shown in Table 1. The minimum pulse density per strip (nominal point density) was 0.5 points/m^2 and the vertical accuracy of the LiDAR system ~~was~~ had a root mean square error (RMSE) < 15 cm ~~root mean square error (RMSE)~~. The resulting point densities for the ~~obtained~~ 2009, 2011 and 2016 data sets ~~surveys~~ were 0.96, 2.14 and 2.77 points/m^2, respectively. The accuracy of the data was calculated by comparing LiDAR and ground GPS elevations, and was estimated ~~for the three data sets~~ to be~~,~~ (expressed as RMSE)~~,~~ < 5 cm ~~in~~ for flat ~~and~~ non-vegetated areas, < 15 cm ~~in~~ for slightly steep and forested areas, and < 50 cm ~~in~~ for steep ~~and~~ densely forested areas.

Table 1. LiDAR flight parameters and point cloud data specifications ~~of~~ from the 2009, 2011 and 2016 surveys (data from ICGC).

	2009	2011	2016
Average flight altitude	2250 m	2440 m	2712 m
Scan angle	48°	40°	31.3 °
Scan frequency	21.5 Hz	25 Hz	24.4 Hz
Pulse rate	89200 Hz	84400 Hz	77100 Hz
Nominal point density	0.5 pt/m^2	0.5 pt/m^2	0.5 pt/m^2
Total point density (for entire datasets)	0.96 pt/m^2	2.14 pt/m^2	2.77 pt/m^2
Ground point density (for analysis area)	0.29 pt/m^2	0.93 pt/m^2	1.32 pt/m^2

A data quality assurance and control process (QA/QC) was performed for each ~~year~~data set. First, ~~the~~ point clouds were~~as~~ distributed in blocks measuring 2 km x 2 km ~~blocks in order~~ to check data completeness and point density. Second, points were georeferenced (x, y and z coordinates) and projected in UTM (Zone 31N) in the

ERTS89 reference system from the aircraft trajectory calculation, using GPS data of the flight and GNSS data from control points of the CatNet network. Elevations were georeferenced to the EGM08D595 geoid~~e~~ and ~~were~~ accurately adjusted, taking into account overlapping zones of different flight strips, but also comparing the LiDAR point cloud with the altitudes of the points located in flat control areas that have been previously measured in the field with GPS. This adjustment reduces ~~the~~ systematic elevation errors. Third, LiDAR topographic points were ~~filtered and~~ classified as ground, vegetation or noise, using automatic filtering ~~routines~~ based on the algorithms of the TerraScan software (Terrasolid, 2016). Moreover, ~~a~~ manual point editing was ~~done~~ performed by experts for an exhaustive verification of real terrain points, paying special attention to barriers, road-torrent intersections, valley bottoms and lateral landslide margins. Finally, a pre-analysis of the resulting data sets (e.g., 3D visualization and segmentation of the files) was performed using the CloudCompare (Girardeau-Montaut, 2015) and ArcGIS (ESRI, 2014) software. This ~~allowed~~ verifi~~y~~ed~~ing~~ that the obtained point clouds provided ~~a~~ good coverage of the study area and an *a priori* adequate average point density for data comparability and DEM generation.

High-resolution bare-earth DEMs were obtained for 2009, 2011 and 2016 by filtering vegetation and noise points. First, ~~For each year, ground points~~ point clouds were compiled into ~~a~~three LAS data sets. For each year, ground points were triangulated and interpolated using the linear interpolation algorithm in ArcGIS (ESRI, 2014), ~~and then~~before being rasterized into a 1-~~-~~m regular grid ~~of~~ with a determined extent ~~using triangulation and subsequent linear interpolation~~ (Wheaton et al., 2010). The ~~grid resolution or cell size was determined according to the average point spacing and density, and the~~ linear interpolation algorithm was used because it provided the most reliable steep terrain surface for the study area. The grid resolution or cell size was determined according to the averaged point spacing and density of the three data sets, as the same resolution is needed for adequate DEM comparison and subtraction (see Section 5.1).

Considering the objectives of the study, a polygon was manually delineated as an analysis area, coinciding with the part of the valley bottom where fluvio-torrential processes act to change~~ing~~ the morphology of the channel, that is, the riverbed. Their limits correspond to the lateral slope change~~,~~ and therefore, only includes the smooth riverbed (< 30º), excluding lateral banks. The three DEMs were clipped using this polygon to obtain isolated DEMs of the ~~specific~~ analysis area.

3.3. Uncertainty analysis and geomorphic change detection

Several sources of error ~~sources~~ (e.g., device errors, meteorological conditions, vegetation cover, point density, data filtering processes~~,~~ and interpolation techniques) affect data ~~and DEM~~ quality and DEM accuracy (Scheidl et al., 2008). Data and DEM comparability ~~needs to be assessed by quantifying uncertainties, which~~ is ~~a key point~~important for ~~an adequate~~accurate geomorphic interpretation.

The approach adopted for this study is summarized in Figure 2~~In the Portainé catchment, a~~A previous visual analysis of point clouds was performed ~~in order to assess~~to evaluate whether their distribution and density ~~of the three point clouds~~ were good enough to perform a conventional DoD analysis. Given the limitations related to ~~densely vegetated steep areas that~~ dense vegetation, such as areas that lack ~~of~~ points, we ~~propose~~ performed a cross-sectional method for a spatially variable uncertainty analysis in mountain torrents that better localizes and implements error thresholds ~~error sources in order to threshold and quantify~~ so that the actual geomorphic change is quantified only when it can be reliably assessed. ~~The approach adopted for this study is summarized in Figure 2 and, for the error analysis, it has This approach had~~ The error analysis had three main steps: individual DEM error quantification; error propagation for multi-temporal data comparison; and probabilistic thresholding of uncertainty at a user-defined confidence interval.

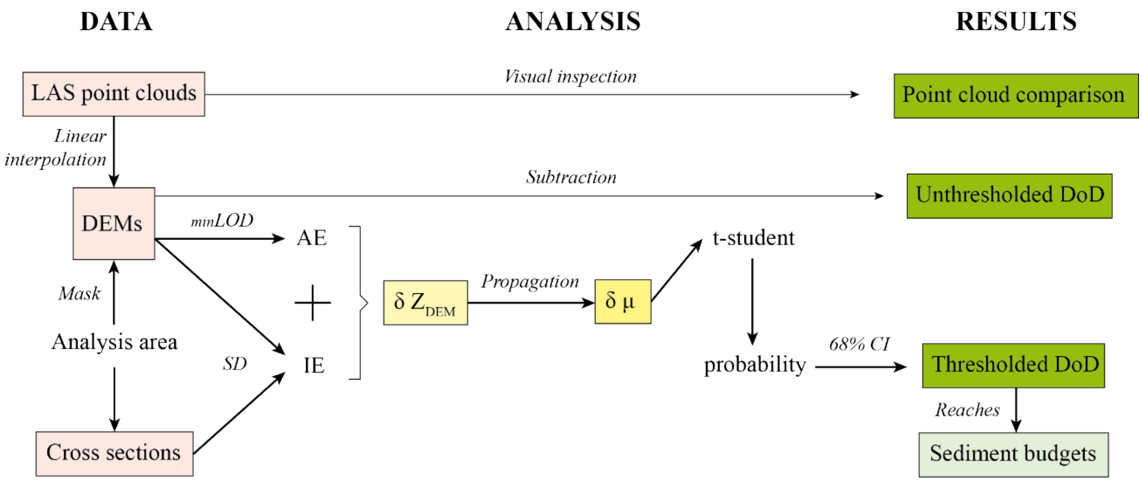

Figure 2. Flowchart showing the methodological approach ~~applied~~ used in this study for multi-temporal airborne LiDAR data analysis.

Individual DEM error quantification

DEM uncertainty (δZ_{DEM}) is defined as the difference in elevation between ~~the true elevation of a~~ real terrain points and ~~its~~ their spatially-paired DEM cells (Wheaton et al., 2010). The quantification of δZ_{DEM} requires ~~a~~ good knowledge of the specific data set and its error sources. ~~Regarding m~~Mountain catchments~~, they~~ are commonly forested and show steep gradients that ~~provoke~~ lead to variabilities in precision, accuracy and point densities~~ at each data set~~. A specific DEM uncertainty analysis ~~considering~~ that considers these ~~different errors~~ uncertainties and their spatial variability is required in such contexts. In this study, we quantified two error sources: (i) aerotriangulation error (AE) and (ii) interpolation error (IE).

The ~~aerotriangulation error (~~AE~~)~~ is the spatial deviation between topographic surveys, namely the errors in the X, Y and Z directions after ~~the~~ aerotriangulation adjustment (Hsieh et al., 2016). This error is the consequence of the constraints of both LiDAR measurements reproducibility and the georeferencing process. ~~which~~This produces a bias that can be detected when comparing data sets acquired at different flight times. ~~It~~ The AE shows a spatially uniform distribution throughout an entire data set and ~~wa~~is estimated by comparing multi-temporal data ~~at~~ from stable areas where no changes are expected (i.e., roads)~~, obtaining a mean single value for 2009, 2011 and 2016 DEMs~~.

First, we ~~carried out~~undertook a DEM-to-DEM comparison (2011-2009, 2016-2011 and 2016-2009) along the road by subtracting ~~new~~ old DEMs ~~to~~ from ~~old~~ new ones ~~in a cell-by-cell basis,~~ and calculating~~ed~~ the standard deviation of elevation differences (between data sets acquired in different flight times) ~~i~~on a cell-by-cell basis. Th~~o~~ese ~~standard~~ deviations for each pair of DEMs were a measure of precision~~, and~~ their mean indicating~~ed~~ the minimum level of detection (${}_{min}$LoD) for each DEM comparison~~s~~. The values were averaged to obtain the mean ${}_{min}$LoD, as follows:

$$ {}_{\mathrm{min}}\mathrm{LoD} = \frac{1}{n}\sum_{i=1}^{n}\sigma\Delta Z \quad (1) $$

where σΔZ ~~being~~ is the mean standard deviation of the elevation difference between new and old DEMs for each DEM-to-DEM comparison (2011-2009, 2016-2011 and 2016-2009)~~,~~ and n ~~being~~ the number of comparisons (3 in our case study).

Second, ~~considering that~~since the ${}_{min}$LoD obtained from Eq~~Q~~. 1 indicates~~d~~ the combination of the individual ~~aerotriangulation errors~~AEs of ~~each~~ two ~~of~~ data sets (propagated error), it can be expressed with the following equation:

$$ {}_{\mathrm{min}}\mathrm{LoD} = \sqrt{(AE_{new})^2 + (AE_{old})^2} \quad (2) $$

where AE_{new} and AE_{old} are the ~~aerotriangulation errors~~AEs of the newer and older DEMs, respectively. ~~in each compared pair.~~ Assuming that the bias is constant and spatially uniform for the ~~entire~~ whole data sets, both values were considered ~~as~~ equal ($AE_{new} = AE_{old} = AE$) and Eq~~Q~~. 2 was transformed into:

$$ AE = \sqrt{\frac{{}_{min}LoD^2}{2}} \quad (3) $$

where AE was calculated as a unique value for the three DEMs.

The ~~interpolation error (~~IE~~)~~ is a ~~significant~~ remarkable ~~error~~ source of error in mountain areas, where DEM surfaces are built from spatially variable point densities. Therefore, multi-temporal comparisons incorporate a different ~~interpolation error~~IE from each DEM, leading to geomorphic changes that are not real, but a result of the subtraction of unreal interpolated surfaces. ~~This error is spatially variable within each data set, so different values need to be calculated within 2009, 2011 and 2016 DEMs.~~ Concerning the studied torrents, ~~the interpolation error varies along the channel according to the *in situ*~~ point densities~~y~~ vary~~ies~~ along the channels according to ~~the~~ *in situ* characteristics~~,~~ and therefore, the IE is spatially variable within each DEM (2009, 2011 and 2016). ~~In order t~~To assess this uncertainty, a 1D analysis of cross~~-~~sectional elevation differences was performed along the channels. We created cross sections every meter and intersected them with the manually delineated polygon (analysis area), obtaining 8,125 sections (5,267 in the Portainé torrent and 2,858 in the Reguerals torrent) with 1-~~-~~m spacing and variable width (Fig. 3~~2~~). DEM cell statistics (e.g., mean elevation, standard deviation and the~~,~~ number of points) were calculated along each section for each year (2009, 2011 and 2016). Assuming a trapezoid-shaped channel with a regular riverbed (smooth and nearly flat), we considered the ~~interpolation error~~IE value at a~~n~~ specific cross section to be~~ing~~ equal to ~~the~~ its mean standard deviation of elevation ~~calculated for each instance~~, as given by the following equation:

$$IE = \sqrt{\frac{1}{n}\sum_{i=1}^{n}(Z_{cell} - Z_{mean})^2} \tag{4}$$

where IE ~~wa~~is estimated as a different value for each cross section and year,~~;~~ n ~~being~~ is the number of cells at each cross section, and Z_{cell} and Z_{mean} ~~being~~ are the elevation of each cell and the average elevation of the cells, respectively.

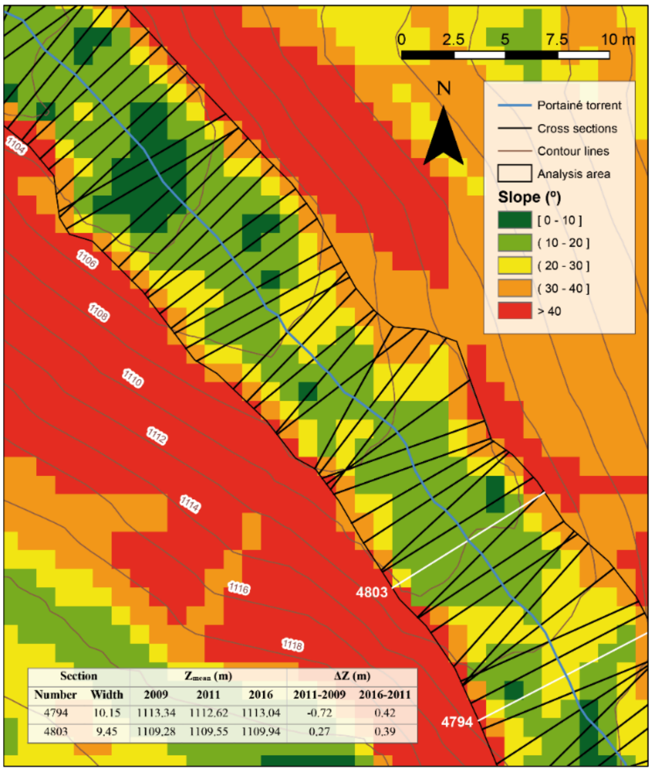

Figure ~~2~~3. Illustration of a specific stretch of the Portainé torrent ~~with~~ showing the locations of the cross sections used for the spatially variable uncertainty analysis. The analysis area corresponds to abrupt lateral ~~abrupt~~ slope changes. The table in the lower part of the figure shows the characteristics and mean elevations ~~from multi-temporal DEM at~~ of two example sections from multi-temporal DEMs (white lines).

Both errors obtained from Eq~~Q~~. 3 (~~aerotriangulation error;~~ AE) and Eq~~Q~~. 4 (~~interpolation error;~~ IE) were combined to obtain DEM uncertainty (δZ_{DEM}) at each cross section as follows:

$$\delta Z_{DEM} = \sqrt{(\mathrm{AE})^2 + (IE)^2} \qquad (5)$$

~~Propagated e~~Error propagation

The multi-temporal comparison of two DEMs ~~to detect geomorphic changes~~ needs to account for the combination ~~or propagation~~ of the elevation errors of each surface. This consists of deriving the quantity of ~~the two~~both DEM errors following the simple error propagation theory that treats inputs as independent (Taylor, 1997). As proposed by Brasington et al. (2003), the propagated error ($\delta\mu$) was determined as follows:

$$\delta\mu = \sqrt{(\delta Z_{DEMnew})^2 + (\delta Z_{DEMold})^2} \qquad (6)$$

where δZ_{DEMnew} and δZ_{DEMold} ~~being~~ are the individual errors in the more recent (DEM_{2011} for 2011-2009 and DEM_{2016} for 2016-2011) and older (DEM_{2009} for 2011-2009 and DEM_{2011} for 2016-2011) surfaces, respectively. In our case, the $\delta\mu$ values were calculated for each cross section and ~~for~~ each ~~considered~~ pair of DEMs considered. This ~~allowed~~ enabled the subsequent accurate assessment of local elevation changes.

Probabilistic thresholding

The significance of uncertainties ($\delta\mu$) in predicted elevation changes (ΔZ) can be assessed in two main ways:~~;~~ using a simple $_{min}$LoD~~,~~ or by probabilistic thresholding at a user-defined confidence interval (Wheaton et al., 2010). The aim of this step is to discard noise~~/error~~ from signals~~,~~ and ~~therefore~~thus, only consider those that we are confident about ~~as~~ being real geomorphic changes (ΔZ_{real}) ~~those that we are confident about~~, ~~by~~ excluding the changes occurring within determined error ranges. If spatial variabilities are ~~accounted~~considered, as in the present study, probabilistic thresholding is the most accurate method (Brasington et al., 2003; Lane et al., 2003). The probability of changes ~~to~~ being real ~~are~~ is calculated using ~~the~~ Student's *t*-distribution, which consists ~~in~~ of calculating the t-score (*t*) of each cross section as follows:

$$t = \frac{|\Delta Z\cancel{Z_{DEMnew}} - \cancel{Z_{DEMold}}|}{\delta_{\mu}} \qquad (7)$$

~~which~~ This equation assesses the significance of the changes, expressed as the absolute elevation difference between new and old DEMs (|ΔZ|=|$Z_{DEM\ new}$ - $Z_{DEM\ old}$|), by comparing it to the propagated error ($\delta\mu$).

T-distribution ~~allowed to obtain~~enables the determination of the probability (p) of ΔZ ~~to~~ being real ~~i~~on a section-by-section basis. ~~Considering~~ Given that we assumed ~~a flat~~the riverbed to be flat along the cross sections, but ~~elevation variations in~~ elevations vary ~~may~~ naturally ~~occur along cross sections~~, ~~the~~ probabilistic thresholding was applied at a specific confidence interval of 68% ($p < 0.32$) to obtain ΔZ_{real}.

~~Following all the mentioned approaches, s~~Sections were excluded ~~with~~ if their probability of the changes ~~to~~ being real ~~higher~~ was greater than 0.32 ~~were excluded~~. ~~and r~~Reliable volumetric elevation changes for the 2009-~~to~~2011 and 2011-~~to~~2016 periods were obtained by multiplying ΔZ_{real} (from the 2011-2009 and 2016-2011 subtractions) ~~by~~ with the width of each cross section (distance between the cross sections is 1 m). This method led to ~~an error-reduced~~the quantification of ~~multi-temporal assessment of the~~ geomorphic activity with fewer errors ~~that allowed establishing sediment budgets and geomorphic changes~~, especially in the reaches where ~~those associated to with the emplacement of the~~ sediment retention barriers are emplaced.

4. Results

4.1. Chronology of torrential events and flexible barriers

~~8~~Eight torrential events of different magnitude, ~~and differing in~~ behavio~~u~~r and sediment load occurred in the 2009-2016 LiDAR temporal window. Five of them obstructed the access road and six ~~of them~~ damaged the sediment retention barriers, which had to be repaired in some cases. Table 2 ~~compiles~~ presents the information of the torrential events recorded in the Portainé catchment and their effects on the barriers. ~~We report that t~~The most intense event occurred in July 2010 and the ~~less~~ least intense one in May 2016.

Table 2. ~~Compilation~~ List of the events, including ~~event~~ date, magnitude and effects (~~torrent, obstructed road crosses and affected barriers~~information obtained from FGC and ICGC (2015) and IGC (2013)).

Event		**Effects and damages**		
Date	**Magnitude**	**Torrent**	**Road crosses**	**Barriers**
2010/07/22	Most significant	Portainé Reguerals	2	7 filled 2 damaged
2010/08/12	Major	Portainé Reguerals	2	0 filled 5 damaged
2011/08/05	Minor	Portainé Reguerals	0	2 filled 1 damaged
2013/07/23	Major	Portainé Reguerals	3	3 filled 3 damaged
2014/08/20	Minor	?	0	-
2014/08/30	Medium	Portainé	1	5 damaged
2015/08/21	Medium	Portainé	1	5 damaged
2016/05/09	Less significant	?	0	-

The ~~fifteen~~ 15 flexible ring-net barriers with~~of~~ similar characteristics were emplaced along the middle reach of the channels ~~in order~~ to retain sediment and produce a stepped ~~the~~ profile to reduce riverbed incision (Fig. 1). These structures are 4-6 m high and 12-24 m wide, ~~and~~ their retention capacity varying~~ies~~ with the specific local slope and channel width. As shown in ~~t~~Table 3, the barriers differ ~~o~~in size and were constructed ~~in~~ at three different ~~dates~~times~~;~~: nine between the end of 2009 and the beginning of 2010 (stage 1);~~,~~ four in 2012 (stage 2) and two in 2014 (stage 3). They ~~all~~ were all filled during different torrential events, except for the ones ~~from~~ emplaced in 2014~~, still~~ that remain empty~~,~~ and another one that was artificially filled after ~~its~~ installation.

Table 3. Sediment retention barriers on the Portainé and ~~the~~ Reguerals torrents (information provided by Mr. C. Fañanás, pers. com.).

Barrier code	Date	Torrent	Elevation (m a.s.l.)	Height (m)	Width (m)	Filling event
0	2009	Caners	1090	4	13.5	2010/07/22
1	2010	Portainé	1308	4	16.8	2010/07/22
2	2009	Portainé	1355	5	13.5	2010/07/22
3	2009	Portainé	1380	5	11.5	2011/08/05
4	2010	Portainé	1405	4	13.5	2010/07/22
5	2009	Portainé	1470	5	20	2010/07/22
6	2010	Reguerals	1490	4	27	2010/07/22
7	2010	Reguerals	1510	4	26	2011/08/05
8	2009	Portainé	1710	6	19.5	2010/07/22
11	2012	Portainé	1345	5.5	16.5	2012 (anthropic)
51	2012	Portainé	1525	4.5	25	2013/07/23
52	2012	Portainé	1555	4.8	27.1	2013/07/23
53	2012	Portainé	1575	5.1	15.1	2013/07/23
A	2014	Reguerals	1615	5	19.2	-
B	2014	Reguerals	1570	6	17.5	-

4.2. Geomorphic ~~C~~changes

3D visualization of airborne LiDAR points ~~allowed~~ enabled us to observe clear geomorphic changes related to anthropic structures. Deposition and erosion were~~as~~ observed upstream and downstream ~~from~~ of the barriers, ~~and erosion downstream~~respectively (Fig. ~~4~~3). In some of the barriers ~~from~~ installed in stage 1, a change in the ~~top~~ highest position of the barrier was identified ~~from the~~when comparing 2011 and 2016 LiDAR data (Fig. ~~3~~4a), produced by ~~resulting from~~ the ring-net flexion ~~due to~~caused by the retained load. The horizontal displacement of the net ~~can~~ could be estimated ~~in those~~for the barriers ~~showing enough~~with sufficient LiDAR points for ~~an~~ accurate measurement. In our study, this ~~phenomenon~~ was ~~detectable and~~ measur~~able~~ed in ~~5~~five barriers (see the results at the end of this section), accounting for an average horizontal displacement of 0.7 m (1.1 m in the example shown in Fig. ~~3~~4a). ~~In cases where the sediment retention~~For the barrier~~s was~~ installed in stage 2, riverbed incision ~~i~~was detected ~~in the 2011-2009 LiDAR comparison~~from 2009 to 2011 (pre-barrier), indicating ~~a~~ natural erosive dynamics (Fig. ~~3~~4b).

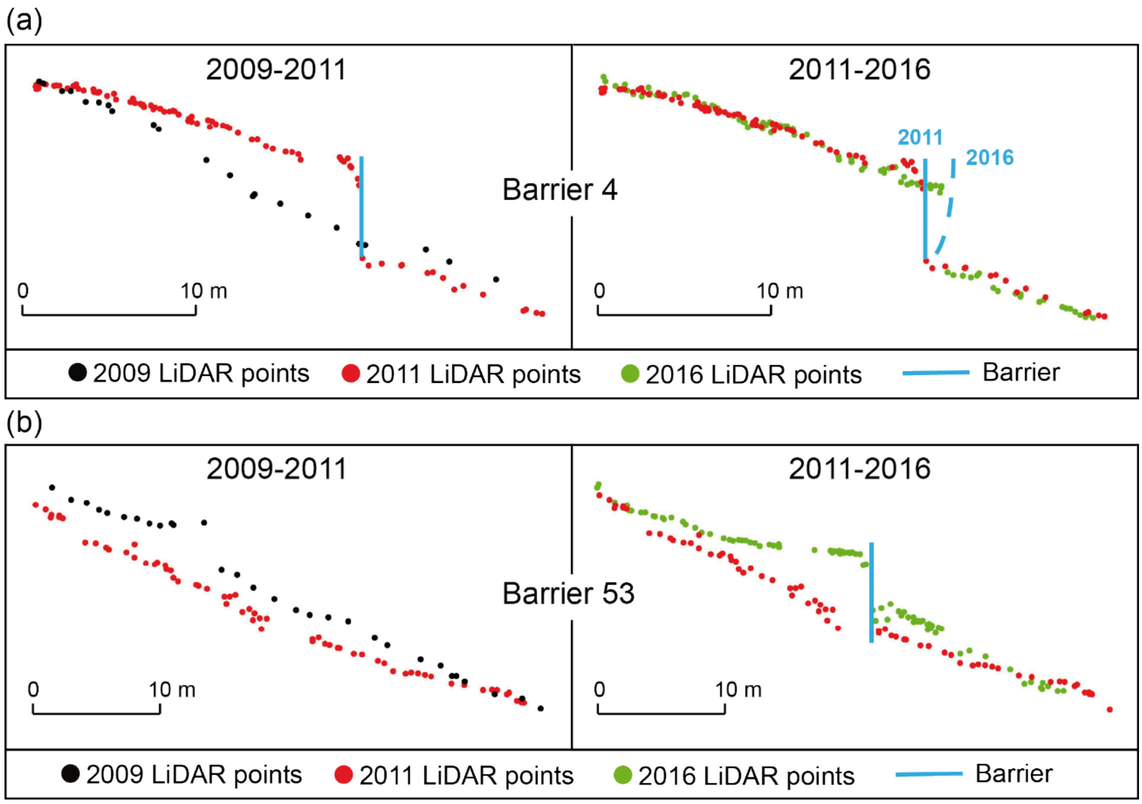

Figure ~~3~~4. Longitudinal sections of two specific stretches of the Portainé torrent showing 2009, 2011 and 2016 ground points (see Fig. 1a for the location of the barriers). (a) Barrier 4, constructed in 2010 and filled in the July 2010 event, illustrating the change ~~of~~ in the barrier position due to ~~the~~ net flexion ~~of the net~~. (b) Barrier 53, constructed in 2012 and filled in the July 2013 event.

As a preliminary approach, the spatial distribution of the geomorphic changes for raw (unthresholded) 2011-2009 (Fig. ~~5~~4a) and 2016-2011 (Fig. ~~5~~4b) comparisons ~~allows us to~~ identified~~y~~ the erosive or depositional nature of the stream stretches, the magnitude of the changes and their relationship with ~~the~~ anthropic structures. Erosion ~~i~~was the most ~~generalized~~ common phenomenon along valley bottoms. The material eroded alongside the torrents ~~i~~was mostly transported during high-discharge flows, sometimes leading to the development of debris flows (and the opposite when deposited). However, there ~~a~~were also other areas where erosion ~~i~~was locally enhanced, such as downstream ~~from~~ of the barriers or road intersections. Depositional geomorphic processes occurred at places where the slope decreased~~s~~ or ~~as a consequence of~~were ~~affected by~~ anthropic structures located. The ~~M~~main areas of accumulation ~~areas~~ ~~a~~were the debris cone formed in the most downstream reach (corresponding to the Caners torrent) and areas upstream ~~from~~ of the sediment retention barriers and road intersections.

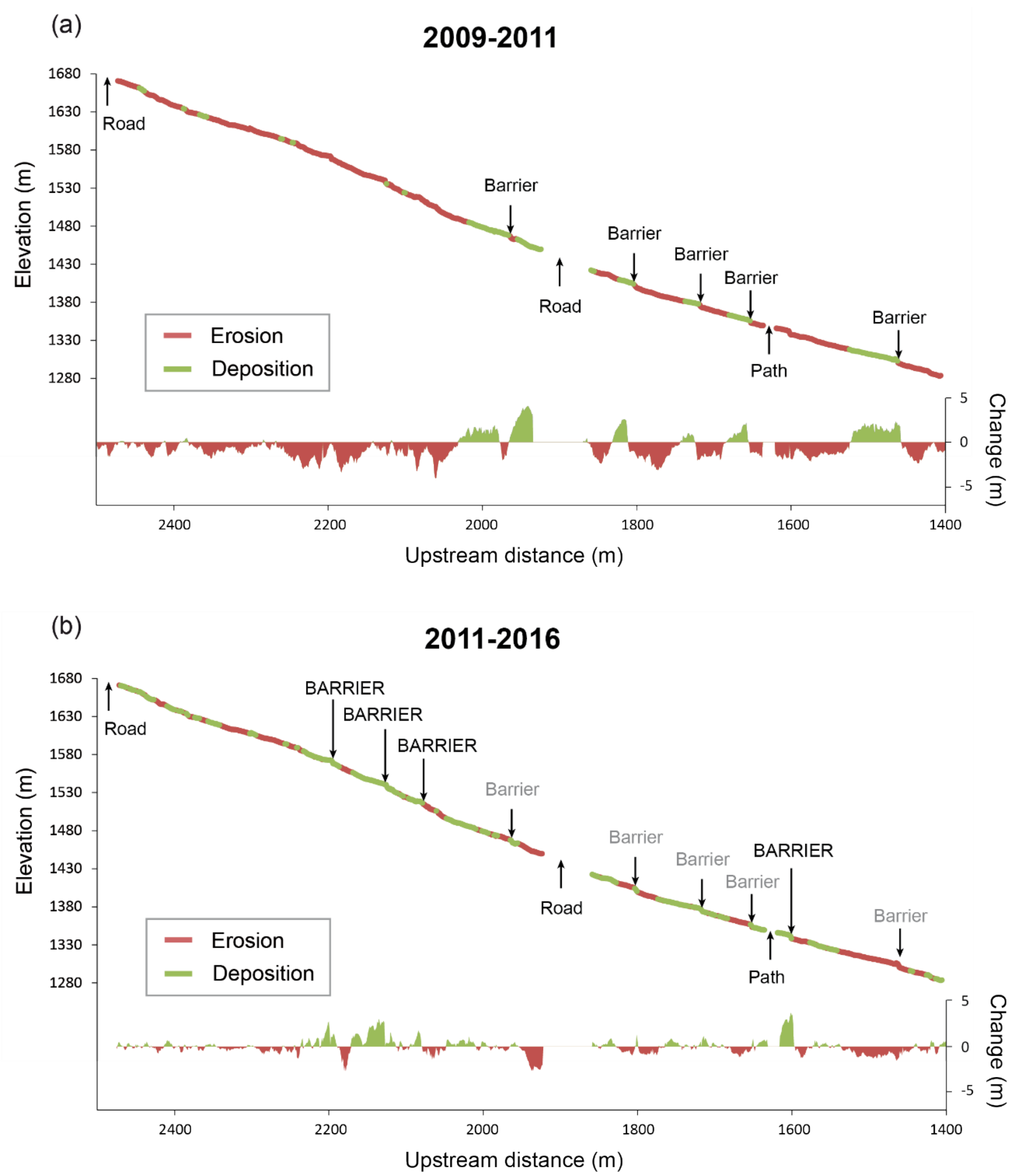

Figure 45. Geomorphic net change in storage terms (unthresholded) along the longitudinal profile of the Portainé torrent, from the road intersection at 1,700 m a.s.l. to the confluence with the Reguerals torrent. The bottom of the profile illustrates the magnitude of the changes. The location of the anthropic structures is indicated by ~~writing~~ the newly ~~emplaced~~ (~~filled~~ between 2011 and 2016) and previously (~~filled~~ between 2009 and 2011) emplaced barriers shown in upper ~~or~~ and lower cases, respectively. (a) Changes between 2009 and 2011. (b) Changes between 2011 and 2016.

Geomorphic changes were ~~then~~ thresholded by ~~means of~~ the spatially variable uncertainty analysis. Table 4 shows the uncertainty analysis and the volumetric geomorphic changes considered real that were obtained for two example cross sections A $_{min}$LoD of 0.1 m was calculated, leading to an AE of 0.07 m ~~aerotriangulation error~~ for the entire data sets. The ~~interpolation error~~IE, calculated from the standard deviation of the mean elevations of each cross section, reached 0.5 m in some areas. $\delta\mu$ values showed~~ a~~ large spatial variability, ranging ~~between~~from 0.1~~ m~~ ~~and~~to 5.4 m;~~,~~ ~~but~~however, the median ~~is~~was 0.9 m and 0.66 m for 2011-2009 and 2016-2011, respectively (see examples in Table 4). ~~The error combination (δZ_{DEM}) and subsequent propagation ($\delta\mu$) allowed thewere used to calculateion of the p~~Probabilities of geomorphic changes ~~to ~~being real (p) were~~. Many of them showed p~~ < 0.32 in many sections (68% confidence interval) and were considered real changes (ΔZ_{real}), whereas geomorphic changes ~~showing ~~with p > 0.32 were discarded.~~ Table 4 shows the uncertainty analysis and the real-considered volumetric geomorphic changes considered real that were obtained for two example cross sections, as an example~~. This thresholding analysis considerably reduced the number of cross sections ~~to be~~that were considered and influenced the final results on geomorphic changes~~ results~~. ~~The thresholding was performed in each section~~ Indeed, ~~for 2011-2009 and 2016-2011, and~~ 57% and 74% of the data were discarded ~~respectively~~ for 2011-2009 and 2016-2011 sediment budget calculations, respectively. ~~However,~~ Nonetheless, those~~e~~ sections ~~recording~~ with changes assumed to be real showed ~~a~~ high reliability~~, so the~~ and were therefore used for geomorphic quantification~~ was based on them~~.~~ Definitely,~~ ~~t~~The uncertainty analysis resulted in a smaller ~~quantity~~ amount of, but more reliable data (see Section 5.1). ~~Indeed, m~~Most active zones, such as the areas surrounding the flexible barriers, were ~~never~~ not discarded due to their high magnitude, proving the effectiveness of the methodology ~~at~~ in these areas.

Table 4. Results of the spatially variable uncertainty analysis for two example sections (see their location in Fig.~~ure~~ 32).~~ The three methodological steps are colored in red, yellow and green, showing the main variables calculated.~~ The ~~v~~Volumes of the geomorphic change were only ~~obtained~~ calculated for thresholded real elevation changes~~, whereas discarded ones are excluded in volumetric calculations~~.

Section		DEM error			Propagated error		Probabilistic thresholding						Volume (m³)	
Nº	Width (m)	δZ_{DEM} (m)			$\delta\mu$ (m)		t		p		Real ΔZ (m)			
		2009	2011	2016	11-09	16-11	11-09	16-11	11-09	16-11	11-09	16-11	11-09	16-11
4794	10.15	0.78	1.04	0.48	1.3	1.14	0.55	0.36	0.29	0.36	-0.72	-	-7.32	-
4803	9.45	0.58	0.29	0.24	0.65	0.38	0.41	1.03	0.34	0.15	-	0.39	-	3.67

For the whole analysis area, the mean magnitude of change, obtained from ~~cross section~~ average~~d~~ vertical changes in the cross sections, ~~i~~was about 1 m (0.90 m for erosion and 1.02 m for deposition), ~~but the number of~~with more erosive sections ~~surpasses the~~occurring than depositional ones. ~~-~~Sediment budgets were calculated for each period of time between the LiDAR flights. The 2011-2009 comparison indicated a total volume of erosion and deposition of 22,042 m³ and 19,204 m³, respectively, indicating a net degradation~~al~~ ~~sediment budget~~ of -2,838 m³ in two years. ~~The~~ ~~q~~Quantification of the 2016-2011 changes also gave a negative sediment budget, but the magnitude was much lower. Indeed, 8,308 m³ of eroded material and 8,161 m³ of deposition ~~led to~~yielded a total volumetric net change of -147 m³ in five years. Th~~e~~ose results ~~represent~~ suggest a~~n~~ tendency for entrenchment ~~tendency~~ (erosion > deposition) ~~of~~ in the studied mountain torrents, with ~~a~~ significant sediment output from the catchment towards the Romadriu River. However, the period between 2009 and 2011 was much more active than that after 2011, as higher volumes were mobilized (both eroded and deposited).

Budget segregation is a very useful ~~process to~~way of characterizing~~e~~ the spatial distribution and magnitude of ~~the~~ geomorphic processes, ~~and~~ therefore~~,~~ leading to a better understanding of the fluvio-torrential dynamics ~~of~~ in the study area. We recalculated the 2011-2009 and 2016-2011 sediment budgets by dividing the channels into reaches according to different morphological (torrents), geomorphological (catchment sectors) or anthropic (~~e.g.,~~ reaches between road intersections) factors. The ~~R~~results are shown in Table 5. The Portainé torrent ~~i~~was more active than the Reguerals torrent, ~~as the~~with ~~magnitude and extension of~~ geomorphic changes of greater magnitude and extension ~~are larger~~, especially for erosion. This explains the narrower and more entrenched morphology of the Portainé torrent, which was also clearly identified in the field. The catchment can be divided into three different sectors with different slopes: the upper reach (location of the Port-Ainé ski station);~~,~~ the middle reach (~~development of~~contains entrenched channels and the ~~emplacement of~~ barriers) and the lower reach (~~existence of~~contains a debris cone in the most downstream part). The upper-middle and middle-lower ~~limits~~ boundaries geographically correspond to the division of the N-S sectors and ~~to~~ the road that crosses the stream at the Montenartró ~~b~~Bridge, respectively (Fig. 1a). From 2009 to 2011, ~~the~~ erosion mostly occurred in the middle reach, ~~and~~with the material deposited in the lower reach. ~~Nonetheless~~However, the 2011-~~ to~~ 2016 period recorded significant accumulations in the middle reach, ~~whereas~~ with erosion dominating~~ed~~ in the lower part. This can be partly explained by the erosive nature of torrential events.~~;~~ ~~w~~While high-~~-~~magnitude events (including debris flows) occurred between 2009 and 2011, producing significant erosion along the channels, the number of events recorded from 2011 to 2016 was~~ere~~ much lower, leading to proportionately more deposition. The ~~R~~reaches between the road intersections showed a more complex erosion-deposition pattern with temporally ~~varying~~ variable tendencies, which ~~is the~~ resulted ~~o~~from the ~~high~~ large influence of the ~~number of existing~~ barriers occurring in such short stretches.

Table 5. Segregation of the sediment budgets obtained from the 2011-2009 and 2016-2011 DEM ~~subtraction~~comparisons. For each reach, we calculated the net volumetric change and indicated ~~the~~ its erosional/degradational ~~(orange background)~~ or depositional/aggradational ~~(green background)~~ tendency.

Criteria	Reach description	Time period	Erosion (m^3)	Deposition (m^3)	Change (m^3)	Dynamics
Torrent (abbr.)	Portainé (Po)	2011-2009	-11,629	6,936	**-4,693**	Degradation
		2016-2011	-4,477	3,497	**-980**	Degradation
	Reguerals (Re)	2011-2009	-4,708	2,167	**-2,541**	Degradation
		2016-2011	-1,618	2,156	**538**	Aggradation
	Caners (Ca)	2011-2009	-5,705	10,101	**4,396**	Aggradation
		2016-2011	-2,213	2,508	**295**	Aggradation
Catchment sector	Upper (low)	2011-2009	-2,441	822	**-1,619**	Degradation
		2016-2011	-1,139	568	**-572**	Degradation

(gradient)	Middle (high)	2011-2009	-19,128	13,023	**-6,105**	Degradation
		2016-2011	-6,112	7,473	**1,362**	Aggradation
	Lower (medium)	2011-2009	-473	5359	**4,886**	Aggradation
		2016-2011	-1,057	120	**-937**	Degradation
Road intersection (max-min altitude)	Po (2360-1965 m)	2011-2009	-1,764	775	**-989**	Degradation
		2016-2011	-1,096	541	**-554**	Degradation
	Po (1965-1700 m)	2011-2009	-1,684	2,015	**331**	Aggradation
		2016-2011	-642	438	**-204**	Degradation
	Po (1700-1450 m)	2011-2009	-4191	2,039	**-2,152**	Degradation
		2016-2011	-1,419	1,731	**312**	Aggradation
	Re (2225-1665 m)	2011-2009	-399	222	**-178**	Degradation
		2016-2011	-180	145	**-34**	Degradation
	Re (1665-1465 m)	2011-2009	-1506	1,450	**-55**	Degradation
		2016-2011	-767	1,107	**339**	Aggradation
	Ca (1465-1035 m)	2011-2009	-12,025	7,344	**-4,681**	Degradation
		2016-2011	-3,147	4,078	**931**	Aggradation
	Ca (1035-950 m)	2011-2009	-473	5,359	**4886**	Aggradation
		2016-2011	-1,057	120	**-937**	Degradation
NET SEDIMENT BUDGET		2011-2009	-22,042	19,204	**-2,838**	Degradation
		2016-2011	-8,308	8,161	**-147**	Degradation

The most significant deposition occurred at the ~~S~~sediment retention barriers, ~~are the most significant deposition areas and~~which played an underlying role in the geomorphic changes recorded along the torrents by modifying their natural evolution. Accumulation upstream ~~from~~ of these structures was quantified ~~from~~ by probabilistic thresholding. The real retained material per barrier range~~d~~s from 146 m^3 to ~~up to~~ 1,311 m^3 and the total retention of the ~~fifteen~~ 15 barriers ~~i~~was 8,278 m^3. Table 6 ~~includes~~ presents the ~~specific~~ volumes accumulated at each barrier and the horizontal displacement of the net where it could be measured. The geomorphic changes of the barriers are discussed in section 5.3.

Table 6. Relationship between dimensions, the calculated volume of filled barriers and the magnitude of the net flexion. The b~~B~~arriers are listed in their order along the ~~in a~~ downstream direction~~ and those retaining a volume of material >1,000 m^3 are marked with a grey background~~.

Barrier code	Height (m)	Width (m)	Torrent	Elevation (m a.s.l.)	Volume (m^3)	Horizontal net displacement (m)
8	6	19.5	Portainé	1710	1302	0.3
53	5.1	15.1	Portainé	1575	303	-
52	4.8	27.1	Portainé	1555	1044	-
51	4.5	25	Portainé	1525	146	-
7	4	26	Reguerals	1510	441	0.5
6	4	27	Reguerals	1490	534	0.4
5	5	20	Portainé	1470	559	?
4	4	13.5	Portainé	1405	589	1.1

3	5	11.5	Portainé	1380	?	1.2
2	5	13.5	Portainé	1355	282	?
11	5.5	16.5	Portainé	1345	535	-
1	4	16.8	Portainé	1308	1230	?
0	4	13.5	Caners	1090	1311	?

Another main deposition area in the 2011-2009 comparison ~~i~~was the debris cone, where 4,904 m^3 of material ~~was~~ accumulated. From 2011 to 2016, erosion prevailed in the cone, leading to a net degradation of -896 m^3 ~~degradational sediment budget~~.

5. Discussion

5.1. Strengths and limitations of airborne LiDAR data in mountain areas

The analysis ~~and comparison~~ of airborne LiDAR data ~~shows underlying applications~~can be applied ~~in~~to the study of hydrogeomorphologically active mountains ~~contexts~~. One of the main advantages is the detection of temporal morphological changes that are ~~u~~indistinguishable in aerial photographs, due to its huge potential for precisely and accurately assessing landscape changes~~, as~~ by easily identifying erosion and deposition zones ~~can be easily identified~~. Moreover, airborne LiDAR ~~allows obtaining~~enables the procurement of extensive data sets that cover~~ing~~ large sectors of the terrain in a short time, which ~~is~~ cannot be achieved with ground-based high-resolution topographic techniques such as terrestrial laser scanning or theodolite measurements. The acquisition of LiDAR data is also useful in remote areas where it is difficult to conduct field surveys ~~can hardly be carried out~~, such as heavily entrenched stretches of steep mountain rivers.

~~Airborne LiDAR~~These kind of data also has ~~also~~ some limitations that need to be considered when assessing the reliability of the data, mainly concerning its accuracy and resolution (Slatton et al., 2007). A 15-~~-~~cm measurement error in point altitude (vertical accuracy) is typically reported by LiDAR manufacturers. The altimetric error is higher in mountain areas ~~characterized by~~with dense vegetation and steep variable gradients. For instance, a vertical accuracy~~ies~~ of ~~<30 cm (Tseng et al., 2013) and~~ 0.25 cm ~~(Biron et al., 2013)~~ has~~ve~~ been ~~quoted~~ reported for ~~flat and~~ forested areas ~~respectively~~(Biron et al., 2013). For the data used in this study, an RMSE < 15 cm ~~RMSE~~ ~~i~~was ~~reported~~obtained, which ~~can~~ decreased to 5 cm in flat areas~~,~~ and was ~~is~~ < 50 cm in steep forested areas. These errors are within the accepted range of values. Point density is another vital factor for evaluating LiDAR data (Rupnik et al., 2015) and can be problematic in mountain areas, as dense vegetation hinders the laser beam from reaching the terrain, giving raise to lower ~~ground point densities and lower~~ess-resolution DEMs. Cavalli and Marchi (2008) ~~work with~~reported a ground data density of 2.5 points/m^2 that decreased~~s~~ to 0.25 points/m^2 under a dense forest canopy. ~~This study~~We took~~akes~~ into account this ~~handicap~~ limitation by ~~carrying out a specific~~ manually filtering ~~of~~ the 2009, 2011 and 2016 point clouds, exclusively paying attention to the analysis area. This~~at editing process~~ considerably minimized the classification errors and ~~allowed obtaining~~produced a higher average ground point density for the analysis area (Table 1).

Regarding the 2009 data, the obtained mean ground point density (Table 1) was lower than the DEM resolution. Using the equation proposed by Landridge et al. (2014), $S=\sqrt{(A/n)}$, the obtained optimal grid resolution (S) for the 2009 data set was 1.86 m and up to 0.86 m for the 2016 data set. As multi-temporal DEMs need to have the same resolution in order to be subtracted, a mean value should be used for DEM generation. A 2-m grid resolution would not take advantage of a significant number of points (in the case of the 2011 and 2016 data sets). Therefore, we generated 1x1-m DEMs for the three data sets. Since some areas from the 2009 model may include highly interpolated unreal surfaces, we analyzed uncertainty in detail, based on the quantification of IEs. This revealed that cross sections with a very low resolution showed a high number of errors and were therefore excluded from morphological budget calculations.

As mountain streams with torrential activity tend to record geomorphic processes with a significant magnitude of change (or signal), ~~in these contexts typically~~ the elevation change ~~i~~was higher than the error ($\Delta Z > \delta\mu$) and thus, ~~so~~ 2D analyses of DoDs could be performed. Whil~~ereas~~ conventional DoD analys~~i~~es ~~are adequate enough~~can be reliably conducted for flat ~~and~~areas with ~~poorly~~little vegetation~~ed areas~~,~~Nevertheless, when dense vegetation covers the steep slopes, it causes~~ it can lead to large interpolation errors ~~can~~ remaining~~that are~~ unidentified for steep slopes with dense vegetation ~~in DoD analyses~~, ~~leading to~~generating errors and unreal topographic changes~~sediment budget calculations in problematic areas~~. We overcame ~~T~~this problem ~~was solved in this study~~ by ~~means of the~~performing a detailed section-by-section 1D analysis for uncertainty estimation along the channels that ~~allowed to~~ excluded data within a determined error range ($\delta\mu$) and probability (confidence interval). ~~Even its higher time and cost compared to~~Although this approach took longer and was more expensive than conventional DoD analyses, ~~The presented approach~~it demonstrate~~d~~s the ~~usefulness~~ utility of ~~the combination of~~combining ~~aerotriangulation~~ AEs and ~~interpolation errors~~IEs for reliable DoD thresholding, morphological budgeting and geomorphic interpretation along mountain steep channels. The first limitation of the designed ~~approach~~ method ~~i~~was the assumption ~~of regular~~that the cross sections are regular~~, which,~~ as they are likely to be irregular in a dynamic erosive system. We ~~overcame such~~addressed this drawback by restricting our analysis ~~area~~ to the smooth riverbed and applying a 68% confidence interval, instead of the commonly used 95% value. ~~Such a~~This confidence interval ~~also This approach also~~ discards the data identified to be insufficiently reliable for comparison ~~when by the uncertainty analysis detects that they are not reliable enough to be compared among them~~, leading to a probable underestimation of the degradational/aggradational effects. Hence, ~~we make~~the final calculations used~~ing~~ ~~less~~fewer, but more reliable data instead of ~~considering~~ a higher amount of data that ~~involves~~included more errors. More data ~~is~~ were discarded when thresholding the 2011-2009 comparison ~~than for the~~compared to the 2016-2011 one (see section 4.2), ~~which is due to~~as the uncertainty ~~elevation being~~ was mostly greater for the first period (most probably due to the lower resolution of the 2009 data set). Factors ~~controlling~~ affecting the percentage of sections ~~that are dismissed~~ excluded from analysis ~~are~~ were mainly point density and the magnitude of the signal. High~~-~~-magnitude geomorphic changes ~~are~~ were never discarded, ~~certainly detecting the most significant geomorphic effects,~~ such as those ~~related to~~associated with the barriers.

5.2. Interpretation of geomorphic changes and catchment dynamics

The ~~G~~geomorphic changes detected, quantified and segregated from multi-temporal LiDAR data provided valuable information ~~for the study of the~~about recent torrential processes ~~of~~ in the Portainé catchment. The main limitation of morphological budgeting in fluvial environments is the compensation of long-term scouring (erosion) and filling (deposition) ~~thorough~~ by extraordinary events. In our study~~ case~~, the mobilized sediment volume was higher in the two-year period from 2009 to 2011 than in the ~~subsequent 5~~five~~-~~ years period from 2011 ~~until~~to 2016 (Table 5). Therefore, the analyz~~s~~ed torrents were considerably more active between 2009 and 2011 as ~~recorded~~ they produced larger geomorphic changes, ~~and~~ with the effects of the fluvio-torrential activity still continuing, but decreasing~~ed~~ later on~~, even if still continued~~. The dynamics observed for the two time periods ~~of time~~ can be explained ~~both~~ by both: (a) the different magnitudes of the torrential events~~,~~ and consequently variations in the eroded and deposited volumes of material, and (b) the ~~consequences~~ effects of the sediment retention barriers changing the flow dynamics, resulting in mainly upstream deposition and downstream and lateral erosion~~, changing the flow dynamics~~. ~~If we consider~~During the LiDAR temporal window, eight high~~-~~-discharge flows ~~are reflected~~occurred (Table 2) and ~~also the emplacement and effects of~~ all the barriers were emplaced (Table 3). Regarding the 2011-2009 ~~subtraction~~comparison, three events occurred (two in 2010 and one in 2011)~~,~~ that filled~~ing~~ nine barriers. The 2016-2011 comparison shows the effects of five events (one in 2013, two in 2014, one in 2015 and one in 2016) and four more sediment retention barriers.

~~Despite~~ Although small rainstorms may move some sediment along the channels, its volume is negligible.~~,~~ ~~and t~~The recorded geomorphic changes ~~are~~ mainly ~~the~~ result ~~of~~from extraordinary torrential events, especially high~~-~~-magnitude debris flows and floods. This is evidenced from the grain size observations ~~o~~in the field, ~~with~~where boulders~~ a~~ predominate~~nce of boulders~~. When quantifying the geomorphic processes associated with extraordinary events, erosion is typically underestimated when the areas eroded during the peak discharge are covered ~~by~~ with deposited material (Fuller et al., 2003).~~,~~ ~~so~~Thus, some erosion is undetectable in multi-temporal DEM comparisons. The torrential flows that occurred from 2009 to 2016 showed very different magnitudes and sediment loads, from well-developed debris flows (e.g., July 2010; Luis-Fonseca et al., 2011) to debris floods (e.g., May 2016; eyewitness~~e~~ accounts). The 2011-2009 geomorphic changes included those affected by the largest event, ~~but also~~as well as another major and minor one. The 2016-2011 comparison ~~record~~ included the effects of one major, three minor and the ~~less significant~~smallest event. The ~~higher magnitude~~ events with a higher magnitude are reflected in the clearly degradational 2011-2009 net budget and ~~in~~ the aggradation of the cone, which ~~can be related to~~are associated with the two major events ~~occurred in~~of 2010. From 2011 to 2016, geomorphic processes in this area ~~a~~were mainly erosive due to the lack of high-magnitude torrential flows, ~~as well as to~~ the retention of material behind the nets and the effect of the "hungry waters" ahead. The ~~effect of the~~ barriers, stepped~~ing the~~ slope and decreasing flow velocity~~,~~ ~~may~~ might have also ~~have~~ reduced the potential effects of the events along the channels, especially for minor floods.

The dynamics of the torrents ~~a~~were mainly degradational, ~~fitting~~ consistent with the ~~apparent~~ erosive tendency of the increasingly entrenched channels. Most of the natural (not human-altered) reaches ~~a~~were erosional, whereas deposition ~~concentrates on~~occurred in specific areas, mainly ~~in~~ at the sediment retention barriers and the debris cone (Fig. 5~~4~~). Indeed, 33% and 25% of the total volumes of deposition from 2011-2009 and 2016-2011, respectively, corresponded to the material retained upstream ~~from~~ of the barriers, whereas the debris cone accounted~~s~~ for ~~the~~ 26% of the deposited volume between 2009 and 2011. Moreover, total erosion volumes ~~may~~ might have been underestimated because of the exclusion of erosive cross sections where the geomorphic change was lower than the error ($\Delta Z < \delta\mu$). Indeed, 53% and 51% of the discarded sections were erosional for the 2011-2009 and 2016-2011 ~~periods~~comparisons, respectively. All these results suggest a generalized incision tendency of the torrents, with local accumulations. As summer convective storms still occur and produce torrential events, such dynamics ~~is~~ are expected to ~~remain on time~~continue.

5.3. *Assessment of the flexible sediment retention barriers*

Flexible barriers are the preferred choice for hydrological correction in mountain areas. Their main advantages over conventional check dams are their lower economic cost and environmental impact, especially as their installation is quite quick and easy, using a helicopter (Mr. C. Fañanás, pers. com.). Furthermore, they only retain high-magnitude debris flows, letting low-magnitude flows go through below the net. However, ~~The~~ sediment retention barriers ~~have a direct impact that highly influence~~strongly affect channel evolution. ~~Once filled,~~ ~~t~~They modify the longitudinal profile of the torrents when they are filled, as the slope changes both upstream and downstream ~~from~~ of the net (Fig. 4~~3~~). ~~Definitively~~Thus, the barriers alter the flow and produce a complex erosion-deposition dynamic~~s~~ that can be assessed in detail, as shown in this study.

Flexible barriers are filled during extraordinary events, leading to significant deposition volumes. They~~ir~~ ~~design characteristics report~~have been reported to present an individual retention capacity of 1,400-2,000 m^3 ~~for the study case~~ (Fañanas-Aguilera et al., 2009). However, we quantified considerably smaller deposition volumes behind the barriers (146-1,311 m^3), suggesting that the real retained volume may be lower than expected. Indeed, the retained volume ~~may depend on~~might be affected by the local morphology of the torrent (gradient and width) and the ~~particular~~ size of the barrier (height and width). Given the dynamic nature of the barriers, acting loads are presumed to deform the ring-net when material is retained. The flexion of the barriers was detected and measured in some barriers, giving valuable information on their behavio~~u~~r.

Table 6 ~~compiles~~ provides the dimensions of the barriers, the estimated retained volumes and the magnitude of net flexion.

Once filled, the~~y~~ barriers induce erosive effects downstream because the ~~water~~ flow falls as a waterfall, progressively eroding the riverbed. In some adjacent slopes, localized incision has occurred due to the lateral deviation of the flow when passing over the deposit (Fig. 6~~5~~a). Such lateral incisions ~~may produce the~~might partially or completely empty~~ing of~~ the barriers. ~~but also~~However, when erosion exposes the anchors, ~~endangers~~ the ~~stability of~~ barriers become less stable and ~~so that~~thus, require repair~~ing~~ and further maintenance ~~is required~~ (Fig. 6~~5~~b). We identified and quantified erosion downstream ~~of some barriers~~ and obtained eroded volumes of 46-703 m^3. These data are of paramount interest for prioritizing the management and maintenance of the barriers.

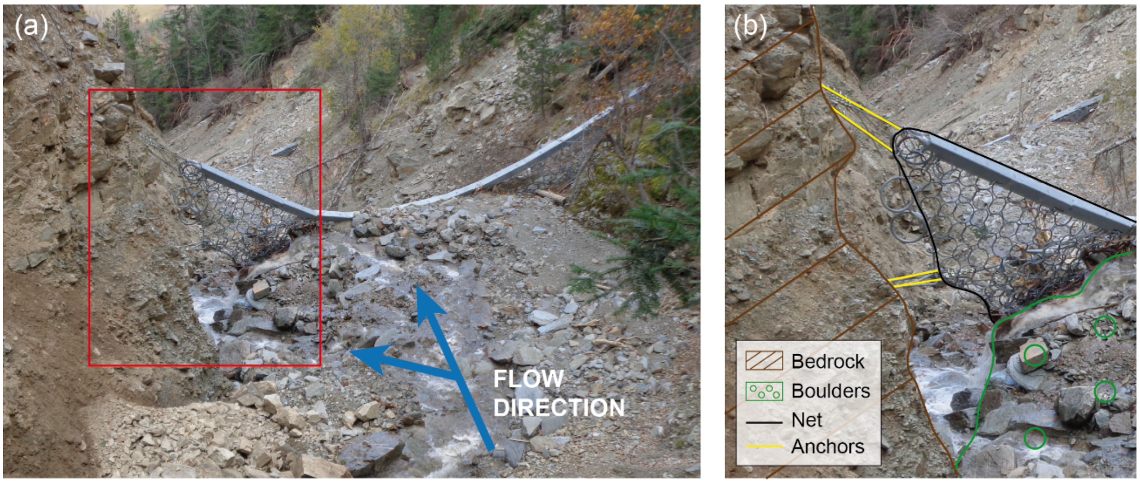

Figure ~~5~~6. Lateral erosion and anchor exposure at barrier 53 (November 2015). (a) Photograph of the barrier and the accumulated material ~~in~~ downstream ~~direction~~. (b) Zoomed ~~picture~~ photograph and drawing of the main features, showing the lateral "hole" with the anchor~~s~~ exposed~~, implying a potential hazard for~~ that might reduce the stability of the barrier.

6. Conclusions

This ~~paper~~ study presents a~~n~~ high-resolution assessment of the geomorphic impact of flexible barriers in torrential channels, including upstream filling and ~~self-induced~~ downstream and lateral erosion that can make barriers unstable, ~~by means of~~using a new LiDAR-based geomorphic approach for improved sediment budgets.

The method ~~considers~~ takes into account spatial variabilities ~~of~~ in data and errors along the channels ~~through~~ by applying a cross-sectional elevation analysis ~~in order~~ to better discretize geomorphic changes. We ~~point out~~propose this approach ~~as an alternative in~~ for studying torrents ~~any~~in densely vegetated ~~and~~ steep mountains ~~torrents,~~ ~~where~~ which produce significant interpolation errors for standard DoD analyses~~methods incorporate significant interpolation errors~~.

~~The interest of this study relies on its usefulness to monitorprovides a high-resolution assessment of engineering structures in remote areas.~~ The main applications for monitoring flexible sediment retention barriers include the: (i) estimation of barrier behavio~~u~~r, effects and consequences; (ii) remote revision and inspection for ~~an~~ appropriate maintenance; (iii) detection of problematic spots and highly erosive reaches; and (iv) selection of priority areas for the installation of new barriers.

~~Last but not least, the used data was not acquired for hydrogeomorphic nor engineering purposes, its usefulness and application has been proved though.~~ The LiDAR data analyzed in this study was useful for hydrogeomorphic research, even if it was not originally acquired for that purpose.~~The design of multi-temporal LiDAR campaigns~~ ~~c~~Choosing ~~best~~ optimal flight parameters for data ~~collection along channels~~ acquisition in abrupt landscapes would provide ~~results that are~~ even more accurate DEMs. Given ~~the~~ its increasing ~~acquisition and~~ availability~~, of~~ airborne LiDAR data~~,~~ ~~definitively these data~~ are emerging~~es~~ as ~~very useful~~a potential tool for monitoring areas that are hard to inspect in the field. In this sense, the presented approach ~~arises as a potential tool for high-resolution assessment~~ can be applied to assessing ~~of~~ structural corrective~~on~~ measures in mountain catchments and ~~has an underlying implication~~provide information for ~~decision-making about~~ future decisions on management strategies.

Acknowledgements

This research was funded by the CHARMA ~~project~~ (CGL2013-40828-R) and PROMONTEC (CGL2017-84720-R) projects ~~of~~ from the Spanish Ministry of Economy, Industry and Competitiveness (MINEICO) and ~~by~~ a PhD studentship ~~of~~ to the lead author (APIF, 2014-2015) ~~paid by~~from the University of Barcelona (UB). LiDAR data were~~as~~ acquired as part of the LiDARCAT project of the Cartographic and Geological Institute of Catalonia (ICGC). ~~The authors~~We wish to thank Professor Jaume Calvet for supporting this study and Mr. Carles Fañanás (DARP) for providing information about historical events and the barriers.

References

Abancó C, Hürlimann M. 2014. Estimate of the debris-flow entrainment using field and topographical data. Natural Hazards 71: 363-383. DOI: 10.1007/s11069-013-0930-5

Abellan A, Derron MH, Jaboyedoff M. 2016. “Use of 3D Point Clouds in Geohazards” Special Issue: Current Challenges and Future Trends (Editorial). Remote Sensing 8: 130. DOI: 10.3390/rs8020130

~~Anders N, Seijmonsbergen AC, Bouten W. 2013. Geomorphological Change Detection Using Object-Based Feature Extraction From Multi-Temporal LiDAR Data. IEEE Geoscience Remote Sensing Letters 10: 1587-1591. DOI: 10.1109/LGRS.2013.2262317~~

Bailly J, Kinzel PJ, Allouis T., Feurer D, Le Coarer Y. 2012. Airborne LiDAR Methods Applied to Riverine Environments. In Fluvial Remote Sensing for Science and Management, Carbonneau PE, Piégay H (eds). John Wiley & Sons, Ltd: Chichester; 141–163.

Batalla RJ, De Jong C, Ergenzinger P, Sala M. 1999. Field observations on hyperconcentrated flows in mountain torrents. Earth Surface Processes and Landforms 24: 247–253. DOI: 10.1002/(SICI)1096-9837(199903)24:3<247::AID-ESP961>3.0.CO;2-1

Biron PM, Chóne G, Buffin-Bélanger T, Demers S, Olsen T. 2013. Improvement of streams hydro-geomorphological assessment using LiDAR DEMs. Earth Surface Processes and Landforms 38: 1808–1821. DOI: 10.1002/esp.3425

Brasington J, Langham J, Rumsby B. 2003. Methodological sensitivity of morphometric estimates of coarse fluvial sediment transport. Geomorphology 53: 299-316. DOI: 10.1016/S0169-555X(02)00320-3

Brasington J, Rumsby BT, Mcvey RA. 2000. Monitoring and modeling morphological change in a braided gravel-bed river using high resolution GPS-based survey. Earth Surface Processes and Landforms 25: 973–990. DOI: 10.1002/1096-9837(200008)25:9<973::AID-ESP111>3.0.CO;2-Y

~~Breien H, de Blasio .V, Elverhøi A, Høeg K. 2008. Erosion and morphology of a debris flow caused by a glacial lake outburst flood, Western Norway. Landslides 5: 271-280. DOI: 10.1007/s10346-008-0118-3~~

~~Bremer M, Sass O. 2012. Combining airborne and terrestrial laser scanning for quantifying erosion and deposition by a debris flow event. Geomorphology 138: 49-60. DOI: 10.1016/j.geomorph.2011.08.024~~

Bull JM, Miller H, Gravley DM, Costello D, Hikuroa DCH, Dix JK. 2010. Assessing debris flows using LIDAR differencing: 18 May 2005 Matata event, New Zealand. Geomorphology 124: 75–84. DOI: 10.1016/j.geomorph.2010.08.011

Cavalli M, Goldin B, Comiti F, Brardinoni F, Marchi L. 2017. Assessment of erosion and deposition in steep mountain basins by differencing sequential digital terrain models. Geomorphology 291: 4–16. DOI: 10.1016/j.geomorph.2016.04.009

Cavalli M, Marchi L. 2008. Characterisation of the surface morphology of an alpine alluvial fan using airborne LiDAR. Natural Hazards and Earth System Sciences 8: 323-333. DOI: 10.5194/nhess-8-323-2008

~~Cavalli M, Tarolli P. 2011. Application of LiDAR technology for rivers analysis. Italian Journal of Engineering Geology and Environment, Special Issue 1: 33–44. DOI: 10.4408/IJEGE.2011-01.S-03~~

Cavalli M, Tarolli P, Marchi L, Dalla Fontana G. 2008. The effectiveness of airborne LiDAR data in the recognition of channel-bed morphology. Catena 73: 249–260. DOI: 10.1016/j.catena.2007.11.001

Chevalier GG, Medina V, Hürlimann M, Bateman A. 2013. Debris-flow susceptibility analysis using fluvio-morphological parameters and data mining: application to the Central-Eastern Pyrenees. Natural Hazards 67: 213–238. DOI: 10.1007/s11069-013-0568-3

~~Chiang SH, Chang KT, Mondini AC, Tsai BW, Chen CY. 2012. Simulation of event-based landslides and debris flows at watershed level. Geomorphology 138: 306-318. DOI: 10.1016/j.geomorph.2011.09.016~~

Croke J, Todd P, Thompson C, Watson F, Denham R, Khanal G. 2013. The use of multi temporal LiDAR to assess basin-scale erosion and deposition following the catastrophic January 2011 Lockyer flood, SE Queensland, Australia. Geomorphology 184: 111–126. DOI: 10.1016/j.geomorph.2012.11.023

~~De las Heras A. 2016. Modificación de la respuesta hidrológica en avenidas torrenciales ante los cambios de usos del suelo en una cuenca de montaña (Portainé, Pirineo leridano). Archivo Digital UPM: Madrid. Available at: http://oa.upm.es/45430/~~

ESRI. 2014. ArcGIS 10.2.2 Desktop. Environmental Systems Research Institute: Redlands

Fañanás C. 2016. Personal communication.

Fañanas-Aguilera C, Aguilar-Marín N, Raïmat-Quintana C, Luis-Fonseca R. 2009. Corrección hidrológica en el barranco de Portainé. In VII Simposio Nacional sobre Taludes y Laderas Inestables, Alonso E, Corominas J, Hürlimann M (eds). CIMNE: Barcelona; 999-1011.

Ferrero AM, Segalini A, Umili G. 2015. Experimental tests for the application of an analytical model for flexible debris flow barrier design. Engineering Geology 185: 33–42. DOI: 10.1016/j.enggeo.2014.12.002

FGC, ICGC. 2015. Seguiment geològic i geotècnic de la carretera d'accés a Port Ainé, 24 d'agost de 2015, NT-150824. Ferrocarrils de la Generalitat de Catalunya and Institut Cartogràfic i Geològic de Catalunya: Barcelona

~~FGC, ICGC. 2016. Seguiment geològic i geotècnic de la carretera d'accés a Port Ainé, 28 de setembre de 2016. Ferrocarrils de la Generalitat de Catalunya and Institut Cartogràfic i Geològic de Catalunya: Barcelona~~

Fuller IC, Large ARG, Charlton ME, Heritage GL, Milan DJ. 2003. Reach-scale sediment transfers: an evaluation of two morphological budgeting approaches. Earth Surface Processes and Landforms 28: 889–903. DOI: 10.1002/esp.1011

Furdada G, de las Heras A, Díez-Herrero A, Martins L, Fernández-Yuste JA, Victoriano A. 2017. The impact of land-use changes on palaeoflood and recent floods magnitude and frequency: Portainé (Eastern Pyrenees, Iberian Peninsula). In: 5th Past Global Changes Open Science Meeting Abstract Book. CSIC: Zaragoza; 253.

Génova M, Díez-Herrero A, Furdada G, Guinau M, Victoriano A. ~~Under review~~Accepted. Dendrogeomorphological evidence of flood frequency changes ~~due to~~and anthropic activities (the Portainé basin, Spanish Pyrenees). Tree-Ring Research.

Girardeau-Montaut D. 2015. CloudCompare 2.6.2. Available at: http://www.cloudcompare.org/

Guha-Sapir D, Hoyois P, Below R. 2016. Annual Disaster Statistical Review 2015 The numbers and trends. CRED, Université catholique de Louvain: Brussels

Hsieh YC, Chan YC, Hu JC. 2016. Digital elevation model differencing and error estimation from multiple sources: A case study from the Meiyuan Shan landslide in Taiwan. Remote Sensing 8: 199. DOI: 10.3390/rs8030199

~~IGC. 2008. Nota tècnica sobre la visita al barranc de Portainé i al barranc des Caners els dies 1 i 2 d'octubre de 2008 en motiu de la torrentada ocorreguda la matinada del dia 12 de setembre de 2008, AP-187/08. Institut Geològic de Catalunya: Barcelona~~

~~IGC. 2010a. Estudi de la torrentada de la nit del dia 11 al 12 de setembre de 2008 al barranc de Portainé (Pallars Sobirà), AP-019/10. Institut Geològic de Catalunya: Barcelona~~

~~IGC. 2010b. Nota de la visita al barranc de Portainé (Pallars Sobirà) arran del episodi de pluges dels dies 22 i 23 de juliol de 2010, AP-046/10. Institut Geològic de Catalunya: Barcelona~~

~~IGC. 2011. Nota de la visita al barranc de Portainé (Pallars Sobirà) arran de l'episodi de pluges del dia 5 d'agost de 2011, AP-054/11. Institut Geològic de Catalunya: Barcelona~~

IGC. 2013~~a~~. Avaluació de la dinàmica torrencial del torrent de Portainé, AP-035/13. Institut Geològic de Catalunya: Barcelona

~~IGC. 2013b. Nota de la visita al barranc de Portainé (Pallars Sobirà) arran de l'episodi de pluges del dia 23 de juliol de 2013, AP-091/13. Institut Geològic de Catalunya: Barcelona~~

~~Imaizumi F, Trappmann D, Matsuoka N, Tsuchiya S, Ohsaka O, Stoffel M. 2016. Biographical sketch of a giant: Deciphering recent debris-flow dynamics from the Ohya landslide body (Japanese Alps). Geomorphology 272: 102-114. DOI: 10.1016/j.geomorph.2015.11.008~~

~~Jaboyedoff M, Oppikofer T, Abellán A, Derron MH, Loye A. Metzger R, Pedrazzini A. 2012. Use of LIDAR in landslide investigations: a review. Natural Hazards 61: 5–28. DOI: 10.1007/s11069-010-9634-2~~

~~Jones AF, Brewer PA, Johnstone E, Macklin MG. 2007. High-resolution interpretative geomorphological mapping of river valley environments using airborne LiDAR data. Earth Surface Processes and Landforms 32: 1574-1592. DOI: 10.1002/esp.1505~~

Lallias-Tacon S, Liébault F, Piégay H. 2014. Step by step error assessment in braided river sediment budget using airborne LiDAR data. Geomorphology 214: 307-323. DOI: 10.1016/j.geomorph.2014.02.014

~~Lane SN, Chandler, JH, Richards, KS. 1994. Developments in monitoring and modelling small-scale river bed topography. Earth Surf. Process. Landforms 19: 349–368. doi:10.1002/esp.3290190406~~

Lane, SN, Westaway RM, Hicks DM. 2003. Estimation of erosion and deposition volumes in a large, gravel-bed, braided river using synoptic remote sensing. Earth Surface Processes and Landforms 28: 249–271. DOI: 10.1002/esp.483

~~Lorente A, Beguería S, Bathurst JC, García-Ruiz JM. 2003. Debris flow characteristics and relationships in the Central Spanish Pyrenees. Natural Hazards and Earth System Sciences 3: 683–692. DOI: 10.5194/nhess-3-683-2003~~

Luis-Fonseca R, Raïmat C, Hürlimann M, Abancó C, Moya J, Fernández J. 2011. Debris-flow protection in recurrent areas of the Pyrenees. Experience of the VX systems from output results collected in the pioneer monitoring station in Spain. In 5th International Conference on Debris-Flow Hazards "Mitigation, Mechanics, Prediction and Assessment", Genevois R, Hamilton DL, Prestininzi A (eds). Research Center CERI, Sapienza Università: Rome; 1063–1071. DOI: 10.4408/IJEGE.2011-03.B-115

Meteocat. 2008. Atles Climátic de Catalunya 1961-1990. Servei Meteorològic de Catalunya: Barcelona

Munich Re. 2016. Annual statistics: natural disasters 2015. Munich Re Group, NatCatSERVICE: Munich

Notebaert B, Verstraeten G, Govers G, Poesen J. 2009. Qualitative and quantitative applications of LiDAR imagery in fluvial geomorphology. Earth Surface Processes and Landforms 34: 217–231. DOI: 10.1002/esp.1705

Ortuño M, Guinau, M, Calvet J, Furdada G, Bordonau J, Ruiz A, Camafort M. 2017. Potential of airborne LiDAR data analysis to detect subtle landforms of slope failure: Portainé, Central Pyrenees. Geomorphology 295: 364–382. DOI: 10.1016/j.geomorph.2017.07.015

Palau RM, Hürlimann M, Pinyol J, Moya J, Victoriano A, Génova M, Puig-Polo C. 2017. Recent debris flows in the Portainé catchment (Eastern Pyrenees, Spain): analysis of monitoring and field data focussing on the 2015 event. Landslides 14: 1161–1170. DOI: 10.1007/s10346-017-0832-9

Passalacqua P, Belmont P, Staley DM, Simley JD, Arrowsmith R, Bode CA, Crosby C, DeLong SB, Glenn NF, Kelly SA, Lague D, Sangireddy H, Schaffrath K, Tarboton DG, Wasklewicz T, Wheaton JM. 2015. Analyzing high resolution topography for advancing the understanding of mass and energy transfer through landscapes: A review. Earth Science Reviews 148: 174-193. DOI: 10.1016/j.earscirev.2015.05.012

Pierson TC, Costa JE. 1987. A rheologic classification of subaerial sediment-water flows. In Debris Flows/Avalanches: Process, Recognition and Mitigation, Reviews in Engineering Geology 7, Costa JE, Wieczorek G (eds). Geological Society of America: Boulder; 1–12.

Pinyol J, Hürlimann M, Furdada G, Moysset M, Palau RM, Victoriano A, González M, Moya J, Guinau M, Raïmat C, Fañanás C. 2017. El barranco de Portainé (Pirineo Central): un laboratorio in situ completo para el estudio de la actividad torrencial. In: IX Simposio Nacional Sobre Taludes y Laderas Inestables, Alonso E, Corominas J, Hürlimann M (eds). CIMNE: Barcelona; 1165–1176.

Portilla M, Chevalier G, Hürlimann M. 2010. Description and analysis of the debris flows occurred during 2008 in the Eastern Pyrenees. Natural Hazards and Earth System Sciences 10: 1635–1645. DOI: 10.5194/nhess-10-1635-2010

~~Rathburn SL, Bennett GL, Wohl EE, Briles C, McElroy B, Sutfin N. 2017. The fate of sediment, wood, and organic carbon eroded during an extreme flood, Colorado Front Range, USA. Geology 45: 499–502. DOI:10.1130/G38935.1~~

Roering JJ, Mackey BH, Marshall JA, Sweeney KE, Deligne NI, Booth AM, Handwerger AL, Cerovski-Darriau C. 2013. “You are HERE”: Connecting the dots with airborne lidar for geomorphic fieldwork. Geomorphology 200: 172–183. DOI: 10.1016/j.geomorph.2013.04.009

Rupnik B, Mongus D, Žalik B. 2015. Point Density Evaluation of Airborne LiDAR Datasets. Journal of Universal Computer Science 21: 587–603. DOI: 10.3217/jucs-021-04-0587

Scheidl C, Rickenmann D. 2011. TopFlowDF – A simple GIS model to simulate debris-flow runout on the fan. In 5th International Conference on Debris-Flow Hazards "Mitigation, Mechanics, Prediction and Assessment", Genevois R, Hamilton DL, Prestininzi A (eds). Research Center CERI, Sapienza Università: Rome; 253-262. DOI: 10.4408/IJEGE.2011-03.B-030

Scheidl C, Rickenmann D, Chiari M. 2008. The use of airborne LiDAR data for the analysis of debris flow events in Switzerland. Natural Hazards and Earth System Sciences 8: 1113–1127. DOI: 10.5194/nhess-8-1113-2008

Slatton KC, Carter WE, Shrestha RL, Dietrich WE. 2007. Airborne Laser Swath Mapping: Achieving the resolution and accuracy required for geosurficial research. Geophysical Research Letters 34: L23S10. DOI: 10.1029/2007GL031939

Taylor JR. 1997. An Introduction to Error Analysis: The Study of Uncertainties in Physical Measurements. University Science Books: Sausalito. ISBN: 0-935702-42-3

Terrasolid. 2016. TerraScan User's Guide. Terrasolid Ltd: Helsinki

~~Thoma DP, Gupta SC, Bauer ME, Kirchoff CE. 2005. Airborne laser scanning for riverbank erosion assessment. Remote Sensing of Environment 95: 493–501. DOI: 10.1016/j.rse.2005.01.012~~

Trapero L, Bech J, Duffourg F, Esteban P, Lorente J. 2013. Mesoscale numerical analysis of the historical November 1982 heavy precipitation event over Andorra (Eastern Pyrenees). Natural Hazards and Earth System Sciences 13: 2969-2990. DOI: 10.5194/nhess-13-2969-2013

~~Tseng CM, Lin CW, Stark CP, Liu JK, Fei LY, Hsieh YC. 2013. Application of a multi-temporal, LiDAR-derived, digital terrain model in a landslide-volume estimation. Earth Surface Processes and Landforms 38: 1587–1601. DOI: 10.1002/esp.3454~~

Victoriano A, Díez-Herrero A, Génova M, Guinau M, Furdada G, Khazaradze G, Calvet J. ~~In press~~2018. Four-topic correlation between flood dendrogeomorphological evidence and hydraulic parameters (the Portainé stream, Iberian Peninsula). Catena 162: 216-229. DOI: 10.1016/j.catena.2017.11.009

Volkwein A, Baumann R, Rickli C, Wendeler C. 2015. Standardization for Flexible Debris Retention Barriers. In Engineering Geology for Society and Territory – Volume 2, Lollino G, Giordan D, Crosta GB, Corominas J, Azzam R, Wasowski J, Sciarra N (eds). Springer: Cham, Heidelberg, New York, Dordrecht, London; 193-196. DOI: 10.1007/978-3-319-09057-3_25

Wendeler C, McArdell BW, Volkwein A, Denk M, Gröner E. 2008. Debris flow mitigation with flexible ring net barriers – field tests and case studies. WIT Transactions on Engineering Sciences 60:23-31. DOI: 10.2495/DEB080031

Wheaton JM, Brasington J, Darby SE, Sear DA. 2010. Accounting for uncertainty in DEMs from repeat topographic surveys: improved sediment budgets. Earth Surface Processes and Landforms 35: 136–156. DOI: 10.1002/esp.1886

- A new LiDAR-based approach to assess defense structures in torrents is proposed.
- Geomorphic effects of floods, altered by sediment retention barriers, were measured.
- Deposition behind barriers, downstream and lateral erosion, and net flexion were detected.
- This analysis is a potential tool for monitoring engineering structures in remote mountain areas.

Geomorphic impact and assessment of flexible barriers using multi-temporal LiDAR data: the Portainé mountain catchment (Pyrenees)

Ane Victoriano[a,*], James Brasington[b], Marta Guinau[a], Glòria Furdada[a], Mariló Cabré[c], Myriam Moysset[c]

[a] RISKNAT Group, Geomodels Institute, Departament de Dinàmica de la Terra i de l'Oceà, Universitat de Barcelona (UB), Barcelona, Spain.

[b] School of Geography, Queen Mary University of London (QMUL), London, UK.

[c] Geoprocessing Area, Institut Cartogràfic i Geològic de Catalunya (ICGC), Barcelona, Spain.

* Corresponding author at: Departament de Dinàmica de la Terra i de l'Oceà, Facultat de Ciències de la Terra, Universitat de Barcelona (UB), Martí i Franquès s/n, 08028 Barcelona, Spain

E-mail address: ane.victoriano@ub.edu (A. Victoriano).

Abstract

Multi-temporal digital elevation models (DEMs) obtained from airborne LiDAR surveys are widely used to detect geomorphic changes in time and quantify sediment budgets. However, they have been rarely applied to study the geomorphic impact of engineering structures in mountain settings. In this study, we assessed the influence and behavior of flexible sediment retention barriers in the Portainé catchment (Spanish Pyrenees), using three LiDAR data sets (2009, 2011 and 2016) that covered a 7-year period. Densely forested mountainous areas present some limitations for reliable DEM analysis due to spatial variabilities in data precision, accuracy and point density. A new methodological approach for robust uncertainty analysis along channels, based on changes in cross-sectional elevations, was used to discriminate noise from real geomorphic changes. The obtained results indicated that erosion occurs along most reaches covering a large area, whereas deposition is localized in specific areas such as those upstream of sediment retention barriers and in the debris cone. Despite the presence of 15 flexible sediment retention barriers, the channels presented net degradation during both 2009-2011 and 2011-2016, with 2,838 and 147 m^3 of material exported from the basin, respectively. For the same periods, the barriers retained 33% and 25% of the total deposition (up to 1,300 m^3 per barrier), respectively, but also induced lateral and downstream incision, the latter reaching 703 m^3 for a single barrier. We detected a horizontal displacement of the net of up to 1.2 m in filled barriers, resulting from net flexion. The interference of the natural river evolution by defense measures has resulted in a complex erosion-deposition pattern. The presented methods show high potential for the hydrogeomorphic study of mountain catchments, especially for a high-resolution assessment of flexible barriers or other engineering structures in remote areas.

Keywords: torrential flow, LiDAR, change detection, flexible barrier, sediment budget.

1. Introduction

Hydrometeorological events represent the most frequent natural disasters occurring on a global scale (Munich Re, 2016), producing significant economic and human losses.

In 2015 alone, floods caused damages estimated to be worth US$ 21.3 billion (c. €20,108 million) and claimed 3,449 lives (Guha-Sapir et al., 2016). In mountainous areas, high-intensity sediment-laden torrential floods are the most destructive geomorphological hazards. Several areas in the Pyrenees have been affected by these phenomena in recent years and their management continues to pose an ongoing challenge (Batalla et al., 1999; Chevalier et al., 2013).

Such phenomena are highly unpredictable, often resulting from short and intense localized precipitation events. The rapid accumulation of drainage through steep mountain basins can lead to high-velocity flows that entrain large volumes of sediment from the bed and banks. These can quickly evolve into floods with a high concentration of sediments that continue to bulk up downstream, with potentially catastrophic consequences. Such flows pose a severe risk to infrastructure, riparian assets and life, particularly where the floods discharge onto the valley floor through populated fans and floodplains. Lithology, gradient and the pattern of drainage accumulation combine to affect the distribution of stream power and sediment transport in mountain catchments. This interaction determines whether the flow becomes a clearwater, hyperconcentrated or a debris one in a single event, depending on the sediment load (Pierson and Costa, 1987). This in turn influences the distribution of runout across the receiving fan piedmont or floodplain (Scheidl and Rickenmann, 2011). We will use the term “torrential” throughout this paper to include all the mentioned flow types and events.

Hydrogeomophic hazards can be dealt with using various kinds of defense measures, depending on the characteristics of the site. Engineering structures are considered a fast and effective way of mitigating risk and include the recently-developed flexible debris flow barriers that are increasingly being emplaced in torrential channels (Luis-Fonseca et al., 2011; Wendeler et al., 2008). While much attention has been paid to the safe design of such retention barriers (Ferrero et al., 2015; Volkwein et al., 2015), their geomorphic effects still require further research, as these directly impact on the effectiveness and stability of the structure itself. Thus, the question that needs to be addressed is how barriers actually behave and influence geomorphological evolution.

Geomorphological risk assessments have been facilitated by the emergence of high-resolution topographic data that have provided new opportunities to quantify the transfer of mass and energy across landscapes (Passalacqua et al., 2015). The acquisition of detailed 3D topographic data, particularly through airborne laser scanning (airborne LiDAR), has rapidly become routine practice for many national mapping agencies to support geological risk assessment. Moreover, such data are now increasingly available to the wider public through open-access data portals, presenting unrivalled opportunities for broad-scale research. Airborne LiDAR data have been used for a wide range of research into natural hazards, such as the geomorphic research on past and/or recent active surficial processes (Abellan et al., 2016; Roering et al., 2013). In fluvial and torrential environments, these data have been used to provide enhanced characterization of drainage systems and the boundary conditions for kinematic and physical models of fluid and sediment transport (Bailly et al., 2012; Biron et al., 2013; Notebaert et al., 2009).

The increasingly routine use of LiDAR data acquisition has led to the development of multi-temporal data sets that sample the same region as a series of timeslices. The derived digital elevation models (DEMs) can then be differenced sequentially to obtain DEMs of difference (DoDs), which reveal not only the horizontal, but also the vertical pattern of topographic change. Such assessments of geomorphic changes based on DoDs provide information on landscape morphology and evolution, as it enables a detailed study of the spatial and temporal patterns in erosion and deposition. Sequential DEM differencing has been applied to a wide range of fluvial systems, including braided gravel-bed rivers with high sediment loads (Brasington et al., 2000; Lane et al., 2003), steep mountain channels (Cavalli et al., 2017), and specific flood or debris flow events (Bull et al., 2010; Croke et al., 2013; Scheidl et al., 2008).

It is essential to consider data uncertainty to avoid the misinterpretation of real geomorphic changes by distinguishing them from background noise generated by different sources of error. Over the last few decades, much attention has been paid to the assessment of DoD uncertainties (Brasington et al., 2003; Cavalli et al., 2017; Lane et al., 2003; Wheaton et al., 2010). It has been reported that a minimum level of detection ($_{min}$LoD) should be estimated for the detection of small elevation changes that are probably associated with errors (Brasington et al., 2000; Fuller et al., 2003).

Regarding mountain environments, the reliable application of airborne LiDAR data is still hampered by many difficulties. Comparability between data sets is a hard task in morphologically complex terrains. However, point cloud georeferencing and the adjustment/alignment process become arduous in mountain regions (Lallias-Tacon et al., 2014). Moreover, elevation accuracy and point density decrease in steep densely forested areas (Cavalli et al., 2008), leading to data sets with temporally variable characteristics among them and spatially variable uncertainties within each. With these limitations, DoD-based analyses cannot be performed properly due to many areas lacking source data, resulting in merely interpolated surfaces that are different in each DEM. Thus, there is a need for a methodology for LiDAR uncertainty analysis based on spatial variabilities along mountain channels and hillslopes.

In this paper, we present a new approach for quantifying geomorphic changes in active and densely forested mountain catchments using multi-temporal airborne LiDAR data. The main objective of this study was to assess the behavior, effectiveness and geomorphic influence of flexible retention barriers. This research provides a high-resolution assessment of the existing engineering structures in remote channels that are difficult to access, identifying the priority areas for the maintenance and future management of the barriers.

2. Study area and torrential activity

This study was carried out in the Portainé (5.7 km long; average gradient, 24.7%) and Reguerals (3 km long; average gradient, 31.3%) mountain torrents of the Pyrenees, the latter being a tributary of the former and referred to as Caners downstream of the confluence (Fig. 1a). The two torrents constitute the Portainé catchment (5.72 km^2), which is located in the Pallars Sobirà County (Catalonia, Spain), and they flow into the Romadriu River, which is part of the Ebro River draining into the Mediterranean Sea. Elevation ranges from 2,439 m a.s.l. (the Torreta de l'Orri peak) to 950 m a.s.l. (the Vallespir hydropower dam), and the torrents merge at 1,285 m a.s.l. A ski resort is located at the headwaters, with its access road along the hillslopes crossing the channels several times. The basin can be divided into two sectors that differ in morphology and hydrogeomorphic processes. The southern one corresponds to the headwaters containing less vegetation and the ski resort. This area is characterized by gentler slopes (10-25º) and a less entrenched drainage network, where torrential processes are not especially relevant. The northern sector is densely forested and shows intense torrential activity along the steep (>25º) and strongly entrenched and confined torrents. These channels have been affected by human activity via the implementation of a multi-barrier system that strongly influences sediment transfer processes. In these reaches, severe flows have occurred in the last decade and a debris cone has formed in the most downstream part.

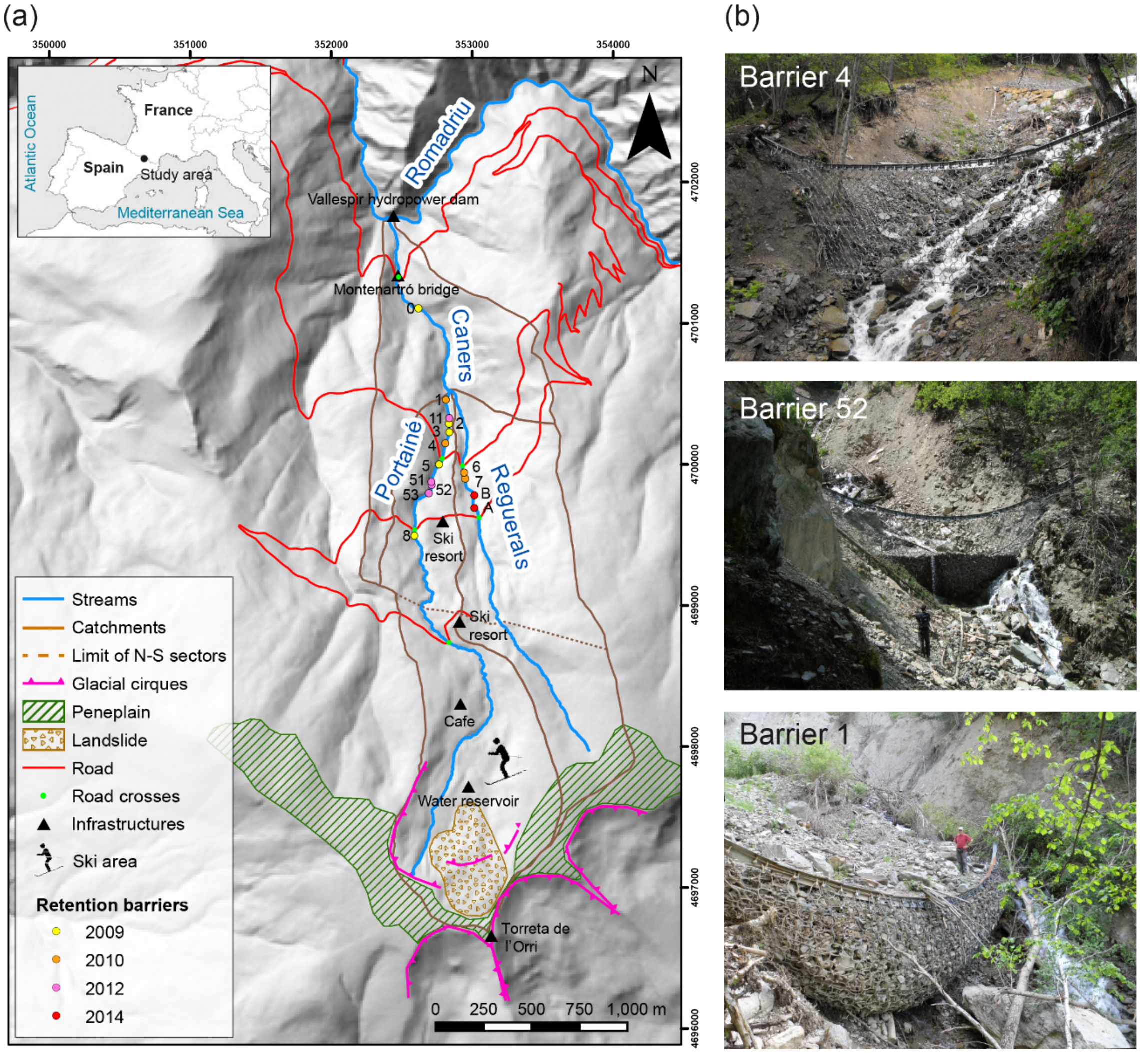

Figure 1. (a) Setting of the study area showing the main geomorphological and anthropic features. The Portainé and Reguerals torrents, as well as the code of each sediment retention barrier, are also indicated. (b) Photographs of some of the barriers showing examples of an empty (barrier 4 in June 2010), partly filled (barrier 52 in June 2013) and completely filled (barrier 1 in June 2013) barrier.

2.1. Geological setting and climate

The region is dominated by highly folded, fractured and weakened Cambro-Ordovician metapelites. Glacial and periglacial processes during the Pleistocene glacial periods gave rise to intense weathering, with the subsequent fluvial erosion resulting in steep slopes and entrenched torrents. Apart from the bedrock, two types of surficial deposits crop out in the Portainé catchment. One is the colluvium, up to 10 m thick, which covers the bedrock along most of its extension. The other are the torrential deposits found in the valley bottoms that have been formed by the deposition of different sediment-laden flows. Both are unconsolidated materials that can be easily eroded and transported, as well as the bedrock (Ortuño et al., 2017).

The climate of the study area is Alpine Mediterranean, with a mean annual rainfall of 800 mm and a mean annual temperature of 5-7°C (Meteocat, 2008). Maximum precipitation in terms of intensity and frequency occurs in the spring and summer, mainly as convective storms. It should be noted that orography controls the generation of convective cells at the top of the drainage basins (Trapero et al., 2013), affecting the local meteorological conditions.

2.2. Hydrogeomorphic hazards and flexible barriers

Fluvio-torrential processes are very intense in the Portainé and Reguerals torrents. Torrential flows, which include some well-known debris flows, produce considerable economic damages to infrastructures and facilities in the catchment, especially due to the obstruction of the access road to the ski resort. Since 2009, €5,800,000 have been invested in road works and €510,000 in mitigation measures (Pinyol et al., 2017). Dendrogeomorphological studies have proved the occurrence of at least ten events from 1969/1970 to 2009/2010 (recurrence interval of 4.5 years), based on the dating of damage indicators on riverbank trees in different geomorphic positions (Génova et al., accepted; Victoriano et al., 2018). Torrential activity has intensified since 2006, with extraordinary flows occurring almost yearly. This increase in the occurrence of torrential events has been linked to anthropic activities in the ski resort area, mainly to the loss of vegetation cover decreasing infiltration capacity, and to the construction of artificial drainage channels for gathering the runoff, all of these together producing higher peak discharges (Furdada et al., 2017). The largest recorded debris flow occurred in September 2008 (prior to the available LiDAR data) and its volume was estimated to be 26,000 m^3 (Portilla et al., 2010), with an average erosion rate of 2.12 m^3/m (Abancó and Hürlimann, 2014).

To reduce the impact of the torrential events, mid-term hydrological corrective measures have been implemented (Luis-Fonseca et al., 2011), consisting of placing VX-160 flexible ring-net barriers along the channels (Fig. 1b). These aim to retain part of the transported material and induce a stepped river profile to reduce flow energy and, therefore, prevent erosion. Since 2009, 15 barriers have been placed in the Portainé catchment, 11 in Portainé and 4 in Reguerals (Fig. 1a). Due to the large sediment loads that are associated with extraordinary events, the barriers were quickly filled, even after a single event. Currently, torrential events still occur, leading to progressively more entrenched ravines and posing a risk to the effectiveness and stability of the barriers.

3. Methods

3.1. Documentary data

We searched for documentary data on recent torrential events and compiled all the available data on their effects on infrastructures. The main data sources were the technical reports of the *Institut Geològic de Catalunya* (IGC) and *Ferrocarrils de la Generalitat de Catalunya* (FGC) (e.g., FGC and ICGC, 2015; IGC, 2013), as well as other scientific works (Palau et al., 2017; Victoriano et al., 2018). The relative magnitude of the events was established according to their repercussion on infrastructures (number of obstructed road crosses and filled barriers) and geomorphological processes (incision, sediment transport and accumulation). Regarding anthropic activities, the emplacement dates and locations of the sediment retention barriers (Fig. 1a) were established thanks to the information provided by Mr. Carles Fañanás (Department of Environment, Government of Catalonia). A complete database was prepared with all this information.

3.2. LiDAR data acquisition and processing

Sequential data sets were collected in August 2009, August-September 2011 and August-September 2016, using a Cessna Caravan 208B aircraft equipped with a Leica ALS50-II topographic LiDAR sensor, owned by the *Institut Cartogràfic i Geològic de Catalunya* (ICGC). The LiDAR flight parameters and data specifications are shown in Table 1. The minimum pulse density per strip (nominal point density) was 0.5 points/m^2 and the vertical accuracy of the LiDAR system had a root mean square error (RMSE) < 15 cm. The resulting point densities for the 2009, 2011 and 2016 data sets were 0.96, 2.14 and 2.77 points/m^2, respectively. The accuracy of the data was calculated by comparing LiDAR and ground GPS elevations, and was estimated to be (expressed as RMSE) < 5 cm for flat non-vegetated areas, < 15 cm for slightly steep and forested areas, and < 50 cm for steep densely forested areas.

Table 1. LiDAR flight parameters and point cloud data specifications from the 2009, 2011 and 2016 surveys (data from ICGC).

	2009	**2011**	**2016**
Average flight altitude	2250 m	2440 m	2712 m
Scan angle	48°	40°	31.3 °
Scan frequency	21.5 Hz	25 Hz	24.4 Hz
Pulse rate	89200 Hz	84400 Hz	77100 Hz
Nominal point density	0.5 pt/m^2	0.5 pt/m^2	0.5 pt/m^2
Total point density (for entire datasets)	0.96 pt/m^2	2.14 pt/m^2	2.77 pt/m^2
Ground point density (for analysis area)	0.29 pt/m^2	0.93 pt/m^2	1.32 pt/m^2

A data quality assurance and control process (QA/QC) was performed for each data set. First, point clouds were distributed in blocks measuring 2 km x 2 km to check data completeness and point density. Second, points were georeferenced (x, y and z coordinates) and projected in UTM (Zone 31N) in the ERTS89 reference system from the aircraft trajectory calculation, using GPS data of the flight and GNSS data from control points of the CatNet network. Elevations were georeferenced to the EGM08D595 geoid and accurately adjusted, taking into account overlapping zones of different flight strips, but also comparing the LiDAR point cloud with the altitudes of the points located in flat control areas that have been previously measured in the field with GPS. This adjustment reduces systematic elevation errors. Third, LiDAR topographic points were classified as ground, vegetation or noise, using automatic filtering based on the algorithms of the TerraScan software (Terrasolid, 2016). Moreover, manual point editing was performed by experts for an exhaustive verification of real terrain points, paying special attention to barriers, road-torrent intersections, valley bottoms and lateral landslide margins. Finally, a pre-analysis of the resulting data sets (e.g., 3D visualization and segmentation of the files) was performed using the CloudCompare (Girardeau-Montaut, 2015) and ArcGIS (ESRI, 2014) software. This verified that the obtained point clouds provided good coverage of the study area and an *a priori* adequate average point density for data comparability and DEM generation.

High-resolution bare-earth DEMs were obtained for 2009, 2011 and 2016 by filtering vegetation and noise points. First, point clouds were compiled into three LAS data sets. For each year, ground points were triangulated and interpolated using the linear interpolation algorithm in ArcGIS (ESRI, 2014), before being rasterized into a 1-m regular grid with a determined extent (Wheaton et al., 2010). The linear interpolation algorithm was used because it provided the most reliable steep terrain surface for the study area. The grid resolution or cell size was determined according to the averaged point spacing and density of the three data sets, as the same resolution is needed for adequate DEM comparison and subtraction (see Section 5.1).

Considering the objectives of the study, a polygon was manually delineated as an analysis area, coinciding with the part of the valley bottom where fluvio-torrential processes act to change the morphology of the channel, that is, the riverbed. Their limits correspond to the lateral slope change and therefore, only includes the smooth riverbed (< 30º), excluding lateral banks. The three DEMs were clipped using this polygon to obtain isolated DEMs of the analysis area.

3.3. Uncertainty analysis and geomorphic change detection

Several sources of error (e.g., device errors, meteorological conditions, vegetation cover, point density, data filtering processes and interpolation techniques) affect data quality and DEM accuracy (Scheidl et al., 2008). Data and DEM comparability is important for accurate geomorphic interpretation.

The approach adopted for this study is summarized in Figure 2A previous visual analysis of point clouds was performed to evaluate whether their distribution and density were good enough to perform a conventional DoD analysis. Given the limitations related to dense vegetation, such as areas that lack points, we performed a cross-sectional method for a spatially variable uncertainty analysis in mountain torrents that better localizes and implements error thresholds so that the actual geomorphic change is quantified only when it can be reliably assessed. The error analysis had three main steps: individual DEM error quantification; error propagation for multi-temporal data comparison; and probabilistic thresholding of uncertainty at a user-defined confidence interval.

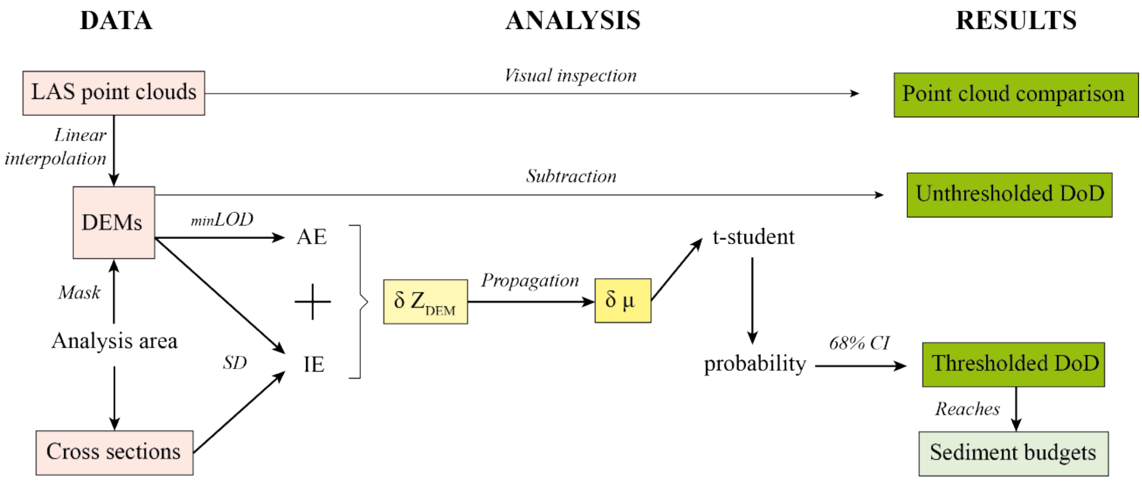

Figure 2. Flowchart showing the methodological approach used in this study for multi-temporal airborne LiDAR data analysis.

Individual DEM error quantification

DEM uncertainty (δZ_{DEM}) is defined as the difference in elevation between real terrain points and their spatially-paired DEM cells (Wheaton et al., 2010). The quantification of δZ_{DEM} requires good knowledge of the specific data set and its error sources. Mountain catchments are commonly forested and show steep gradients that lead to variabilities in precision, accuracy and point densities. A specific DEM uncertainty analysis that considers these uncertainties and their spatial variability is required in such contexts. In this study, we quantified two error sources: (i) aerotriangulation error (AE) and (ii) interpolation error (IE).

The AE is the spatial deviation between topographic surveys, namely the errors in the X, Y and Z directions after aerotriangulation adjustment (Hsieh et al., 2016). This error is the consequence of the constraints of both LiDAR measurement reproducibility and the georeferencing process. This produces a bias that can be detected when comparing data sets acquired at different flight times. The AE shows a spatially uniform distribution throughout an entire data set and is estimated by comparing multi-temporal data from stable areas where no changes are expected (i.e., roads).

First, we undertook a DEM-to-DEM comparison (2011-2009, 2016-2011 and 2016-2009) along the road by subtracting old DEMs from new ones and calculating the standard deviation of elevation differences (between data sets acquired in different flight times) on a cell-by-cell basis. These deviations for each pair of DEMs were a measure of precision, their mean indicating the minimum level of detection ($_{min}$LoD) for each DEM comparison. The values were averaged to obtain the mean $_{min}$LoD, as follows:

$$_{\min}\mathrm{LoD} = \frac{1}{n}\sum_{i=1}^{n} \sigma \Delta Z \quad (1)$$

where σΔZ is the mean standard deviation of the elevation difference between new and old DEMs for each DEM-to-DEM comparison (2011-2009, 2016-2011 and 2016-2009) and *n* the number of comparisons (3 in our case study).

Second, since the $_{\min}$LoD obtained from Eq. 1 indicates the combination of the individual AEs of two data sets (propagated error), it can be expressed with the following equation:

$$_{\min}\mathrm{LoD} = \sqrt{(AE_{new})^2 + (AE_{old})^2} \quad (2)$$

where AE_{new} and AE_{old} are the AEs of the newer and older DEMs, respectively. Assuming that the bias is constant and spatially uniform for the whole data sets, both values were considered equal ($AE_{new} = AE_{old} = AE$) and Eq. 2 was transformed into:

$$AE = \sqrt{\frac{_{min}LoD^2}{2}} \quad (3)$$

where *AE* was calculated as a unique value for the three DEMs.

The IE is a remarkable source of error in mountain areas, where DEM surfaces are built from spatially variable point densities. Therefore, multi-temporal comparisons incorporate a different IE from each DEM, leading to geomorphic changes that are not real, but a result of the subtraction of unreal interpolated surfaces. Concerning the studied torrents, point densities vary along the channels according to *in situ* characteristics and therefore, the IE is spatially variable within each DEM (2009, 2011 and 2016). To assess this uncertainty, a 1D analysis of cross-sectional elevation differences was performed along the channels. We created cross sections every meter and intersected them with the manually delineated polygon (analysis area), obtaining 8,125 sections (5,267 in the Portainé torrent and 2,858 in the Reguerals torrent) with 1-m spacing and variable width (Fig. 3). DEM cell statistics (e.g., mean elevation, standard deviation and the number of points) were calculated along each section for each year (2009, 2011 and 2016). Assuming a trapezoid-shaped channel with a regular riverbed (smooth and nearly flat), we considered the IE value at a specific cross section to be equal to its mean standard deviation of elevation, as given by the following equation:

$$IE = \sqrt{\frac{1}{n}\sum_{i=1}^{n} (Z_{cell} - Z_{mean})^2} \quad (4)$$

where *IE* is estimated as a different value for each cross section and year, *n* is the number of cells at each cross section, and Z_{cell} and Z_{mean} are the elevation of each cell and the average elevation of the cells, respectively.

Both errors obtained from Eq. 3 (AE) and Eq. 4 (IE) were combined to obtain DEM uncertainty (δZ_{DEM}) at each cross section as follows:

$$\delta Z_{DEM} = \sqrt{(\mathrm{AE})^2 + (IE)^2} \quad (5)$$

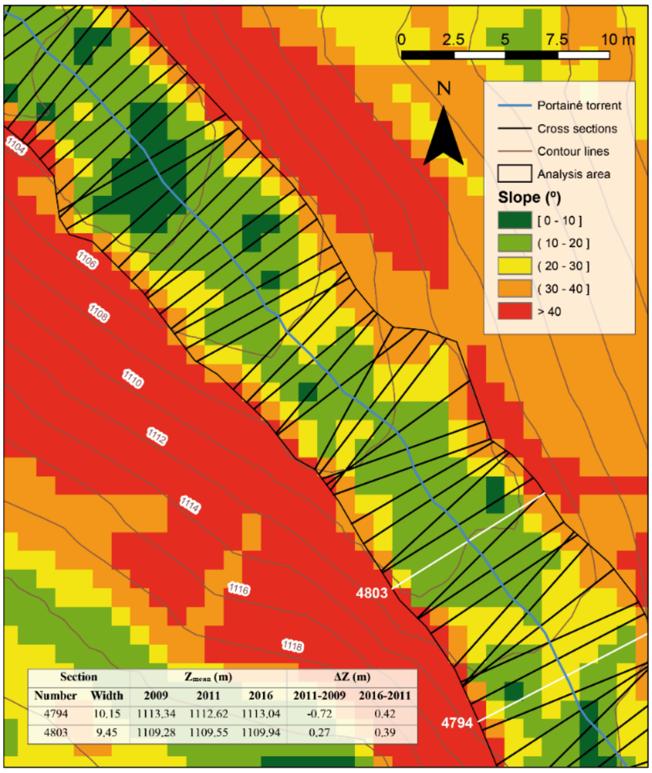

Section		Z_{mean} (m)			ΔZ (m)	
Number	Width	2009	2011	2016	2011-2009	2016-2011
4794	10.15	1113.34	1112.62	1113.04	-0.72	0.42
4803	9.45	1109.28	1109.55	1109.94	0.27	0.39

Figure 3. Illustration of a specific stretch of the Portainé torrent showing the locations of the cross sections used for the spatially variable uncertainty analysis. The analysis area corresponds to abrupt lateral slope changes. The table in the lower part of the figure shows the characteristics and mean elevations of two example sections from multi-temporal DEMs (white lines).

Error propagation

The multi-temporal comparison of two DEMs needs to account for the combination of the elevation errors of each surface. This consists of deriving the quantity of both DEM errors following the simple error propagation theory that treats inputs as independent (Taylor, 1997). As proposed by Brasington et al. (2003), the propagated error ($\delta\mu$) was determined as follows:

$$\delta\mu = \sqrt{(\delta Z_{DEMnew})^2 + (\delta Z_{DEMold})^2} \tag{6}$$

where δZ_{DEMnew} and δZ_{DEMold} are the individual errors in the more recent (DEM_{2011} for 2011-2009 and DEM_{2016} for 2016-2011) and older (DEM_{2009} for 2011-2009 and DEM_{2011} for 2016-2011) surfaces, respectively. In our case, the $\delta\mu$ values were calculated for each cross section and each pair of DEMs considered. This enabled the subsequent accurate assessment of local elevation changes.

Probabilistic thresholding

The significance of uncertainties ($\delta\mu$) in predicted elevation changes (ΔZ) can be assessed in two main ways: using a simple $_{min}$LoD or by probabilistic thresholding at a user-defined confidence interval (Wheaton et al., 2010). The aim of this step is to discard noise from signals and thus, only consider those that we are confident about being real geomorphic changes (ΔZ_{real}), excluding the changes occurring within determined error ranges. If spatial variabilities are considered, as in the present study, probabilistic thresholding is the most accurate method (Brasington et al., 2003; Lane et al., 2003). The probability of changes being real is calculated using Student's t-distribution, which consists of calculating the t-score (t) of each cross section as follows:

$$t = \frac{|\Delta Z|}{\delta_\mu} \tag{7}$$

This equation assesses the significance of the changes, expressed as the absolute elevation difference between new and old DEMs ($|\Delta Z| = |Z_{DEM\ new} - Z_{DEM\ old}|$), by comparing it to the propagated error ($\delta\mu$).

T-distribution enables the determination of the probability (p) of ΔZ being real on a section-by-section basis. Given that we assumed the riverbed to be flat along the cross sections, but elevations vary naturally, probabilistic thresholding was applied at a specific confidence interval of 68% ($p < 0.32$) to obtain ΔZ_{real}.

Sections were excluded if their probability of the changes being real was greater than 0.32. Reliable volumetric elevation changes for the 2009-2011 and 2011-2016 periods were obtained by multiplying ΔZ_{real} (from the 2011-2009 and 2016-2011 subtractions) with the width of each cross section (distance between the cross sections is 1 m). This method led to the quantification of geomorphic activity with fewer errors, especially in the reaches where sediment retention barriers are emplaced.

4. Results

4.1. Chronology of torrential events and flexible barriers

Eight torrential events of different magnitude, behavior and sediment load occurred in the 2009-2016 LiDAR temporal window. Five of them obstructed the access road and six damaged the sediment retention barriers, which had to be repaired in some cases. Table 2 presents the information of the torrential events recorded in the Portainé catchment and their effects on the barriers. The most intense event occurred in July 2010 and the least intense one in May 2016.

Table 2. List of the events, including date, magnitude and effects (information obtained from FGC and ICGC (2015) and IGC (2013).

Event		Effects and damages		
Date	**Magnitude**	**Torrent**	**Road crosses**	**Barriers**
2010/07/22	Most significant	Portainé Reguerals	2	7 filled 2 damaged
2010/08/12	Major	Portainé Reguerals	2	0 filled 5 damaged
2011/08/05	Minor	Portainé Reguerals	0	2 filled 1 damaged
2013/07/23	Major	Portainé Reguerals	3	3 filled 3 damaged
2014/08/20	Minor	?	0	-

2014/08/30	Medium	Portainé	1	5 damaged
2015/08/21	Medium	Portainé	1	5 damaged
2016/05/09	Less significant	?	0	-

The 15 flexible ring-net barriers with similar characteristics were emplaced along the middle reach of the channels to retain sediment and produce a stepped profile to reduce riverbed incision (Fig. 1). These structures are 4-6 m high and 12-24 m wide, their retention capacity varying with the specific local slope and channel width. As shown in Table 3, the barriers differ in size and were constructed at three different times: nine between the end of 2009 and the beginning of 2010 (stage 1); four in 2012 (stage 2) and two in 2014 (stage 3). They were all filled during different torrential events, except for the ones emplaced in 2014 that remain empty and another one that was artificially filled after installation.

Table 3. Sediment retention barriers on the Portainé and Reguerals torrents (information provided by Mr. C. Fañanás, pers. com.).

Barrier code	Date	Torrent	Elevation (m a.s.l.)	Height (m)	Width (m)	Filling event
0	2009	Caners	1090	4	13.5	2010/07/22
1	2010	Portainé	1308	4	16.8	2010/07/22
2	2009	Portainé	1355	5	13.5	2010/07/22
3	2009	Portainé	1380	5	11.5	2011/08/05
4	2010	Portainé	1405	4	13.5	2010/07/22
5	2009	Portainé	1470	5	20	2010/07/22
6	2010	Reguerals	1490	4	27	2010/07/22
7	2010	Reguerals	1510	4	26	2011/08/05
8	2009	Portainé	1710	6	19.5	2010/07/22
11	2012	Portainé	1345	5.5	16.5	2012 (anthropic)
51	2012	Portainé	1525	4.5	25	2013/07/23
52	2012	Portainé	1555	4.8	27.1	2013/07/23
53	2012	Portainé	1575	5.1	15.1	2013/07/23
A	2014	Reguerals	1615	5	19.2	-
B	2014	Reguerals	1570	6	17.5	-

4.2. Geomorphic changes

3D visualization of airborne LiDAR points enabled us to observe clear geomorphic changes related to anthropic structures. Deposition and erosion were observed upstream and downstream of the barriers, respectively (Fig. 4). In some of the barriers installed in stage 1, a change in the highest position of the barrier was identified when comparing 2011 and 2016 LiDAR data (Fig. 4a), produced by the ring net flexion caused by the retained load. The horizontal displacement of the net could be estimated for the barriers with sufficient LiDAR points for accurate measurement. In our study, this was measured in five barriers (see the results at the end of this section), accounting for an average horizontal displacement of 0.7 m (1.1 m in the example shown in Fig. 4a). For the barriers installed in stage 2, riverbed incision was detected from 2009 to 2011 (pre-barrier), indicating natural erosive dynamics (Fig. 4b).

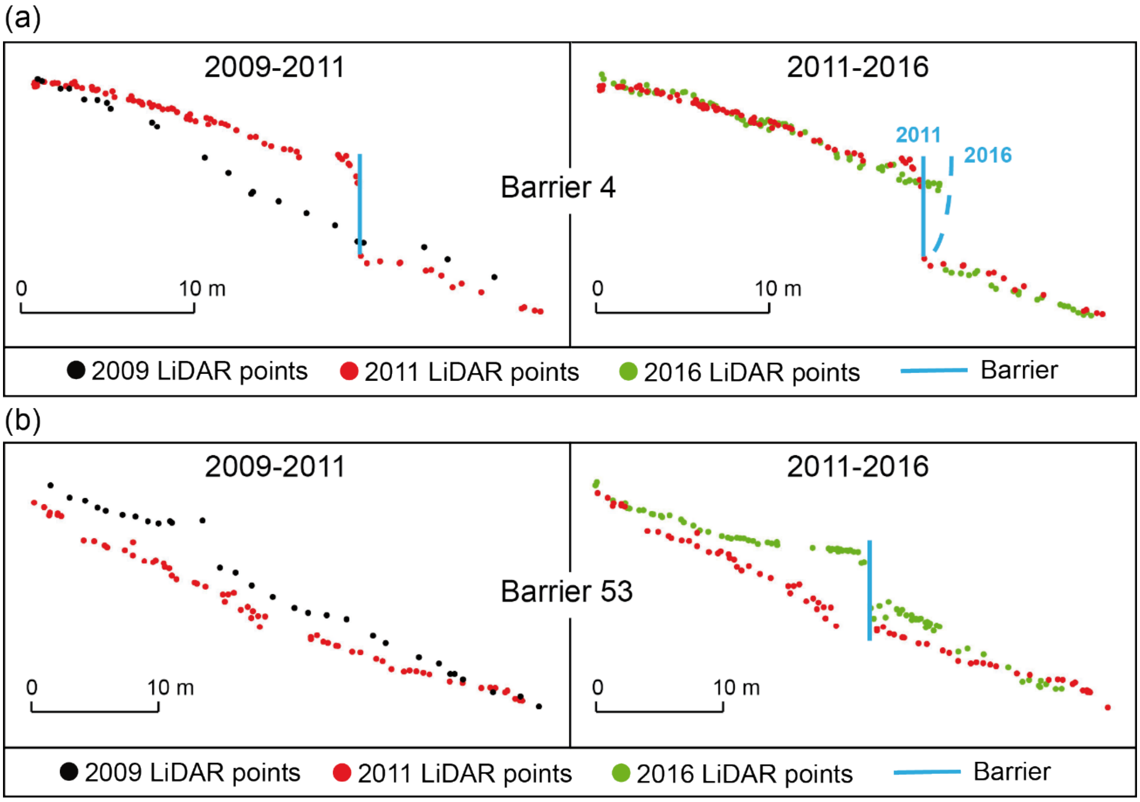

Figure 4. Longitudinal sections of two specific stretches of the Portainé torrent showing 2009, 2011 and 2016 ground points (see Fig. 1a for the location of the barriers). (a) Barrier 4, constructed in 2010 and filled in the July 2010 event, illustrating the change in the barrier position due to net flexion. (b) Barrier 53, constructed in 2012 and filled in the July 2013 event.

As a preliminary approach, the spatial distribution of the geomorphic changes for raw (unthresholded) 2011-2009 (Fig. 5a) and 2016-2011 (Fig. 5b) comparisons identified the erosive or depositional nature of the stream stretches, the magnitude of the changes and their relationship with anthropic structures. Erosion was the most common phenomenon along valley bottoms. The material eroded alongside the torrents was mostly transported during high-discharge flows, sometimes leading to the development of debris flows (and the opposite when deposited). However, there were also other areas where erosion was locally enhanced, such as downstream of the barriers or road intersections. Depositional geomorphic processes occurred at places where the slope decreased or anthropic structures located. The main areas of accumulation were the debris cone formed in the most downstream reach (corresponding to the Caners torrent) and areas upstream of the sediment retention barriers and road intersections.

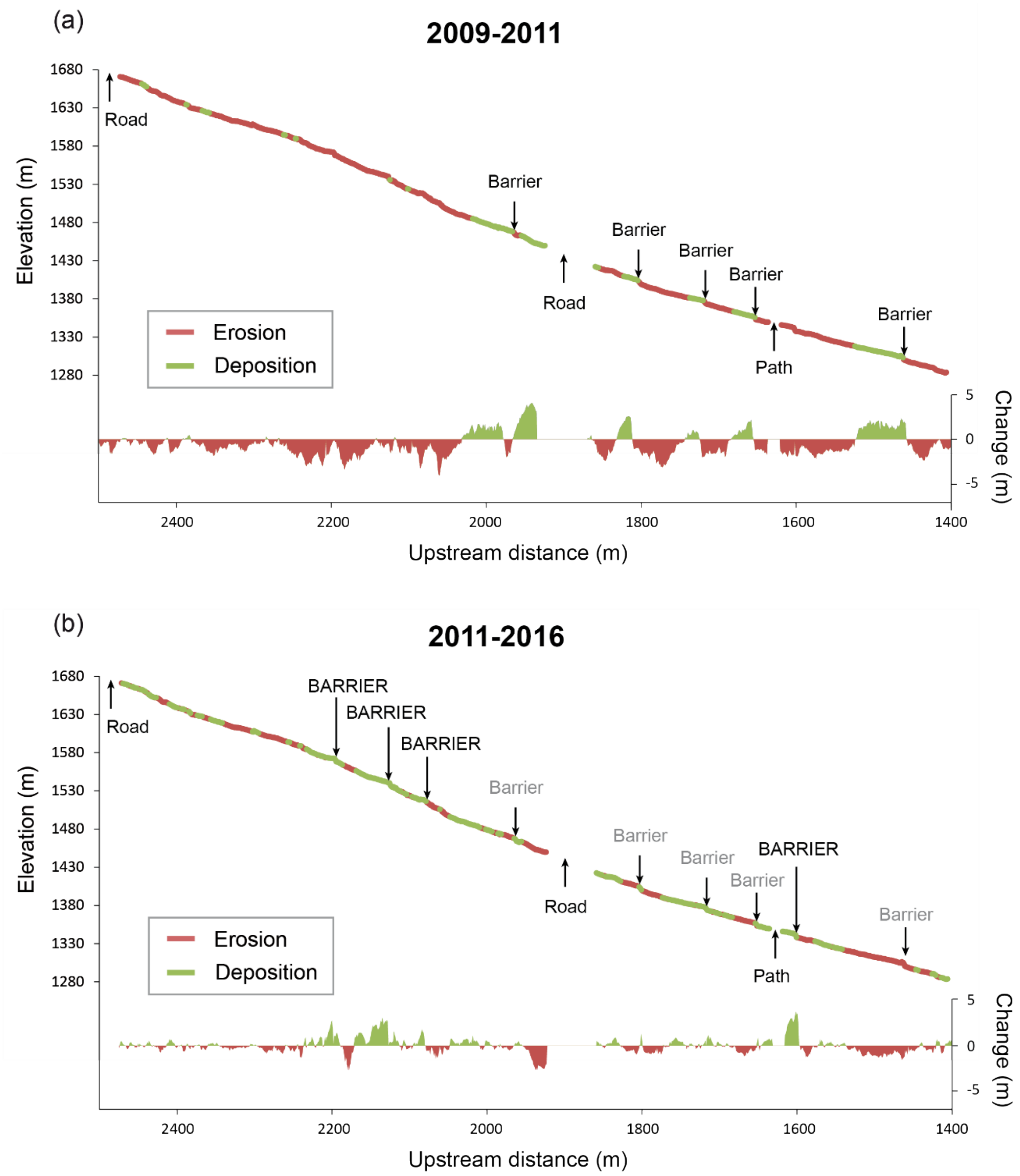

Figure 5. Geomorphic net change in storage terms (unthresholded) along the longitudinal profile of the Portainé torrent, from the road intersection at 1,700 m a.s.l. to the confluence with the Reguerals torrent. The bottom of the profile illustrates the magnitude of the changes. The location of the anthropic structures is indicated by the newly (between 2011 and 2016) and previously (between 2009 and 2011) emplaced barriers shown in upper and lower cases, respectively. (a) Changes between 2009 and 2011. (b) Changes between 2011 and 2016.

Geomorphic changes were thresholded by the spatially variable uncertainty analysis. Table 4 shows the uncertainty analysis and the volumetric geomorphic changes considered real that were obtained for two example cross sections A $_{min}$LoD of 0.1 m was calculated, leading to an AE of 0.07 m for the entire data sets. The IE, calculated from the standard deviation of the mean elevations of each cross section, reached 0.5 m in some areas. $\delta\mu$ values showed large spatial variability, ranging from 0.1 to 5.4 m; however, the median was 0.9 m and 0.66 m for 2011-2009 and 2016-2011, respectively (see examples in Table 4). Probabilities of geomorphic changes being real (p) were < 0.32 in many sections (68% confidence interval) and were considered real changes (ΔZ_{real}), whereas geomorphic changes with p > 0.32 were discarded.. This thresholding analysis considerably reduced the number of cross sections that were considered and influenced the final results on geomorphic changes. Indeed, 57% and 74% of the data were discarded for 2011-2009 and 2016-2011 sediment budget calculations, respectively. Nonetheless, those sections with changes assumed to be real showed high reliability and were therefore used for geomorphic quantification. The uncertainty analysis resulted in a smaller amount of, but more reliable data (see Section 5.1). Most active zones, such as the areas surrounding the flexible barriers, were not discarded due to their high magnitude, proving the effectiveness of the methodology in these areas.

Table 4. Results of the spatially variable uncertainty analysis for two example sections (see their location in Fig. 3). The volumes of the geomorphic change were only calculated for thresholded real elevation changes.

Section		**DEM error**			**Propagated error**		**Probabilistic thresholding**						**Volume (m^3)**	
Nº	Width (m)	δZ_{DEM} (m)			$\delta\mu$ (m)		t		p		Real ΔZ (m)			
		2009	2011	2016	11-09	16-11	11-09	16-11	11-09	16-11	11-09	16-11	11-09	16-11
4794	10.15	0.78	1.04	0.48	1.3	1.14	0.55	0.36	0.29	0.36	-0.72	-	-7.32	-
4803	9.45	0.58	0.29	0.24	0.65	0.38	0.41	1.03	0.34	0.15	-	0.39	-	3.67

For the whole analysis area, the mean magnitude of change, obtained from average vertical changes in the cross sections, was about 1 m (0.90 m for erosion and 1.02 m for deposition), with more erosive sections occurring than depositional ones. Sediment budgets were calculated for each period of time between the LiDAR flights. The 2011-2009 comparison indicated a total volume of erosion and deposition of 22,042 m^3 and 19,204 m^3, respectively, indicating a net degradation of -2,838 m^3 in two years. Quantification of the 2016-2011 changes also gave a negative sediment budget, but the magnitude was much lower. Indeed, 8,308 m^3 of eroded material and 8,161 m^3 of deposition yielded a total volumetric net change of -147 m^3 in five years. These results suggest a tendency for entrenchment (erosion > deposition) in the studied mountain torrents, with significant sediment output from the catchment towards the Romadriu River. However, the period between 2009 and 2011 was much more active than that after 2011, as higher volumes were mobilized (both eroded and deposited).

Budget segregation is a very useful way of characterizing the spatial distribution and magnitude of geomorphic processes, therefore leading to a better understanding of the fluvio-torrential dynamics in the study area. We recalculated the 2011-2009 and 2016-2011 sediment budgets by dividing the channels into reaches according to different morphological (torrents), geomorphological (catchment sectors) or anthropic (reaches between road intersections) factors. The results are shown in Table 5. The Portainé torrent was more active than the Reguerals torrent, with geomorphic changes of greater magnitude and extension, especially for erosion. This explains the narrower and more entrenched morphology of the Portainé torrent, which was also clearly identified in the field. The catchment can be divided into three different sectors with different slopes: the upper reach (location of the Port-Ainé ski station); the middle reach (contains entrenched channels and the barriers) and the lower reach (contains a debris cone in the most downstream part). The upper-middle and middle-lower boundaries geographically correspond to the division of the N-S sectors and the road that crosses the stream at the Montenartró Bridge, respectively (Fig. 1a). From 2009 to 2011, erosion mostly occurred in the middle reach, with the material deposited in the lower reach. However, the 2011-2016 period recorded significant accumulations in the middle reach, with erosion dominating in the lower part. This can be partly explained by the erosive nature of torrential events. While high-magnitude events (including debris flows) occurred between 2009 and 2011, producing significant erosion along the channels, the number of events recorded from 2011 to 2016 was much lower, leading to proportionately more deposition. The reaches between the road intersections showed a more complex erosion-deposition pattern with temporally variable tendencies, which resulted from the large influence of the barriers occurring in such short stretches.

Table 5. Segregation of the sediment budgets obtained from the 2011-2009 and 2016-2011 DEM comparisons. For each reach, we calculated the net volumetric change and indicated its erosional/degradational or depositional/aggradational tendency.

Criteria	Reach description	Time period	Erosion (m^3)	Deposition (m^3)	Change (m^3)	Dynamics
Torrent (abbr.)	Portainé (Po)	2011-2009	-11,629	6,936	**-4,693**	Degradation
		2016-2011	-4,477	3,497	**-980**	Degradation
	Reguerals (Re)	2011-2009	-4,708	2,167	**-2,541**	Degradation
		2016-2011	-1,618	2,156	**538**	Aggradation
	Caners (Ca)	2011-2009	-5,705	10,101	**4,396**	Aggradation
		2016-2011	-2,213	2,508	**295**	Aggradation
Catchment sector (gradient)	Upper (low)	2011-2009	-2,441	822	**-1,619**	Degradation
		2016-2011	-1,139	568	**-572**	Degradation
	Middle (high)	2011-2009	-19,128	13,023	**-6,105**	Degradation
		2016-2011	-6,112	7,473	**1,362**	Aggradation
	Lower (medium)	2011-2009	-473	5359	**4,886**	Aggradation
		2016-2011	-1,057	120	**-937**	Degradation
Road intersection (max-min altitude)	Po (2360-1965 m)	2011-2009	-1,764	775	**-989**	Degradation
		2016-2011	-1,096	541	**-554**	Degradation
	Po (1965-1700 m)	2011-2009	-1,684	2,015	**331**	Aggradation
		2016-2011	-642	438	**-204**	Degradation
	Po (1700-1450 m)	2011-2009	-4191	2,039	**-2,152**	Degradation
		2016-2011	-1,419	1,731	**312**	Aggradation
	Re (2225-1665 m)	2011-2009	-399	222	**-178**	Degradation
		2016-2011	-180	145	**-34**	Degradation
	Re (1665-1465 m)	2011-2009	-1506	1,450	**-55**	Degradation
		2016-2011	-767	1,107	**339**	Aggradation

	Ca (1465-1035 m)	2011-2009	-12,025	7,344	**-4,681**	Degradation
		2016-2011	-3,147	4,078	**931**	Aggradation
	Ca (1035-950 m)	2011-2009	-473	5,359	**4886**	Aggradation
		2016-2011	-1,057	120	**-937**	Degradation
NET SEDIMENT BUDGET		2011-2009	-22,042	19,204	**-2,838**	Degradation
		2016-2011	-8,308	8,161	**-147**	Degradation

The most significant deposition occurred at the sediment retention barriers, which played an underlying role in the geomorphic changes recorded along the torrents by modifying their natural evolution. Accumulation upstream of these structures was quantified by probabilistic thresholding. The real retained material per barrier ranged from 146 m^3 to 1,311 m^3 and the total retention of the 15 barriers was 8,278 m^3. Table 6 presents the volumes accumulated at each barrier and the horizontal displacement of the net where it could be measured. The geomorphic changes of the barriers are discussed in section 5.3.

Table 6. Relationship between dimensions, the calculated volume of filled barriers and the magnitude of the net flexion. The barriers are listed in their order along the downstream direction.

Barrier code	Height (m)	Width (m)	Torrent	Elevation (m a.s.l.)	Volume (m^3)	Horizontal net displacement (m)
8	6	19.5	Portainé	1710	1302	0.3
53	5.1	15.1	Portainé	1575	303	-
52	4.8	27.1	Portainé	1555	1044	-
51	4.5	25	Portainé	1525	146	-
7	4	26	Reguerals	1510	441	0.5
6	4	27	Reguerals	1490	534	0.4
5	5	20	Portainé	1470	559	?
4	4	13.5	Portainé	1405	589	1.1
3	5	11.5	Portainé	1380	?	1.2
2	5	13.5	Portainé	1355	282	?
11	5.5	16.5	Portainé	1345	535	-
1	4	16.8	Portainé	1308	1230	?
0	4	13.5	Caners	1090	1311	?

Another main deposition area in the 2011-2009 comparison was the debris cone, where 4,904 m^3 of material accumulated. From 2011 to 2016, erosion prevailed in the cone, leading to a net degradation of -896 m^3.

5. Discussion

5.1. Strengths and limitations of airborne LiDAR data in mountain areas

The analysis of airborne LiDAR data can be applied to the study of hydrogeomorphologically active mountains. One of the main advantages is the detection of temporal morphological changes that are indistinguishable in aerial photographs, due to its huge potential for precisely and accurately assessing landscape changes by easily identifying erosion and deposition zones. Moreover, airborne LiDAR enables the procurement of extensive data sets that cover large sectors of the terrain in a short time, which cannot be achieved with ground-based high-resolution topographic techniques such as terrestrial laser scanning or theodolite measurements. The acquisition of LiDAR data is also useful in remote areas where it is difficult to conduct field surveys, such as heavily entrenched stretches of steep mountain rivers.

These kind of data also has some limitations that need to be considered when assessing the reliability of the data, mainly concerning its accuracy and resolution (Slatton et al., 2007). A 15-cm measurement error in point altitude (vertical accuracy) is typically reported by LiDAR manufacturers. The altimetric error is higher in mountain areas with dense vegetation and steep variable gradients. For instance, a vertical accuracy of 0.25 cm has been reported for forested areas (Biron et al., 2013). For the data used in this study, an RMSE < 15 cm was obtained, which decreased to 5 cm in flat areas and was < 50 cm in steep forested areas. These errors are within the accepted range of values. Point density is another vital factor for evaluating LiDAR data (Rupnik et al., 2015) and can be problematic in mountain areas, as dense vegetation hinders the laser beam from reaching the terrain, giving rise to lower -resolution DEMs. Cavalli and Marchi (2008) reported a ground data density of 2.5 points/m^2 that decreased to 0.25 points/m^2 under a dense forest canopy. We took into account this limitation by manually filtering the 2009, 2011 and 2016 point clouds, exclusively paying attention to the analysis area. This considerably minimized the classification errors and produced a higher average ground point density for the analysis area (Table 1).

Regarding the 2009 data, the obtained mean ground point density (Table 1) was lower than the DEM resolution. Using the equation proposed by Landridge et al. (2014), $S=\sqrt{(A/n)}$, the obtained optimal grid resolution (S) for the 2009 data set was 1.86 m and up to 0.86 m for the 2016 data set. As multi-temporal DEMs need to have the same resolution in order to be subtracted, a mean value should be used for DEM generation. A 2-m grid resolution would not take advantage of a significant number of points (in the case of the 2011 and 2016 data sets). Therefore, we generated 1x1-m DEMs for the three data sets. Since some areas from the 2009 model may include highly interpolated unreal surfaces, we analyzed uncertainty in detail, based on the quantification of IEs. This revealed that cross sections with a very low resolution showed a high number of errors and were therefore excluded from morphological budget calculations.

As mountain streams with torrential activity tend to record geomorphic processes with a significant magnitude of change (or signal), the elevation change was higher than the error ($\Delta Z>\delta\mu$) and thus, 2D analyses of DoDs could be performed. While conventional DoD analysis can be reliably conducted for flat areas with little vegetation, it can lead to large interpolation errors remaining unidentified for steep slopes with dense vegetation, generating errors and unreal topographic changes. We overcame this problem by performing a detailed section-by-section 1D analysis for uncertainty estimation along the channels that excluded data within a determined error range ($\delta\mu$) and probability (confidence interval). Although this approach took longer and was more expensive than conventional DoD analyses, it demonstrated the utility of combining AEs and IEs for reliable DoD thresholding, morphological budgeting and geomorphic interpretation along mountain steep channels. The first limitation of the designed method was the assumption that the cross sections are regular, as they are likely to be irregular in a dynamic erosive system. We addressed this drawback by restricting our analysis to the smooth riverbed and applying a 68% confidence interval, instead of the commonly used 95% value. This confidence interval discards the data identified to be insufficiently reliable for comparison , leading to a probable underestimation of the degradational/aggradational effects. Hence, the final calculations used fewer, but more reliable data instead of a higher amount of data that included more errors. More data were discarded when thresholding the 2011-2009 comparison compared to the 2016-2011 one (see section 4.2), as the uncertainty was mostly greater for the first period (most probably due to the lower resolution of the 2009 data set). Factors affecting the percentage of sections excluded from analysis were mainly point density and the magnitude of the signal. High-magnitude geomorphic changes were never discarded, such as those associated with the barriers.

5.2. Interpretation of geomorphic changes and catchment dynamics

The geomorphic changes detected, quantified and segregated from multi-temporal LiDAR data provided valuable information about recent torrential processes in the Portainé catchment. The main limitation of morphological budgeting in fluvial environments is the compensation of long-term scouring (erosion) and filling (deposition) by extraordinary events. In our study, the mobilized sediment volume was higher in the two-year period from 2009 to 2011 than in the five–year period from 2011 to 2016 (Table 5). Therefore, the analyzed torrents were considerably more active between 2009 and 2011 as they produced larger geomorphic changes, with the effects of the fluvio-torrential activity still continuing, but decreasing later on. The dynamics observed for the two time periods can be explained by both: (a) the different magnitudes of the torrential events and consequently variations in the eroded and deposited volumes of material, and (b) the effects of the sediment retention barriers changing the flow dynamics, resulting in mainly upstream deposition and downstream and lateral erosion. During the LiDAR temporal window, eight high-discharge flows occurred (Table 2) and all the barriers were emplaced (Table 3). Regarding the 2011-2009 comparison, three events occurred (two in 2010 and one in 2011) that filled nine barriers. The 2016-2011 comparison shows the effects of five events (one in 2013, two in 2014, one in 2015 and one in 2016) and four more sediment retention barriers.

Although small rainstorms may move some sediment along the channels, its volume is negligible. The recorded geomorphic changes mainly result from extraordinary torrential events, especially high-magnitude debris flows and floods. This is evidenced from the grain size observations in the field, where boulders predominate. When quantifying the geomorphic processes associated with extraordinary events, erosion is typically underestimated when the areas eroded during the peak discharge are covered with deposited material (Fuller et al., 2003). Thus, some erosion is undetectable in multi-temporal DEM comparisons. The torrential flows that occurred from 2009 to 2016 showed very different magnitudes and sediment loads, from well-developed debris flows (e.g., July 2010; Luis-Fonseca et al., 2011) to debris floods (e.g., May 2016; eyewitness accounts). The 2011-2009 geomorphic changes included those affected by the largest event, as well as another major and minor one. The 2016-2011 comparison included the effects of one major, three minor and the smallest event. The events with a higher magnitude are reflected in the clearly degradational 2011-2009 net budget and the aggradation of the cone, which are associated with the two major events of 2010. From 2011 to 2016, geomorphic processes in this area were mainly erosive due to the lack of high-magnitude torrential flows, the retention of material behind the nets and the effect of the "hungry waters" ahead. The barriers, stepped slope and decreasing flow velocity might have also reduced the potential effects of the events along the channels, especially for minor floods.

The dynamics of the torrents were mainly degradational, consistent with the erosive tendency of the increasingly entrenched channels. Most of the natural (not human-altered) reaches were erosional, whereas deposition occurred in specific areas, mainly at the sediment retention barriers and the debris cone (Fig. 5). Indeed, 33% and 25% of the total volumes of deposition from 2011-2009 and 2016-2011, respectively, corresponded to the material retained upstream of the barriers, whereas the debris cone accounted for 26% of the deposited volume between 2009 and 2011. Moreover, total erosion volumes might have been underestimated because of the exclusion of erosive cross sections where the geomorphic change was lower than the error ($\Delta Z < \delta\mu$). Indeed, 53% and 51% of the discarded sections were erosional for the 2011-2009 and 2016-2011 comparisons, respectively. All these results suggest a generalized incision tendency of the torrents, with local accumulations. As summer convective storms still occur and produce torrential events, such dynamics are expected to continue.

5.3. Assessment of the flexible sediment retention barriers

Flexible barriers are the preferred choice for hydrological correction in mountain areas. Their main advantages over conventional check dams are their lower economic cost and environmental impact, especially as their installation is quite quick and easy, using a helicopter (Mr. C. Fañanás, pers. com.). Furthermore, they only retain high-magnitude debris flows, letting low-magnitude flows go through below the net. However, sediment retention barriers strongly affect channel evolution. They modify the longitudinal profile of the torrents when they are filled, as the slope changes both upstream and downstream of the net (Fig. 4). Thus, the barriers alter the flow and produce a complex erosion-deposition dynamic that can be assessed in detail, as shown in this study.

Flexible barriers are filled during extraordinary events, leading to significant deposition volumes. They have been reported to present an individual retention capacity of 1,400-2,000 m^3 (Fañanas-Aguilera et al., 2009). However, we quantified considerably smaller deposition volumes behind the barriers (146-1,311 m^3), suggesting that the real retained volume may be lower than expected. Indeed, the retained volume might be affected by the local morphology of the torrent (gradient and width) and the size of the barrier (height and width). Given the dynamic nature of the barriers, acting loads are presumed to deform the ring net when material is retained. The flexion of the barriers was detected and measured in some barriers, giving valuable information on their behavior. Table 6 provides the dimensions of the barriers, the estimated retained volumes and the magnitude of net flexion.

Once filled, the barriers induce erosive effects downstream because the flow falls as a waterfall, progressively eroding the riverbed. In some adjacent slopes, localized incision has occurred due to the lateral deviation of the flow when passing over the deposit (Fig. 6a). Such lateral incisions might partially or completely empty the barriers. However, when erosion exposes the anchors, the barriers become less stable and thus, require repair and further maintenance (Fig. 6b). We identified and quantified erosion downstream and obtained eroded volumes of 46-703 m^3. These data are of paramount interest for prioritizing the management and maintenance of the barriers.

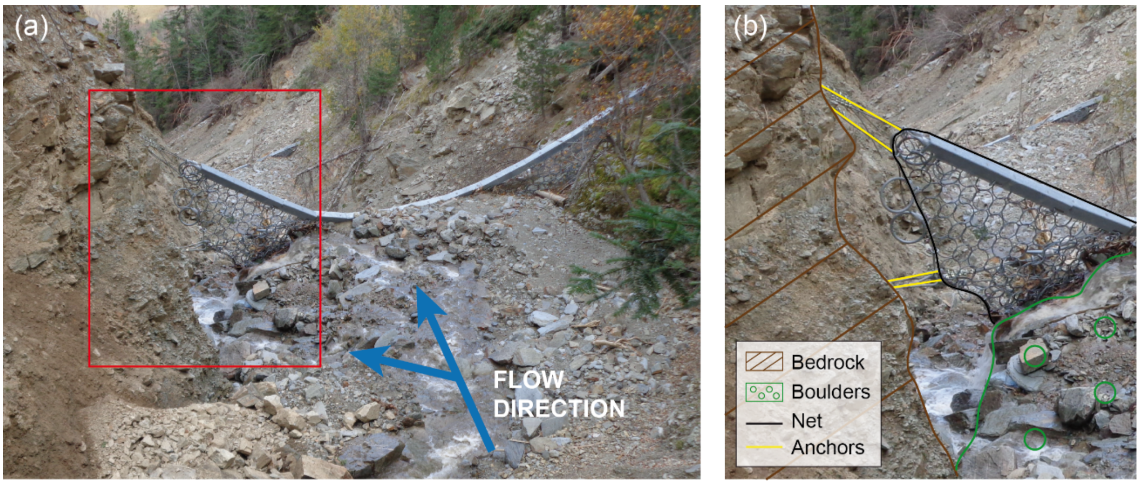

Figure 6. Lateral erosion and anchor exposure at barrier 53 (November 2015). (a) Photograph of the barrier and the accumulated material downstream. (b) Zoomed photograph and drawing of the main features, showing the lateral “hole” with the anchor exposed that might reduce the stability of the barrier.

6. Conclusions

This study presents a high-resolution assessment of the geomorphic impact of flexible barriers in torrential channels, including upstream filling and downstream and lateral erosion that can make barriers unstable, using a new LiDAR-based geomorphic approach for improved sediment budgets. The method takes into account spatial variabilities in data and errors along the channels by applying a cross-sectional elevation analysis to better discretize geomorphic changes. We propose this approach for studying torrents in densely vegetated steep mountains, which produce significant interpolation errors for standard DoD analyses.

The main applications for monitoring flexible sediment retention barriers include the: (i) estimation of barrier behavior, effects and consequences; (ii) remote revision and inspection for appropriate maintenance; (iii) detection of problematic spots and highly erosive reaches; and (iv) selection of priority areas for the installation of new barriers.

The LiDAR data analyzed in this study was useful for hydrogeomorphic research, even if it was not originally acquired for that purpose. Choosing optimal flight parameters for data acquisition in abrupt landscapes would provide even more accurate DEMs. Given its increasing availability, airborne LiDAR data are emerging as a potential tool for monitoring areas that are hard to inspect in the field. In this sense, the presented approach can be applied to assess structural corrective measures in mountain catchments and provide information for future decisions on management strategies.

Acknowledgements

This research was funded by the CHARMA (CGL2013-40828-R) and PROMONTEC (CGL2017-84720-R) projects from the Spanish Ministry of Economy, Industry and Competitiveness (MINEICO) and a PhD studentship to the lead author (APIF, 2014-2015) from the University of Barcelona (UB). LiDAR data were acquired as part of the LiDARCAT project of the Cartographic and Geological Institute of Catalonia (ICGC). We wish to thank Professor Jaume Calvet for supporting this study and Mr. Carles Fañanás (DARP) for providing information about historical events and the barriers.

References

Abancó C, Hürlimann M. 2014. Estimate of the debris-flow entrainment using field and topographical data. Natural Hazards 71: 363-383. DOI: 10.1007/s11069-013-0930-5

Abellan A, Derron MH, Jaboyedoff M. 2016. "Use of 3D Point Clouds in Geohazards" Special Issue: Current Challenges and Future Trends (Editorial). Remote Sensing 8: 130. DOI: 10.3390/rs8020130

Bailly J, Kinzel PJ, Allouis T., Feurer D, Le Coarer Y. 2012. Airborne LiDAR Methods Applied to Riverine Environments. In Fluvial Remote Sensing for Science and Management, Carbonneau PE, Piégay H (eds). John Wiley & Sons, Ltd: Chichester; 141–163.

Batalla RJ, De Jong C, Ergenzinger P, Sala M. 1999. Field observations on hyperconcentrated flows in mountain torrents. Earth Surface Processes and Landforms 24: 247–253. DOI: 10.1002/(SICI)1096-9837(199903)24:3<247::AID-ESP961>3.0.CO;2-1

Biron PM, Chóne G, Buffin-Bélanger T, Demers S, Olsen T. 2013. Improvement of streams hydro-geomorphological assessment using LiDAR DEMs. Earth Surface Processes and Landforms 38: 1808–1821. DOI: 10.1002/esp.3425

Brasington J, Langham J, Rumsby B. 2003. Methodological sensitivity of morphometric estimates of coarse fluvial sediment transport. Geomorphology 53: 299-316. DOI: 10.1016/S0169-555X(02)00320-3

Brasington J, Rumsby BT, Mcvey RA. 2000. Monitoring and modeling morphological change in a braided gravel-bed river using high resolution GPS-based survey. Earth Surface Processes and Landforms 25: 973–990. DOI: 10.1002/1096-9837(200008)25:9<973::AID-ESP111>3.0.CO;2-Y

Bull JM, Miller H, Gravley DM, Costello D, Hikuroa DCH, Dix JK. 2010. Assessing debris flows using LIDAR differencing: 18 May 2005 Matata event, New Zealand. Geomorphology 124: 75–84. DOI: 10.1016/j.geomorph.2010.08.011

Cavalli M, Goldin B, Comiti F, Brardinoni F, Marchi L. 2017. Assessment of erosion and deposition in steep mountain basins by differencing sequential digital terrain models. Geomorphology 291: 4–16. DOI: 10.1016/j.geomorph.2016.04.009

Cavalli M, Marchi L. 2008. Characterisation of the surface morphology of an alpine alluvial fan using airborne LiDAR. Natural Hazards and Earth System Sciences 8: 323-333. DOI: 10.5194/nhess-8-323-2008

Cavalli M, Tarolli P, Marchi L, Dalla Fontana G. 2008. The effectiveness of airborne LiDAR data in the recognition of channel-bed morphology. Catena 73: 249–260. DOI: 10.1016/j.catena.2007.11.001

Chevalier GG, Medina V, Hürlimann M, Bateman A. 2013. Debris-flow susceptibility analysis using fluvio-morphological parameters and data mining: application to the Central-Eastern Pyrenees. Natural Hazards 67: 213–238. DOI: 10.1007/s11069-013-0568-3

Croke J, Todd P, Thompson C, Watson F, Denham R, Khanal G. 2013. The use of multi temporal LiDAR to assess basin-scale erosion and deposition following the catastrophic January 2011 Lockyer flood, SE Queensland, Australia. Geomorphology 184: 111–126. DOI: 10.1016/j.geomorph.2012.11.023

ESRI. 2014. ArcGIS 10.2.2 Desktop. Environmental Systems Research Institute: Redlands

Fañanás C. 2016. Personal communication.

Fañanas-Aguilera C, Aguilar-Marín N, Raïmat-Quintana C, Luis-Fonseca R. 2009. Corrección hidrológica en el barranco de Portainé. In VII Simposio Nacional sobre Taludes y Laderas Inestables, Alonso E, Corominas J, Hürlimann M (eds). CIMNE: Barcelona; 999-1011.

Ferrero AM, Segalini A, Umili G. 2015. Experimental tests for the application of an analytical model for flexible debris flow barrier design. Engineering Geology 185: 33–42. DOI: 10.1016/j.enggeo.2014.12.002

FGC, ICGC. 2015. Seguiment geològic i geotècnic de la carretera d'accés a Port Ainé, 24 d'agost de 2015, NT-150824. Ferrocarrils de la Generalitat de Catalunya and Institut Cartogràfic i Geològic de Catalunya: Barcelona

Fuller IC, Large ARG, Charlton ME, Heritage GL, Milan DJ. 2003. Reach-scale sediment transfers: an evaluation of two morphological budgeting approaches. Earth Surface Processes and Landforms 28: 889–903. DOI: 10.1002/esp.1011

Furdada G, de las Heras A, Díez-Herrero A, Martins L, Fernández-Yuste JA, Victoriano A. 2017. The impact of land-use changes on palaeoflood and recent floods magnitude and frequency: Portainé (Eastern Pyrenees, Iberian Peninsula). In: 5th Past Global Changes Open Science Meeting Abstract Book. CSIC: Zaragoza; 253.

Génova M, Díez-Herrero A, Furdada G, Guinau M, Victoriano A. Accepted. Dendrogeomorphological evidence of flood frequency changes and anthropic activities (the Portainé basin, Spanish Pyrenees). Tree-Ring Research.

Girardeau-Montaut D. 2015. CloudCompare 2.6.2. Available at: http://www.cloudcompare.org/
Guha-Sapir D, Hoyois P, Below R. 2016. Annual Disaster Statistical Review 2015 The numbers and trends. CRED, Université catholique de Louvain: Brussels
Hsieh YC, Chan YC, Hu JC. 2016. Digital elevation model differencing and error estimation from multiple sources: A case study from the Meiyuan Shan landslide in Taiwan. Remote Sensing 8: 199. DOI: 10.3390/rs8030199
IGC. 2013. Avaluació de la dinàmica torrencial del torrent de Portainé, AP-035/13. Institut Geològic de Catalunya: Barcelona
Lallias-Tacon S, Liébault F, Piégay H. 2014. Step by step error assessment in braided river sediment budget using airborne LiDAR data. Geomorphology 214: 307-323. DOI: 10.1016/j.geomorph.2014.02.014
Lane, SN, Westaway RM, Hicks DM. 2003. Estimation of erosion and deposition volumes in a large, gravel-bed, braided river using synoptic remote sensing. Earth Surface Processes and Landforms 28: 249–271. DOI: 10.1002/esp.483
Luis-Fonseca R, Raïmat C, Hürlimann M, Abancó C, Moya J, Fernández J. 2011. Debris-flow protection in recurrent areas of the Pyrenees. Experience of the VX systems from output results collected in the pioneer monitoring station in Spain. In 5th International Conference on Debris-Flow Hazards “Mitigation, Mechanics, Prediction and Assessment”, Genevois R, Hamilton DL, Prestininzi A (eds). Research Center CERI, Sapienza Università: Rome; 1063–1071. DOI: 10.4408/IJEGE.2011-03.B-115
Meteocat. 2008. Atles Climátic de Catalunya 1961-1990. Servei Meteorològic de Catalunya: Barcelona
Munich Re. 2016. Annual statistics: natural disasters 2015. Munich Re Group, NatCatSERVICE: Munich
Notebaert B, Verstraeten G, Govers G, Poesen J. 2009. Qualitative and quantitative applications of LiDAR imagery in fluvial geomorphology. Earth Surface Processes and Landforms 34: 217–231. DOI: 10.1002/esp.1705
Ortuño M, Guinau, M, Calvet J, Furdada G, Bordonau J, Ruiz A, Camafort M. 2017. Potential of airborne LiDAR data analysis to detect subtle landforms of slope failure: Portainé, Central Pyrenees. Geomorphology 295: 364–382. DOI: 10.1016/j.geomorph.2017.07.015
Palau RM, Hürlimann M, Pinyol J, Moya J, Victoriano A, Génova M, Puig-Polo C. 2017. Recent debris flows in the Portainé catchment (Eastern Pyrenees, Spain): analysis of monitoring and field data focussing on the 2015 event. Landslides 14: 1161–1170. DOI: 10.1007/s10346-017-0832-9
Passalacqua P, Belmont P, Staley DM, Simley JD, Arrowsmith R, Bode CA, Crosby C, DeLong SB, Glenn NF, Kelly SA, Lague D, Sangireddy H, Schaffrath K, Tarboton DG, Wasklewicz T, Wheaton JM. 2015. Analyzing high resolution topography for advancing the understanding of mass and energy transfer through landscapes: A review. Earth Science Reviews 148: 174-193. DOI: 10.1016/j.earscirev.2015.05.012
Pierson TC, Costa JE. 1987. A rheologic classification of subaerial sediment-water flows. In Debris Flows/Avalanches: Process, Recognition and Mitigation, Reviews in

Engineering Geology 7, Costa JE, Wieczorek G (eds). Geological Society of America: Boulder; 1–12.

Pinyol J, Hürlimann M, Furdada G, Moysset M, Palau RM, Victoriano A, González M, Moya J, Guinau M, Raïmat C, Fañanás C. 2017. El barranco de Portainé (Pirineo Central): un laboratorio in situ completo para el estudio de la actividad torrencial. In: IX Simposio Nacional Sobre Taludes y Laderas Inestables, Alonso E, Corominas J, Hürlimann M (eds). CIMNE: Barcelona; 1165–1176.

Portilla M, Chevalier G, Hürlimann M. 2010. Description and analysis of the debris flows occurred during 2008 in the Eastern Pyrenees. Natural Hazards and Earth System Sciences 10: 1635–1645. DOI: 10.5194/nhess-10-1635-2010

Roering JJ, Mackey BH, Marshall JA, Sweeney KE, Deligne NI, Booth AM, Handwerger AL, Cerovski-Darriau C. 2013. "You are HERE": Connecting the dots with airborne lidar for geomorphic fieldwork. Geomorphology 200: 172–183. DOI: 10.1016/j.geomorph.2013.04.009

Rupnik B, Mongus D, Žalik B. 2015. Point Density Evaluation of Airborne LiDAR Datasets. Journal of Universal Computer Science 21: 587–603. DOI: 10.3217/jucs-021-04-0587

Scheidl C, Rickenmann D. 2011. TopFlowDF – A simple GIS model to simulate debris-flow runout on the fan. In 5th International Conference on Debris-Flow Hazards "Mitigation, Mechanics, Prediction and Assessment", Genevois R, Hamilton DL, Prestininzi A (eds). Research Center CERI, Sapienza Università: Rome; 253-262. DOI: 10.4408/IJEGE.2011-03.B-030

Scheidl C, Rickenmann D, Chiari M. 2008. The use of airborne LiDAR data for the analysis of debris flow events in Switzerland. Natural Hazards and Earth System Sciences 8: 1113–1127. DOI: 10.5194/nhess-8-1113-2008

Slatton KC, Carter WE, Shrestha RL, Dietrich WE. 2007. Airborne Laser Swath Mapping: Achieving the resolution and accuracy required for geosurficial research. Geophysical Research Letters 34: L23S10. DOI: 10.1029/2007GL031939

Taylor JR. 1997. An Introduction to Error Analysis: The Study of Uncertainties in Physical Measurements. University Science Books: Sausalito. ISBN: 0-935702-42-3

Terrasolid. 2016. TerraScan User's Guide. Terrasolid Ltd: Helsinki

Trapero L, Bech J, Duffourg F, Esteban P, Lorente J. 2013. Mesoscale numerical analysis of the historical November 1982 heavy precipitation event over Andorra (Eastern Pyrenees). Natural Hazards and Earth System Sciences 13: 2969-2990. DOI: 10.5194/nhess-13-2969-2013

Victoriano A, Díez-Herrero A, Génova M, Guinau M, Furdada G, Khazaradze G, Calvet J. 2018. Four-topic correlation between flood dendrogeomorphological evidence and hydraulic parameters (the Portainé stream, Iberian Peninsula). Catena 162: 216-229. DOI: 10.1016/j.catena.2017.11.009

Volkwein A, Baumann R, Rickli C, Wendeler C. 2015. Standardization for Flexible Debris Retention Barriers. In Engineering Geology for Society and Territory – Volume 2, Lollino G, Giordan D, Crosta GB, Corominas J, Azzam R, Wasowski J, Sciarra N (eds). Springer: Cham, Heidelberg, New York, Dordrecht, London; 193-196. DOI: 10.1007/978-3-319-09057-3_25

Wendeler C, McArdell BW, Volkwein A, Denk M, Gröner E. 2008. Debris flow mitigation with flexible ring net barriers – field tests and case studies. WIT Transactions on Engineering Sciences 60:23-31. DOI: 10.2495/DEB080031

Wheaton JM, Brasington J, Darby SE, Sear DA. 2010. Accounting for uncertainty in DEMs from repeat topographic surveys: improved sediment budgets. Earth Surface Processes and Landforms 35: 136–156. DOI: 10.1002/esp.1886

(a) (b)

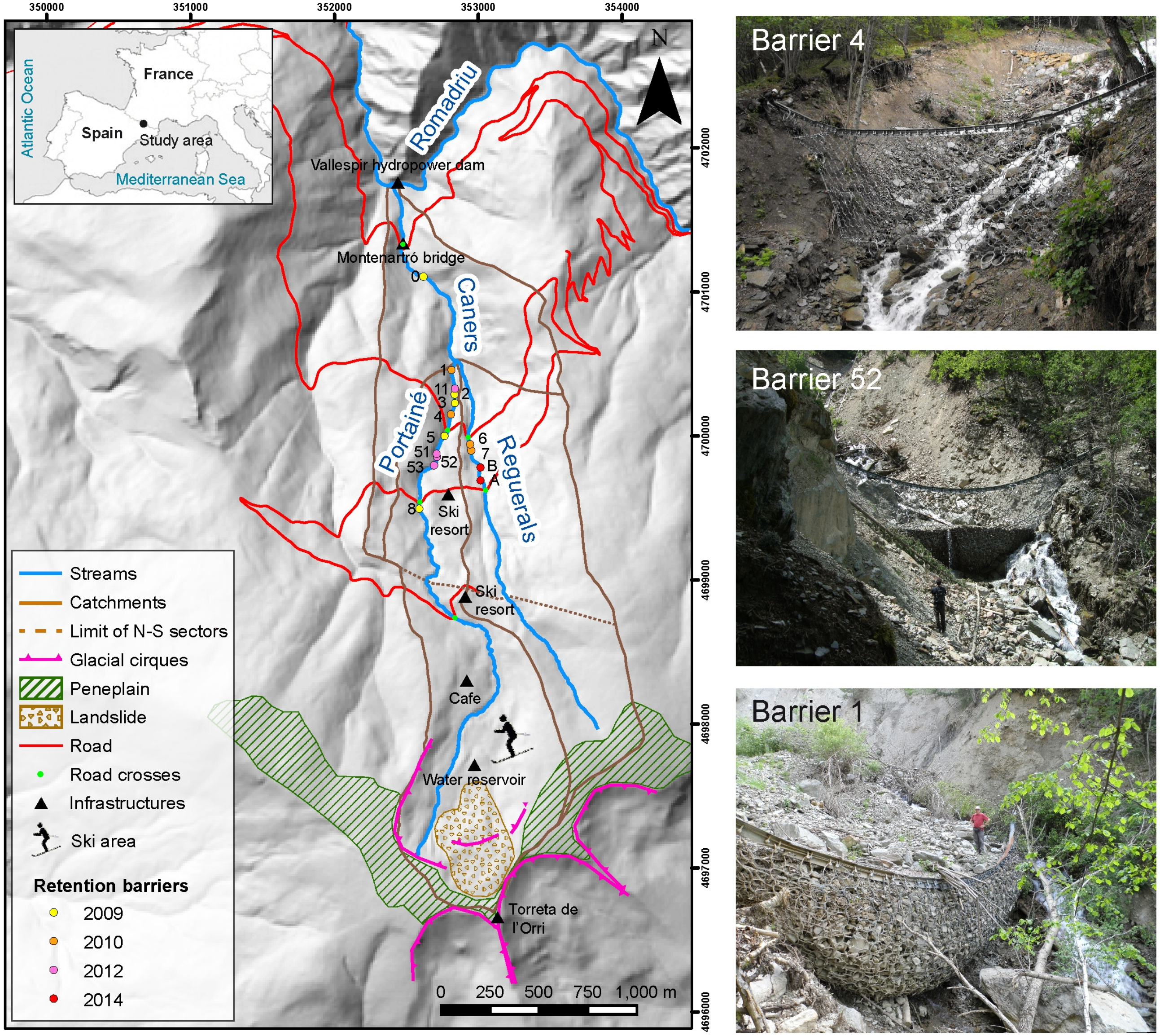

350000
351000
352000
353000
354000
4702000
4701000
4700000
4699000
4698000
4697000
4696000
N
France
Spain
Atlantic Ocean
Study area
Mediterranean Sea
Romadriu
Vallespir hydropower dam
Montenartró bridge
Caners
Portainé
Reguerals
Ski resort
Ski resort
Cafe
Water reservoir
Torreta de l'Orri
0
1
11
2
3
4
5
6
7
B
A
51
52
53
8
0 250 500 750 1,000 m
Streams
Catchments
Limit of N-S sectors
Glacial cirques
Peneplain
Landslide
Road
Road crosses
Infrastructures
Ski area
Retention barriers
2009
2010
2012
2014
Barrier 4
Barrier 52
Barrier 1

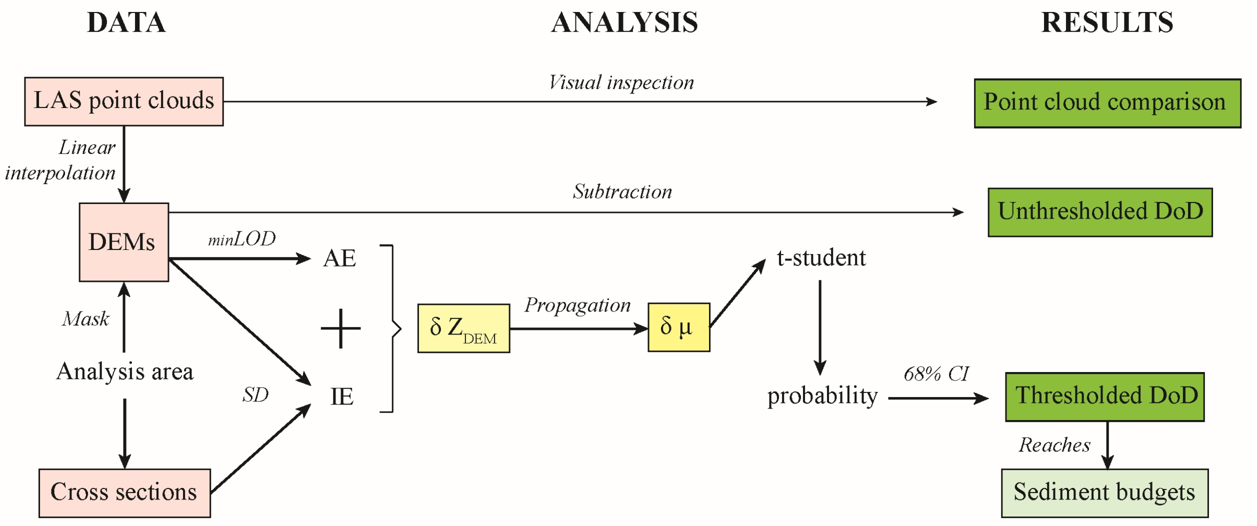
DATA
ANALYSIS
RESULTS
LAS point clouds
Visual inspection
Point cloud comparison
Linear interpolation
DEMs
Subtraction
Unthresholded DoD
minLOD
AE
+
IE
Mask
Analysis area
SD
Cross sections
δ Z DEM
Propagation
δ μ
t-student
probability
68% CI
Thresholded DoD
Reaches
Sediment budgets

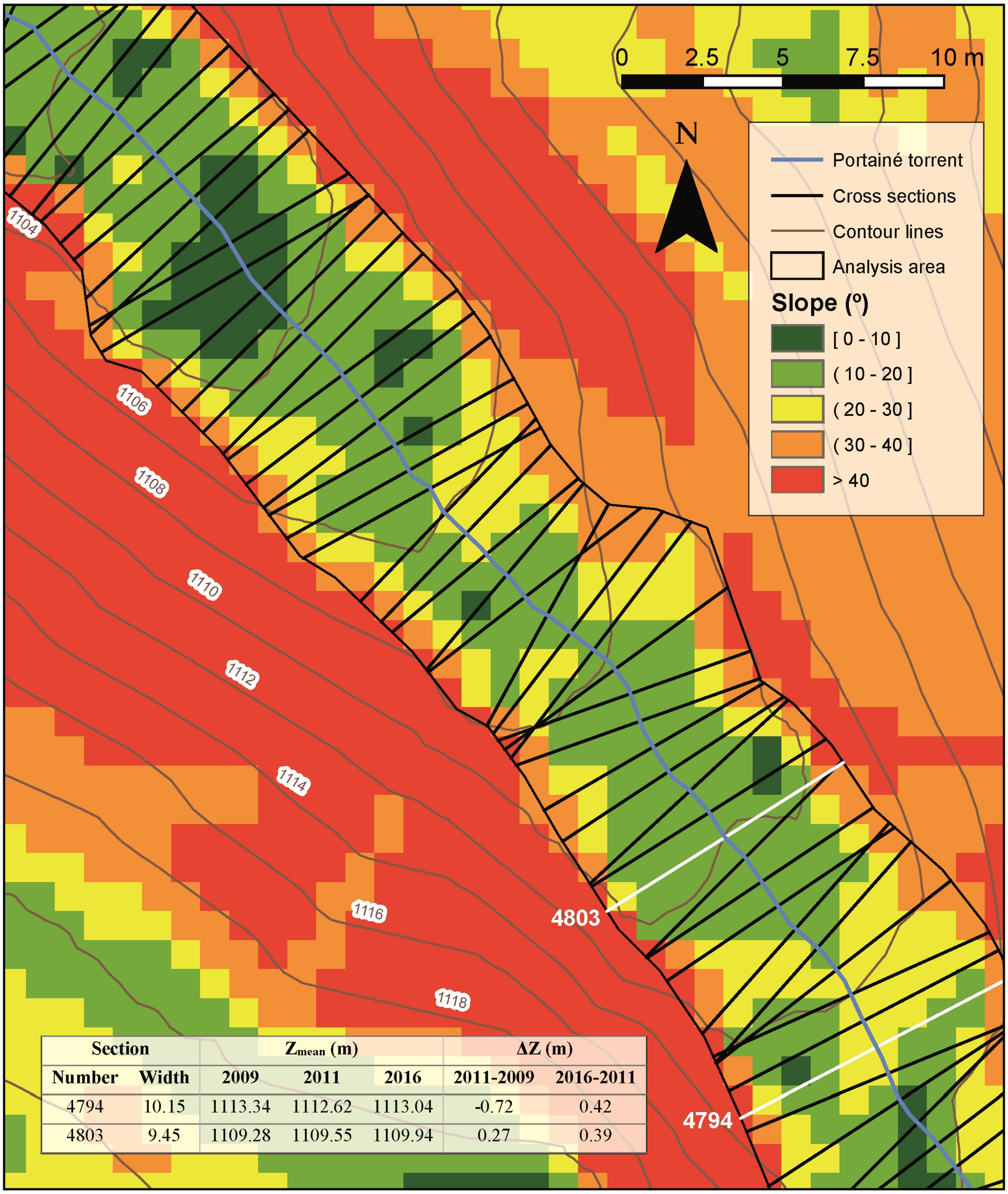

Section		Z_{mean} (m)			ΔZ (m)	
Number	Width	2009	2011	2016	2011-2009	2016-2011
4794	10.15	1113.34	1112.62	1113.04	-0.72	0.42
4803	9.45	1109.28	1109.55	1109.94	0.27	0.39

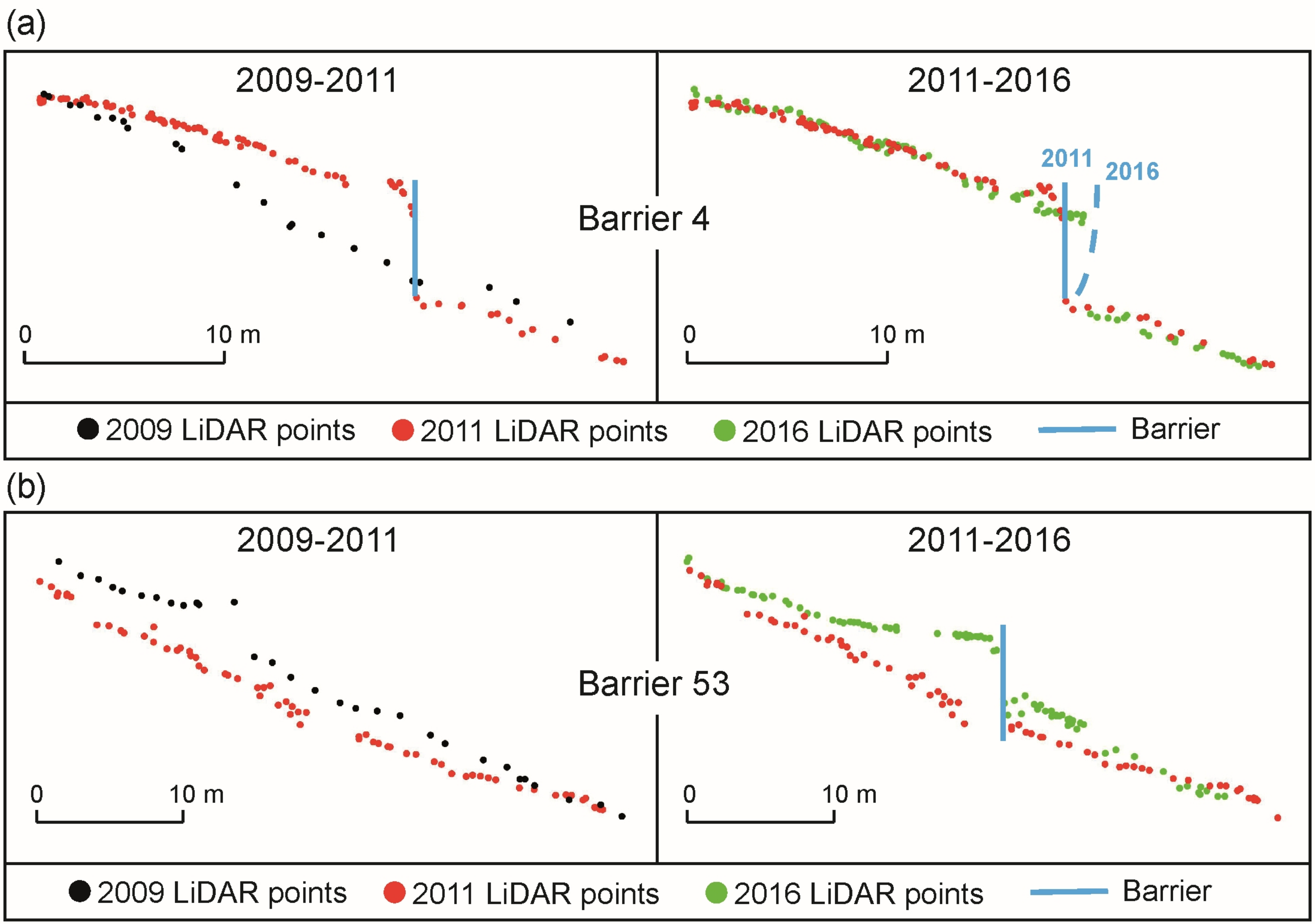

(a)
2009-2011
2011-2016
Barrier 4
2011
2016
0
10 m
0
10 m
2009 LiDAR points
2011 LiDAR points
2016 LiDAR points
Barrier
(b)
2009-2011
2011-2016
Barrier 53
0
10 m
0
10 m
2009 LiDAR points
2011 LiDAR points
2016 LiDAR points
Barrier

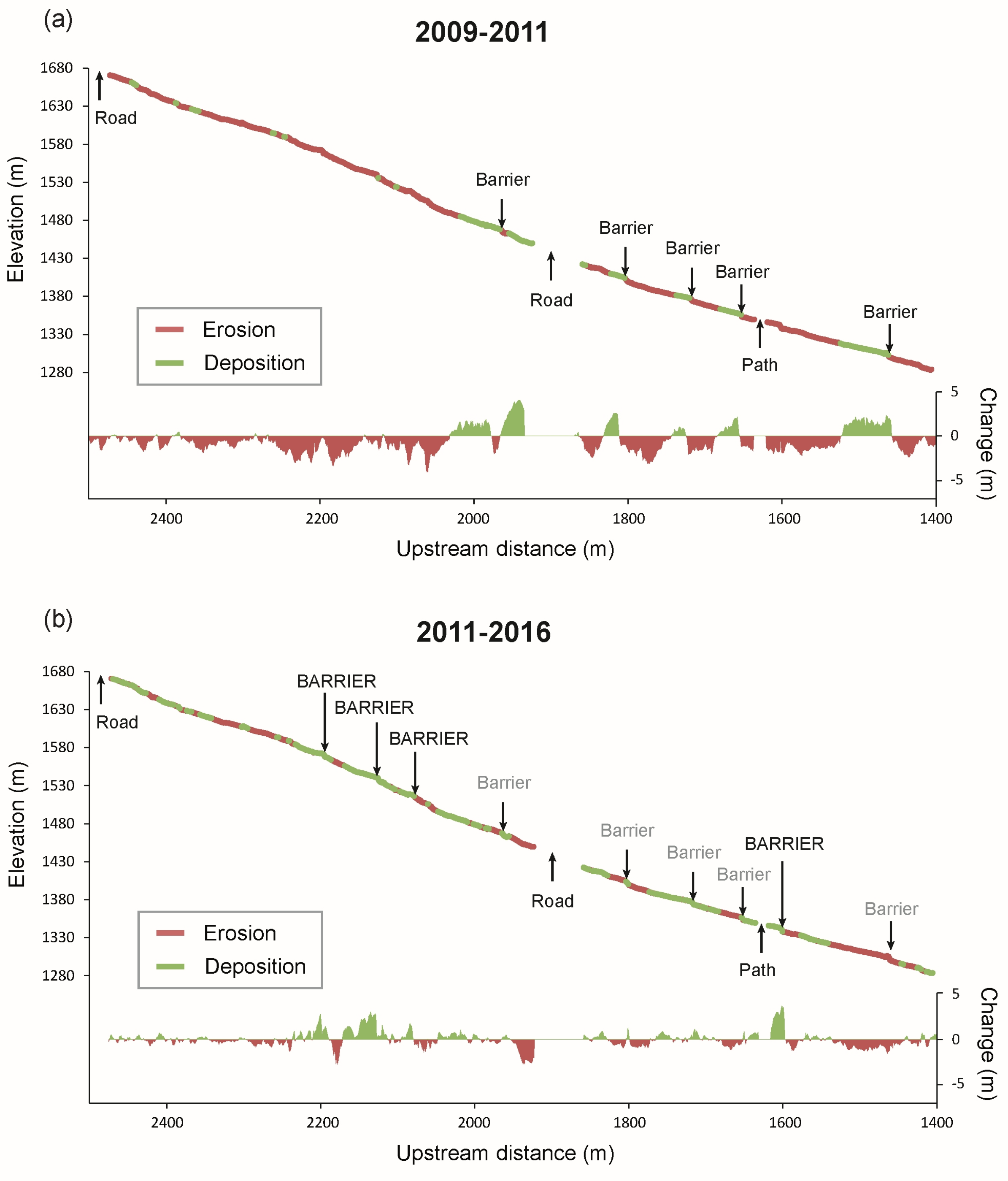

(a)
2009-2011
Elevation (m)
1680
1630
1580
1530
1480
1430
1380
1330
1280
Road
Barrier
Road
Barrier
Barrier
Barrier
Path
Barrier
Erosion
Deposition
Change (m)
5
0
-5
2400
2200
2000
1800
1600
1400
Upstream distance (m)
(b)
2011-2016
Elevation (m)
1680
1630
1580
1530
1480
1430
1380
1330
1280
Road
BARRIER
BARRIER
BARRIER
Barrier
Road
Barrier
Barrier
Barrier
BARRIER
Path
Barrier
Erosion
Deposition
Change (m)
5
0
-5
2400
2200
2000
1800
1600
1400
Upstream distance (m)

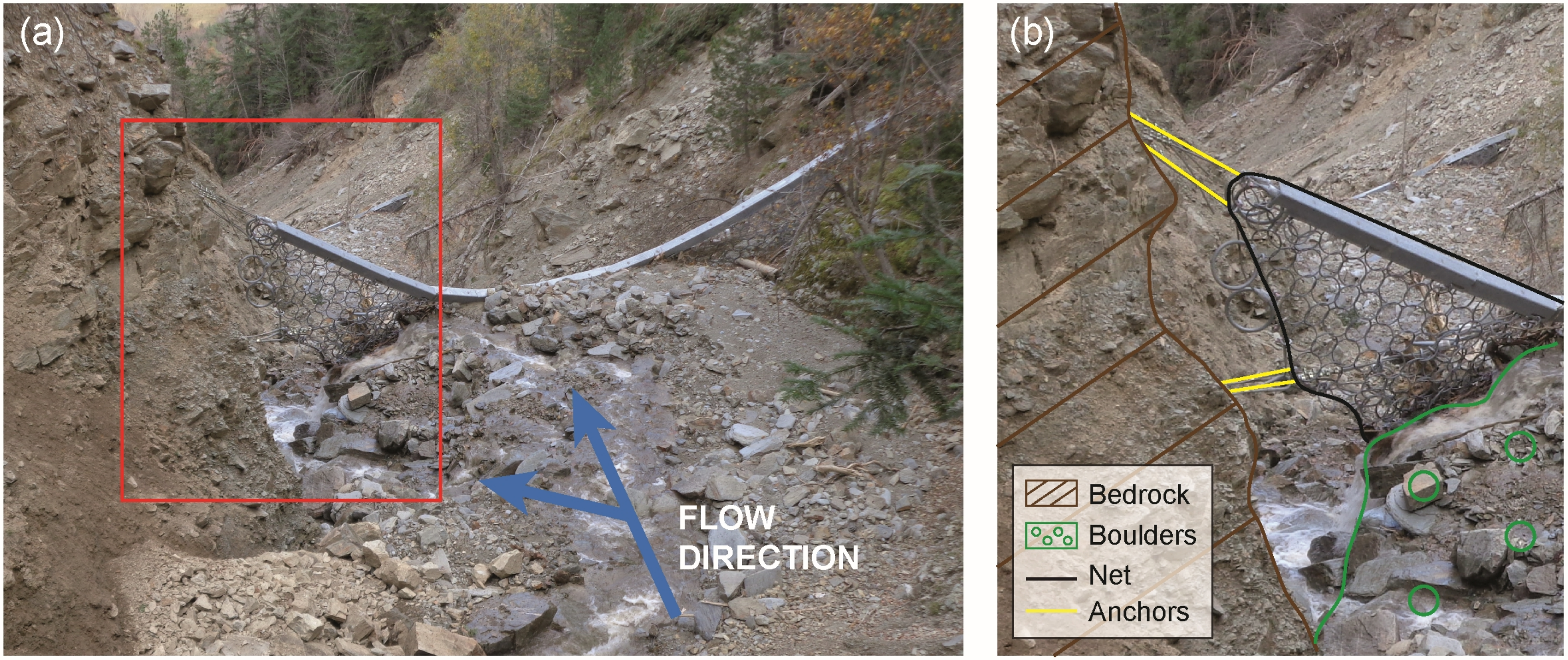
(a)
FLOW
DIRECTION
(b)
Bedrock
Boulders
Net
Anchors

Table 1. LiDAR flight parameters and point cloud data specifications from the 2009, 2011 and 2016 surveys (data from ICGC).

	2009	**2011**	**2016**
Average flight altitude	2250 m	2440 m	2712 m
Scan angle	48°	40°	31.3 °
Scan frequency	21.5 Hz	25 Hz	24.4 Hz
Pulse rate	89200 Hz	84400 Hz	77100 Hz
Nominal point density	0.5 pt/m^2	0.5 pt/m^2	0.5 pt/m^2
Total point density (for entire datasets)	0.96 pt/m^2	2.14 pt/m^2	2.77 pt/m^2
Ground point density (for analysis area)	0.29 pt/m^2	0.93 pt/m^2	1.32 pt/m^2

Table 2. List of the events, including date, magnitude and effects (information obtained from FGC and ICGC (2015) and IGC (2013).

Event		Effects and damages		
Date	**Magnitude**	**Torrent**	**Road crosses**	**Barriers**
2010/07/22	Most significant	Portainé Reguerals	2	7 filled 2 damaged
2010/08/12	Major	Portainé Reguerals	2	0 filled 5 damaged
2011/08/05	Minor	Portainé Reguerals	0	2 filled 1 damaged
2013/07/23	Major	Portainé Reguerals	3	3 filled 3 damaged
2014/08/20	Minor	?	0	-
2014/08/30	Medium	Portainé	1	5 damaged
2015/08/21	Medium	Portainé	1	5 damaged
2016/05/09	Less significant	?	0	-

Table 3. Sediment retention barriers on the Portainé and Reguerals torrents (information provided by Mr. C. Fañanás, pers. com.).

Barrier code	**Date**	**Torrent**	**Elevation (m a.s.l.)**	**Height (m)**	**Width (m)**	**Filling event**
0	2009	Caners	1090	4	13.5	2010/07/22
1	2010	Portainé	1308	4	16.8	2010/07/22
2	2009	Portainé	1355	5	13.5	2010/07/22
3	2009	Portainé	1380	5	11.5	2011/08/05
4	2010	Portainé	1405	4	13.5	2010/07/22
5	2009	Portainé	1470	5	20	2010/07/22
6	2010	Reguerals	1490	4	27	2010/07/22
7	2010	Reguerals	1510	4	26	2011/08/05
8	2009	Portainé	1710	6	19.5	2010/07/22
11	2012	Portainé	1345	5.5	16.5	2012 (anthropic)
51	2012	Portainé	1525	4.5	25	2013/07/23
52	2012	Portainé	1555	4.8	27.1	2013/07/23
53	2012	Portainé	1575	5.1	15.1	2013/07/23
A	2014	Reguerals	1615	5	19.2	-
B	2014	Reguerals	1570	6	17.5	-

Table 4. Results of the spatially variable uncertainty analysis for two example sections (see their location in Fig. 3). The volumes of the geomorphic change were only calculated for thresholded real elevation changes.

Section		**DEM error**			**Propagated error**		**Probabilistic thresholding**						**Volume (m^3)**	
Nº	Width (m)	δZ_{DEM} (m)			$\delta\mu$ (m)		t		p		Real ΔZ (m)			
		2009	2011	2016	11-09	16-11	11-09	16-11	11-09	16-11	11-09	16-11	11-09	16-11
4794	10.15	0.78	1.04	0.48	1.3	1.14	0.55	0.36	0.29	0.36	-0.72	-	-7.32	-
4803	9.45	0.58	0.29	0.24	0.65	0.38	0.41	1.03	0.34	0.15	-	0.39	-	3.67

Table 5. Segregation of the sediment budgets obtained from the 2011-2009 and 2016-2011 DEM comparisons. For each reach, we calculated the net volumetric change and indicated its erosional/degradational or depositional/aggradational tendency.

Criteria	Reach description	Time period	Erosion (m^3)	Deposition (m^3)	Change (m^3)	Dynamics
Torrent (abbr.)	Portainé (Po)	2011-2009	-11,629	6,936	**-4,693**	Degradation
		2016-2011	-4,477	3,497	**-980**	Degradation
	Reguerals (Re)	2011-2009	-4,708	2,167	**-2,541**	Degradation
		2016-2011	-1,618	2,156	**538**	Aggradation
	Caners (Ca)	2011-2009	-5,705	10,101	**4,396**	Aggradation
		2016-2011	-2,213	2,508	**295**	Aggradation
Catchment sector (gradient)	Upper (low)	2011-2009	-2,441	822	**-1,619**	Degradation
		2016-2011	-1,139	568	**-572**	Degradation
	Middle (high)	2011-2009	-19,128	13,023	**-6,105**	Degradation
		2016-2011	-6,112	7,473	**1,362**	Aggradation
	Lower (medium)	2011-2009	-473	5359	**4,886**	Aggradation
		2016-2011	-1,057	120	**-937**	Degradation
Road intersection (max-min altitude)	Po (2360-1965 m)	2011-2009	-1,764	775	**-989**	Degradation
		2016-2011	-1,096	541	**-554**	Degradation
	Po (1965-1700 m)	2011-2009	-1,684	2,015	**331**	Aggradation
		2016-2011	-642	438	**-204**	Degradation
	Po (1700-1450 m)	2011-2009	-4191	2,039	**-2,152**	Degradation
		2016-2011	-1,419	1,731	**312**	Aggradation
	Re (2225-1665 m)	2011-2009	-399	222	**-178**	Degradation
		2016-2011	-180	145	**-34**	Degradation
	Re (1665-1465 m)	2011-2009	-1506	1,450	**-55**	Degradation
		2016-2011	-767	1,107	**339**	Aggradation
	Ca (1465-1035 m)	2011-2009	-12,025	7,344	**-4,681**	Degradation
		2016-2011	-3,147	4,078	**931**	Aggradation
	Ca (1035-950 m)	2011-2009	-473	5,359	**4886**	Aggradation
		2016-2011	-1,057	120	**-937**	Degradation
NET SEDIMENT BUDGET		2011-2009	-22,042	19,204	**-2,838**	Degradation
		2016-2011	-8,308	8,161	**-147**	Degradation

Table 6. Relationship between dimensions, the calculated volume of filled barriers and the magnitude of the net flexion. The barriers are listed in their order along the downstream direction.

Barrier code	**Height (m)**	**Width (m)**	**Torrent**	**Elevation (m a.s.l.)**	**Volume (m^3)**	**Horizontal net displacement (m)**
8	6	19.5	Portainé	1710	1302	0.3
53	5.1	15.1	Portainé	1575	303	-
52	4.8	27.1	Portainé	1555	1044	-
51	4.5	25	Portainé	1525	146	-
7	4	26	Reguerals	1510	441	0.5
6	4	27	Reguerals	1490	534	0.4
5	5	20	Portainé	1470	559	?
4	4	13.5	Portainé	1405	589	1.1
3	5	11.5	Portainé	1380	?	1.2
2	5	13.5	Portainé	1355	282	?
11	5.5	16.5	Portainé	1345	535	-
1	4	16.8	Portainé	1308	1230	?
0	4	13.5	Caners	1090	1311	?